11-2017

Numerical Modeling to Evaluate the Performance of Slow-Release Candles for Groundwater Remediation

Chuyang Liu
University of Nebraska-Lincoln, liucyl@hotmail.com

NUMERICAL MODELING TO EVALUATE THE PERFORMANCE OF SLOW-RELEASE CANDLES FOR GROUNDWATER REMEDIATION

by

Chuyang Liu

A THESIS

Presented to the Faculty of

The Graduate College at the University of

Nebraska In Partial Fulfillment of Requirements

For the Degree of Master of Science

Major: Civil Engineering

Under the Supervision of Professor Yusong Li

Lincoln, Nebraska

November, 2017

NUMERICAL MODELING TO EVALUATE THE PERFORMANCE OF SLOW-RELEASE CANDLES FOR GROUNDWATER REMEDIATION

Chuyang Liu, M.S.

University of Nebraska, 2017

Advisor: Yusong Li

Slow-release candles (SRC) have been developed as a cost-effective technology to treat groundwater contaminants by passively delivering oxidants into the subsurface over a long time. In this thesis, a numerical model has been developed to simulate oxidant release kinetics, transport, and reaction in a field scale. Parameters of the model were obtained from a field site with SRC installed. Modeling results showed that the radius of influence of oxidants was influenced by the relative contribution of reaction and solute transport, and the limited lateral spreading could be an issue to restrict the application of SRC.

Enhanced aeration could increase or decrease the radius of influence of a candle, dependent on the incoming contaminant concentration. Enhanced mixing due to aeration could reduce the concentration of persulfate adjacent to the candle. It can greatly improve the radius of influence when incoming contaminant concentration is relatively low. When incoming contaminant concentration is very high, it may lead to reduced radius of influence. In the slow-release system design, if extra supply of oxidant in a candle was considered and suitable aeration rates was designed, the demand of boring and labor work could be greatly reduced by using

larger interval distances. In the meantime, the effective duration time could also be increased.

The model developed in this work can be adapted to simulate SRC remediation under various field scenarios. It can be a tool to help design and optimize the SRC for various oxidant and targeting contaminants.

Acknowledgements

At the end of my master studies, I wish to deeply thank my advisor, Dr. Yusong Li, for teaching me research related skills from ABC and guiding me to grow into a mature researcher. Without her generous help, I would not be able to effectively control my emotions affected by the surrounding troubles and the processes of research would be more difficult. She always encouraged me to see things in a bigger picture and supported me to study interested objects. With her guidance, I was able to change my specialization from Structural/Transportation Engineering to Water Resources Engineering. I appreciate the opportunity she gave to me to study and build connections to other professionals.

I also wish to express my sincerely thanks to Dr. Steve Comfort for giving me field trip opportunities to enhance my experiences. Without the insight from the field site, the simulation processes would not be that smoothly. He generously helped me the reaction-related portion of my research and offered an opportunity to share my work among his students. Special thanks go to James Reece. Without the field data he provided, my model would be less reliable. My respectful gratitude also goes to Ann Kambhu for her academic and life supports. Without her help, I would need more time to get familiar with the research area and graduate study. She has helped me to develop an ability to finish things on time with better quality and enjoy the rest part of the life.

I would like to sincerely thank my committee members, Dr. Shannon Bartelt-Hunt and Dr. Xu Li, for all their assistance and shared knowledge. Finally, I had my deepest appreciation to my parents for their patience, understanding, and lovely care.

Table of Contents

List of Figures

Chapter 1

Project Overview and Objectives

1.1. Project Overview

Environmental Protection Agency (EPA) reported about 294,000 sites required a remediation under current polices (EPA, 2014). Among those sites, chlorinated solvents and petroleum are worldwide contaminants to threat the groundwater quality. Those contaminants are persistent and toxic. Typically, they require at least decades to be naturally alleviated and caused serious health problems, including cancers. In addition, those contaminants could be widespread as non-aqueous phase liquids (NAPL) sources and transported by density effects and groundwater flow.

In-situ chemical oxidation (ISCO) is a relatively mature technology that injects the oxidants into the subsurface and let oxidants to react with NAPLs (Wiesner, Grant, & Hutchins, 1996). However, delivering oxidants into the low permeability zone is still a challenge for ISCO, and oxidants prefer to go through less resistant area and might bypass the target zone. After an ISCO treatment, NAPL may still remain in the low permeability zone, and concentration of contaminants would go up again by dissolution and diffusion after the remediation (rebound).

To overcome the shortcomings of ISCO, slow-release candles were developed(Christenson, Kambhu, & Comfort, 2012; Kambhu, Comfort, Chokejaroenrat,

& Sakulthaew, 2012; Kambhu, Gren, Tang, Comfort, & Harris, 2017; Lee et al., 2008). Slow-release candles are made of a mixture of environmental safe material (i.e. wax) and oxidants. They can be installed into the low permeability zone, and could semi-passively deliver the oxidants to the surrounding area over days to years. For example, Lee simulated a slow-release system to release about 1.65 kg permanganate (i.e. a type of oxidant) daily over 6.6 years without continuously injection.

While the efficiency of slow-release candles have been demonstrated in several field sites, it is necessary to develop a quantitative approach to evaluate their performance under different site conditions. A numerical model that couples oxidant release, transport, and reaction would be a powerful tool to evaluate the performance of slow release candle and help optimal site design.

1.2. Objectives

The objectives of this study was:

I. To develop a numerical model to simulate oxidant release, transport and reaction with contaminants;

II. To use the model to evaluate the radius of influence of slow-release candles under various field scenarios.

1.3. Thesis Organizations

This thesis consists of 7 Chapters. Following this introduction chapter 1, Chapter 2 identifies that research need based on a literature review. Chapter 3 describes the field

site that provides realistic base parameters for model development. Chapter 4 describes the process of developing a sodium persulfate release model. Chapter 5 provides a model to simulate sodium persulfate release and transport in a field site with simplified flow field. In addition, Chapter 6 couples sodium persulfate release, transport, and reaction to predict the radius of influence with/without aeration. Finally, a conclusion is summarized and suggestions for future work are provided in Chapter 7.

References

Christenson, M. D., Kambhu, A., & Comfort, S. D. (2012). Using slow-release permanganate candles to remove TCE from a low permeable aquifer at a former landfill. *Chemosphere*, *89*(6), 680–687. https://doi.org/10.1016/j.chemosphere.2012.06.009

EPA, U. S. (2014). In Situ Chemical Oxidation. Retrieved from http://www.epa.gov/ada/gw/isco.html

Kambhu, A., Comfort, S., Chokejaroenrat, C., & Sakulthaew, C. (2012). Developing slow-release persulfate candles to treat BTEX contaminated groundwater. *Chemosphere*, *89*(6), 656–664. https://doi.org/10.1016/j.chemosphere.2012.06.004

Kambhu, A., Gren, M., Tang, W., Comfort, S., & Harris, C. E. (2017). Remediating 1,4-dioxane-contaminated water with slow-release persulfate and zerovalent iron. *Chemosphere*, *175*, 170–177. https://doi.org/10.1016/j.chemosphere.2017.02.044

Lee, E. S., Woo, N. C., Schwartz, F. W., Lee, B. S., Lee, K. C., Woo, M. H., … Kim, H.

K. (2008). Characterization of controlled-release KMnO4 (CRP) barrier system for groundwater remediation: A pilot-scale flow-tank study. *Chemosphere*, *71*(5), 902–910. https://doi.org/10.1016/j.chemosphere.2007.11.037

Wiesner, M. R., Grant, M. C., & Hutchins, S. R. (1996). Reduced permeability in groundwater remediation systems: Role of mobilized colloids and injected chemicals. *Environmental Science and Technology*, *30*(11), 3184–3191. https://doi.org/10.1021/es950784u

Chapter 2

Background and Literature Review

2.1. Introduction

Groundwater and soil contaminated sites arose a public attention in the 1970s and became a worldwide problem because of several disasters, such as the cancer incidence in the love canal area. According to Environmental Protection Agency (EPA), there are about 294,000 sites required a remediation under current polices (EPA, 2014). In the past, those sites were drycleaners, gas stations, military sites, manufacturing sites, which discharged gas, detergent and/or other organic solvents into groundwater. Figure 1 illustrates the number of sites that require remediation owned by different local or federal agencies.

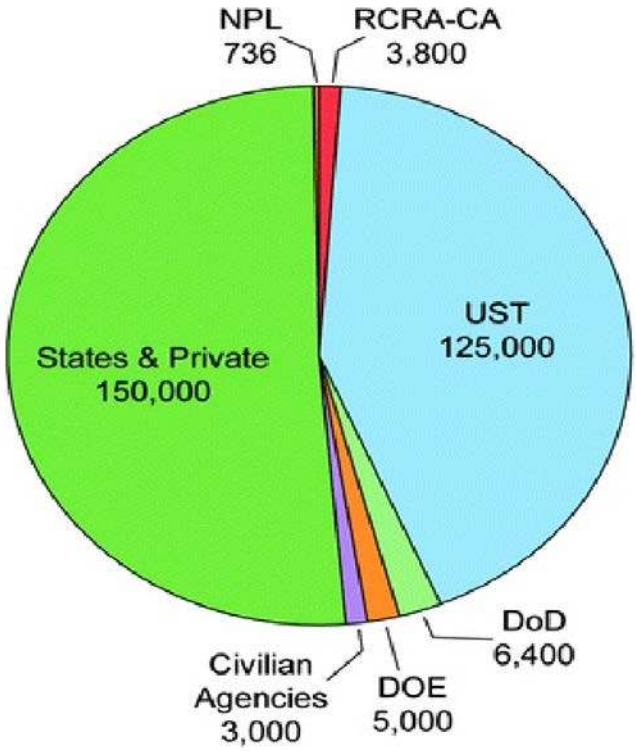

Figure 1. Total number of sites requring a remediation (EPA, 2014)

Based on the toxicity and prevalence of contaminants among those sites, benzene, toluene, ethylbenzene, and xylene (BTEX) are a group of the highest priority compounds that contaminated the soil and groundwater. BTEX are typically components in gasoline. They have low solubility, are less dense than water, and are carcinogenic. The presence of BTEX can be persistent and can serve as a long term source that releases a highly toxic plume in the contaminated site. EPA sets a maximum contaminant level (MCL) as a limit for drinking water quality. For benzene, the MCL is 5 ppb; for toluene, the MCL is 1,000 ppb; for ethylbenzene, the MCL is 700 ppb; for xylene, the MCL is 10,000 ppb (EPA, 2017).

Various remediation technologies were developed to treat these contaminants and meet water regulations. Among them, in situ chemical oxidation (ISCO) is a common and relative mature technology since 1990s ((Liu, Chen, Wang, Shi, & Shi, 2017; Thepsithar & Roberts, 2006; Wiesner, Grant, & Hutchins, 1996)). In ISCO, oxidants are injected into the subsurface to react with contaminants, as shown in Figure 2. In many sites, ISCO has demonstrated an ability for rapid treatment. For high concentration areas, ISCO typically has a moderate cost compared to other remediation techniques. However, the cost of ISCO is relatively high for dilute plumes of contaminants, which is a common situation in many sites. In addition, ISCO is not very effective to treat contaminants in low permeability zones. Injected oxidant solutions tend to transport in higher permeable zones, and bypass the lower permeable zones. When contaminants in the low permeability zones are not completely treated, rebound (i.e. the process of contaminants transported back again after the remediation) commonly occurs.

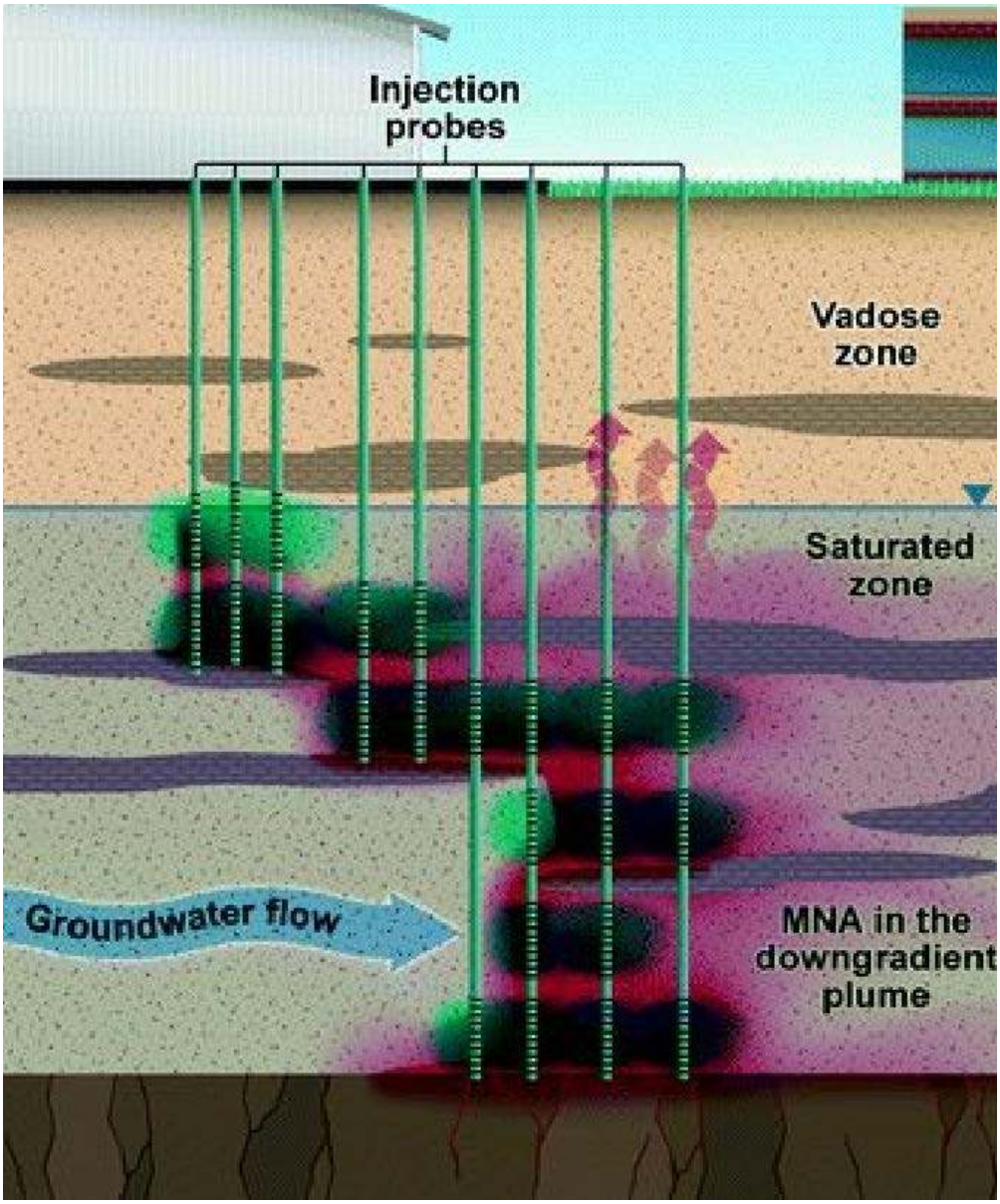

Figure 2. Illustration of ISCO to treat contaminated groundwater

To overcome the disadvantages of ISCO, an innovative technology called slow-release candle (SRC) has been developed (Ross et al., 2005; Lee et al., 2006, 2007, 2008; Christenson et al., 2016; Kambhu et al., 2012; 2017).

2.2. Slow-Release Candle

SRC takes a passive approach, where a controlled-release oxidant is inserted into the subsurface and allowed to dissolve and intercept the contaminant over many years. In the SRC, candle is made of a mixture of environmentally safe materials (such as wax) and oxidants. Instead of active injection of oxidants, slow-release candles gradually deliver the oxidants out of a candle by diffusion (i.e. concentration gradient) and semi-passively transport the oxidants to the surrounding area by groundwater flow (i.e. dispersion, advection, and diffusion). Compared to the traditional ISCO, SRC requires less labor, is easier to replace and has higher efficiency in some specific situations such as low permeability zones with lower cost. In recent years, various have been devoted to study various aspects of SRC technology, including components, formulation, types of candles, the types and activation methods of oxidants, release kinetics and release simulation, and treatment efficiency in the laboratory experiment and in the field.

There are two types of SRC: encapsulated systems and matrix systems. In the encapsulated system, oxidants are covered by coating materials like a core in a shell; while in the matrix system, oxidants are uniformly distributed in the matrix(E. S. Lee & Schwartz, 2007b). Although the coating techniques are being rapidly developed, the encapsulated system is typically limited by its duration and stability (E. S. Lee & Schwartz, 2007b). Here, we mainly focused on review of the research of the matrix system. In the matrix system, sodium/potassium permanganate and persulfate are two most widely encapsulated oxidants.

Bolar wax, piccolyte resin S115, epolene C-16, and paraffin wax are most widely used matric materials to encapsulate sodium/potassium permanganate. Release kinetics of such candles were extensively studied (M. Christenson, Kambhu, Reece, Comfort, & Brunner, 2016; Ross, Murdoch, Freedman, & Siegrist, 2005). Based on batch experiments, Ross investigated the release histories of 18 different formulations of permanganate SRC(Ross et al., 2005). Kambhu studied the influence of the formulation and geometry on the treatment efficiency (Kambhu, Comfort, Chokejaroenrat, & Sakulthaew, 2012). For the same formulation, Kambhu also tested the influence of geometry size. Based on unpublished data, she found that the release kinetics were very sensitive to the radius of a candle, but not to the height of a candle.

For a certain formulation and geometry, mathematical modeling and laboratory experiments were integrated to investigate and predict the release kinetic of oxidants. Lee conducted a column test to measure MnO_4^- release for a 20 day period , which was then fitted to a numerical model to obtain a best-matched diffusion coefficient in a rod shaped candle(E. S. Lee & Schwartz, 2007a). Based on the diffusion coefficient and basic candle parameters (e.g., mass of oxidants, radius and height of a candle), long term slow-release of a $KMnO_4$ candle was simulated over 1344 days (~3.7 yrs) which could treat a plume by releasing 500 g of MnO_4^- daily in average. In another similar study, Liang (C. Liang & Chen, 2017) measured the release of sodium persulfate candle and modified the numerical model by adding porosity into consideration. Based on the simulation, Liang found the minimum longevity of a persulfate rod was a function of candle dimensions (C. Liang & Chen, 2017). To optimize the release of a slow-release system, Lee developed a

generalized modeling approach which adjusted solubility of the oxidant, bulk diffusion coefficients, or initial loading of oxidant(E. S. Lee & Schwartz, 2007b) to satisfy the requirements of specific contaminants and location. Based on the simulation results, Lee illustrated a hybrid candle, which consists of an inner matrix system and outer encapsulation, which could provide a long-term constant release, with merits of easier SRC system design and lower costs compared to a traditional slow-release matrix candle (E. S. Lee & Schwartz, 2007b).

With the promising release rate and predictable longevity, Lee operated pilot scale flow tank experiments to characterize the slow-release permanganate barrier system. They also conducted a large flow-tank study to determine the efficacy of slow-release permanganate barrier system to treat dissolved TCE plume(B. S. Lee et al., 2009; E. S. Lee, Woo, et al., 2008). Experiments indicated that the slow-release permanganate barrier system was able to provide a persistent permanganate plume in natural sands with soil oxidant demands of 3.7-11 g MnO_4^-/kg and removed 74% of the TCE after three barriers for a plume with average concentration of 87 ppb. In addition, Christenson first applied the slow-release permanganate candles in the field and successfully reduced TCE concentrations to 32%-15% of the initial concentration after the first 15 months of treatment. The TCE concentration of site had 89% reduction after 5 years with yearly maintenance (M. D. Christenson, Kambhu, & Comfort, 2012; M. Christenson et al., 2016).

Comparing with sodium/potassium permanganate, persulfate was a relatively new oxidant applied in the ISCO, intending to overcome some limitations of permanganate.

Only a limited number of studies are devoted to study slow-release persulfate candles, which focus on the reaction kinetics for various contaminants and activation methods in the lab scale. Kambhu developed slow-release persulfate candle to treat BTEX and 1,4 dioxane contaminated water (Kambhu et al., 2012; Kambhu, Gren, Tang, Comfort, & Harris, 2017). Liang studied slow-release persulfate candles to treat tertiary-butyl ether (MTBE) contaminated groundwater (S. H. Liang, Kao, Kuo, Chen, & Yang, 2011). Chokejaroenrat conducted laboratory experiments to use persulfate candles to treat methyl orange (Chokejaroenrat et al., 2015). They found persulfate was effective to remediate some organic compounds while permanganate might not. In addition, persulfate might not decrease hydraulic conductivity by solid oxidant products.

2.3. Numerical Simulation of Slow-Release Candles for Remediation

Numerical simulation can be a very efficient and economical method to investigate the long term performance of a complicated slow-release system. Lee developed a 2-D model to couple oxidant release, transport, and reaction in a in situ remediation scenario using the controlled release of permanganate (E. S. Lee, Liu, Schwartz, Kim, & Ibaraki, 2008). In this work, advection dispersion was coupled with a first order decay reaction. Advection was accounted for by a deterministic particle motion approach, and dispersion was accounted for by adding a random component to the particle motion. Simulation results matched well with the previous pilot experiment. In addition, Lee investigated the lateral spreading needed to fill the gaps of oxidant's plume. He proposed to use doublet wells to overcome the lateral spreading limits, which is a cost-effective solution.

Although Lee's model provided a way to further investigate the slow-release system with basic physics (i.e. 2D simulation, constant oxidant release, w/o dispersion, and constant decay as reaction rate), some over simplifications could lead to bad judgments. For instance, the assumption of constant release rate is not realistic, which would underestimate the initial treatment and overestimate the later treatment. Assumption of a constant decay for the reaction is not applicable to common treatment reaction. Various studies have shown that oxidant release rates are not constant, typically higher initially and gradually reduced(Kambhu, Comfort, Chokejaroenrat, & Sakulthaew, 2012; E. S. Lee, Woo, et al., 2008; Roseman & Higuchi, 1970). In general, a much more comprehensive model, considering realistic release kinetics, reactions, and aquifer properties is needed to optimize the system design.

References

Chokejaroenrat, C., Sakulthaew, C., Satapanajaru, T., Tikhamram, T., Pho-Ong, A., & Mulseesuk, T. (2015). Treating Methyl Orange in a Two-Dimensional Flow Tank by *In Situ* Chemical Oxidation Using Slow-Release Persulfate Activated with Zero-Valent Iron. *Environmental Engineering Science*, *32*(12), 1007–1015. https://doi.org/10.1089/ees.2015.0110

Christenson, M. D., Kambhu, A., & Comfort, S. D. (2012). Using slow-release permanganate candles to remove TCE from a low permeable aquifer at a former landfill. *Chemosphere*, *89*(6), 680–687. https://doi.org/10.1016/j.chemosphere.2012.06.009

Christenson, M., Kambhu, A., Reece, J., Comfort, S., & Brunner, L. (2016). A five-year performance review of field-scale, Slow-release permanganate candles with recommendations for second-generation improvements. *Chemosphere*, *150*, 239–247. https://doi.org/10.1016/j.chemosphere.2016.01.125

EPA. (2017). National Primary Drinking Water Regulations. Retrieved from https://www.epa.gov/ground-water-and-drinking-water/national-primary-drinking-water-regulations

EPA, U. S. (2014). In Situ Chemical Oxidation. Retrieved from http://www.epa.gov/ada/gw/isco.html

Kambhu, A., Comfort, S., Chokejaroenrat, C., & Sakulthaew, C. (2012). Developing slow-release persulfate candles to treat BTEX contaminated groundwater. *Chemosphere*, *89*(6), 656–664. https://doi.org/10.1016/j.chemosphere.2012.06.004

Kambhu, A., Gren, M., Tang, W., Comfort, S., & Harris, C. E. (2017). Remediating 1,4-dioxane-contaminated water with slow-release persulfate and zerovalent iron. *Chemosphere*, *175*, 170–177. https://doi.org/10.1016/j.chemosphere.2017.02.044

Lee, B. S., Kim, J. H., Lee, K. C., Kim, Y. Bin, Schwartz, F. W., Lee, E. S., … Lee, M. K. (2009). Efficacy of controlled-release KMnO4 (CRP) for controlling dissolved TCE plume in groundwater: A large flow-tank study. *Chemosphere*, *74*(6), 745–750. https://doi.org/10.1016/j.chemosphere.2008.10.062

Lee, E. S., Liu, G., Schwartz, F. W., Kim, Y., & Ibaraki, M. (2008). Model-based evaluation of controlled-release systems in the remediation of dissolved plumes in

groundwater. *Chemosphere*, *72*(2), 165–173. https://doi.org/10.1016/j.chemosphere.2008.01.078

Lee, E. S., & Schwartz, F. W. (2007a). Characteristics and applications of controlled-release KMnO4 for groundwater remediation. *Chemosphere*, *66*(11), 2058–2066. https://doi.org/10.1016/j.chemosphere.2006.09.093

Lee, E. S., & Schwartz, F. W. (2007b). Characterization and optimization of long-term controlled release system for groundwater remediation: A generalized modeling approach. *Chemosphere*, *69*(2), 247–253. https://doi.org/10.1016/j.chemosphere.2007.04.037

Lee, E. S., Woo, N. C., Schwartz, F. W., Lee, B. S., Lee, K. C., Woo, M. H., … Kim, H. K. (2008). Characterization of controlled-release KMnO4 (CRP) barrier system for groundwater remediation: A pilot-scale flow-tank study. *Chemosphere*, *71*(5), 902–910. https://doi.org/10.1016/j.chemosphere.2007.11.037

Liang, C., & Chen, C. Y. (2017). Characterization of a Sodium Persulfate Sustained Release Rod for in Situ Chemical Oxidation Groundwater Remediation. *Industrial and Engineering Chemistry Research*, *56*(18), 5271–5276. https://doi.org/10.1021/acs.iecr.7b00082

Liang, S. H., Kao, C. M., Kuo, Y. C., Chen, K. F., & Yang, B. M. (2011). In situ oxidation of petroleum-hydrocarbon contaminated groundwater using passive ISCO system. *Water Research*, *45*(8), 2496–2506. https://doi.org/10.1016/j.watres.2011.02.005

Liu, Y., Chen, J., Wang, Q., Shi, L., & Shi, Y. (2017). The principle and effect of transfer agent for the removal of PCE during in situ chemical oxidation. *Environmental Science and Pollution Research*, *24*(26), 21011–21023. https://doi.org/10.1007/s11356-017-9411-9

Roseman, T. J., & Higuchi, W. I. (1970). Release of Medroxyprogesterone Acetate from a Silicone Polymer. *Journal of Pharmaceutical Sciences*, *59*(3), 353–357.

Ross, C., Murdoch, L. C., Freedman, D. L., & Siegrist, R. L. (2005). Characteristics of Potassium Permanganate Encapsulated in Polymer. *Journal of Environmental Engineering*, *131*(8), 1203–1211. https://doi.org/10.1061/(ASCE)0733-9372(2005)131:8(1203)

Thepsithar, P., & Roberts, E. P. L. (2006). Removal of phenol from contaminated kaolin using electrokinetically enhanced in situ chemical oxidation. *Environmental Science and Technology*, *40*(19), 6098–6103. https://doi.org/10.1021/es060883f

Wiesner, M. R., Grant, M. C., & Hutchins, S. R. (1996). Reduced permeability in groundwater remediation systems: Role of mobilized colloids and injected chemicals. *Environmental Science and Technology*, *30*(11), 3184–3191. https://doi.org/10.1021/es950784u

Chapter 3

Field Site Description and Analysis

Recently, Airlift Environmental (Lincoln, NE) has installed persulfate candles into the Textron site, a field site contaminated with BTEX. Although the eventual purpose of the thesis is not to simulate the field site, we analyzed the field site to gather realistic site conditions to form the base parameters for model development. In this Chapter, a 3-D soil lithology model was developed by integrating the available well boring data. The water table of the site was analyzed based on monitoring data from the monitoring wells on the site. Rough estimation of groundwater flow velocity of the site was developed based on Darcy's Law.

3.1. General Site Information

The Textron site is located at 2100 Vine Street in Lincoln, NE and encompasses approximately 15 acres. This site was an old factory that manufactured products such as golf carts and engines over a period of 100 years. Figure 3 presents the general location of the Textron site (i.e. the orange irregular pentagon), which is bound by Vine Street on the south, Antelope Valley Parkway on the west, the railroad on the north, and 22nd Street on the east.

Figure 3. Geographic location of the Textron site

A previous investigation by Terracon Consultants, Inc. indicated that the groundwater under the site has been contaminated with chlorinated solvents and petroleum compounds. Detected petroleum compounds include benzene and hexane. Detected VOCs include 1,1-DCE, 1,1-DCA, cis 1,2-DCE, TCE, PCE, vinyl chloride, trans 1,2-DCE and 1,1,2,2-PCE. Most of these contaminants were detected in the mid-east part of the site. Eight monitoring wells were installed in the site to monitor contaminant concentration. The locations of the wells are noted in the Figure 4. Figure 4 is a digitized map developed using AutoCAD.

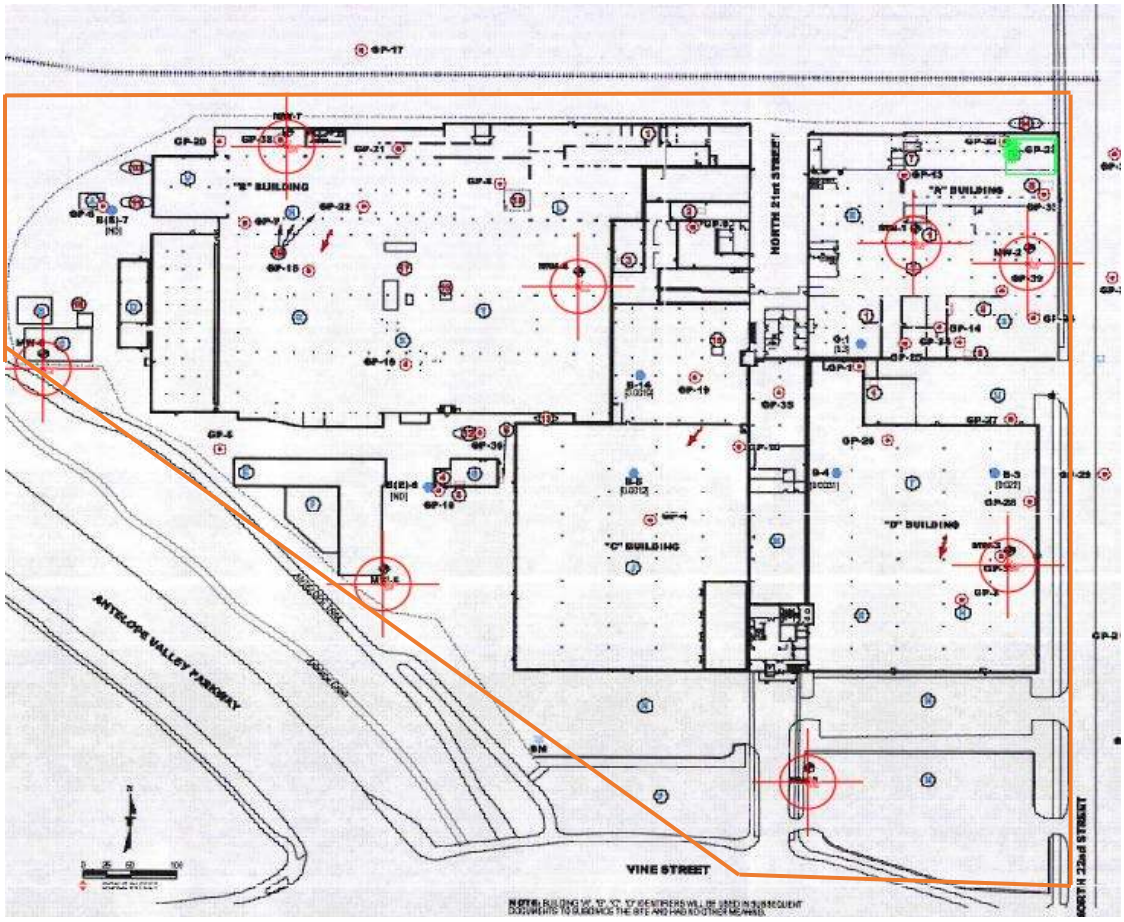

Figure 4. Site diagram with horizontal borders, eight monitoring wells, and the test area.

To evaluate the efficiency of slow release candles developed by Airlift Inc., a small area in the top right corner of the site (shown in Figure 4 as a green rectangle) was further investigated. BTEX were detected in the test area. Figure 5 provides the contaminant concentration distribution map in the test area. As shown in the map, all contaminants have higher concentration in the upper-left of the test area.

21 wells to place the candles were assigned in the upper-left of the test area as shown in Figure 6. There were 6 rows of wells with an interval of 3 ft between each row.

For each row, there were 3 or 4 wells with 3 ft. interval between two wells. The wells were arranged so that the wells in the next row positioned in the middle of two wells in the previous row (Figure 6).

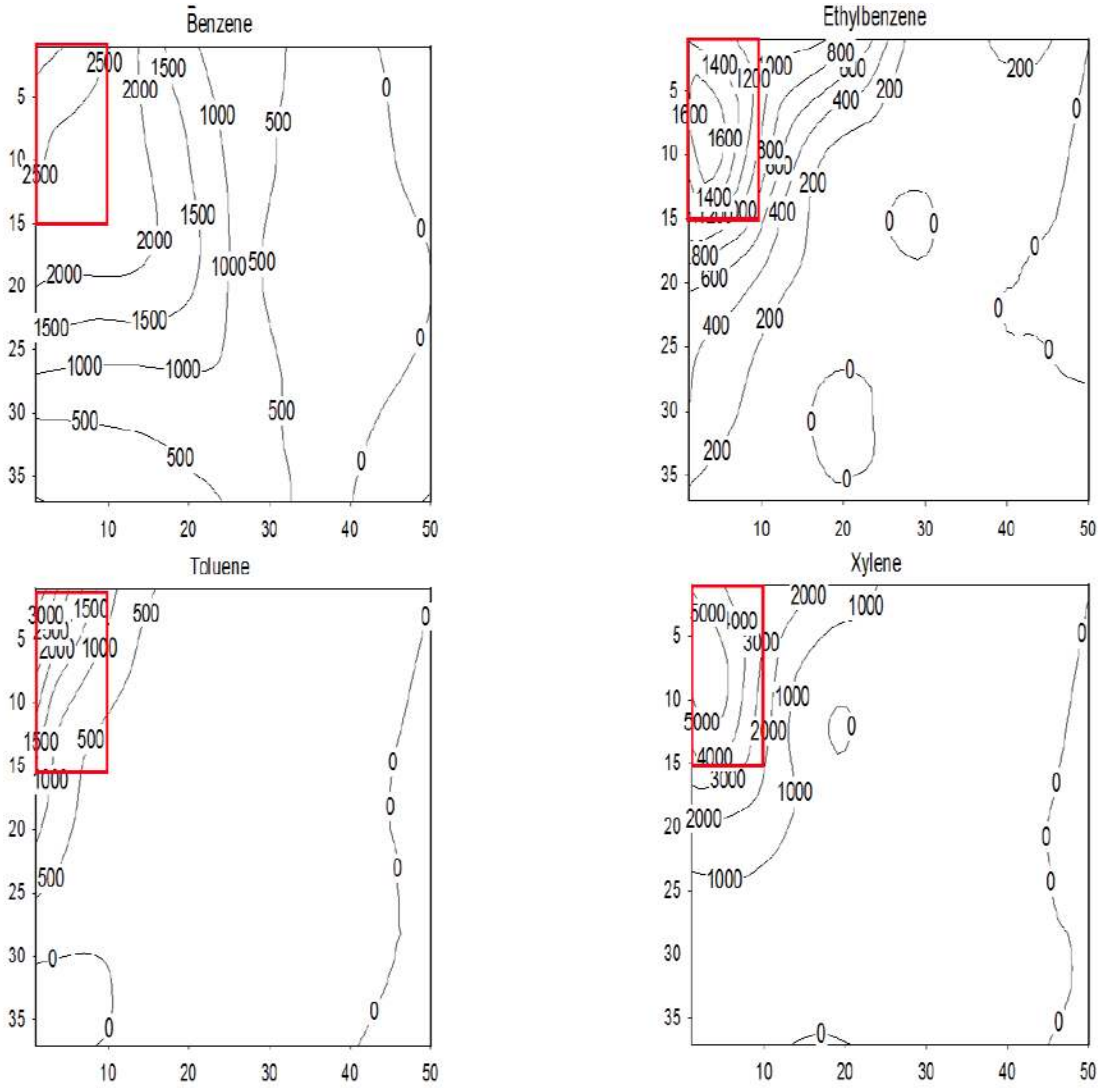

Figure 5. Main contaminants concentration maps in the test area (provided by the Airlift)

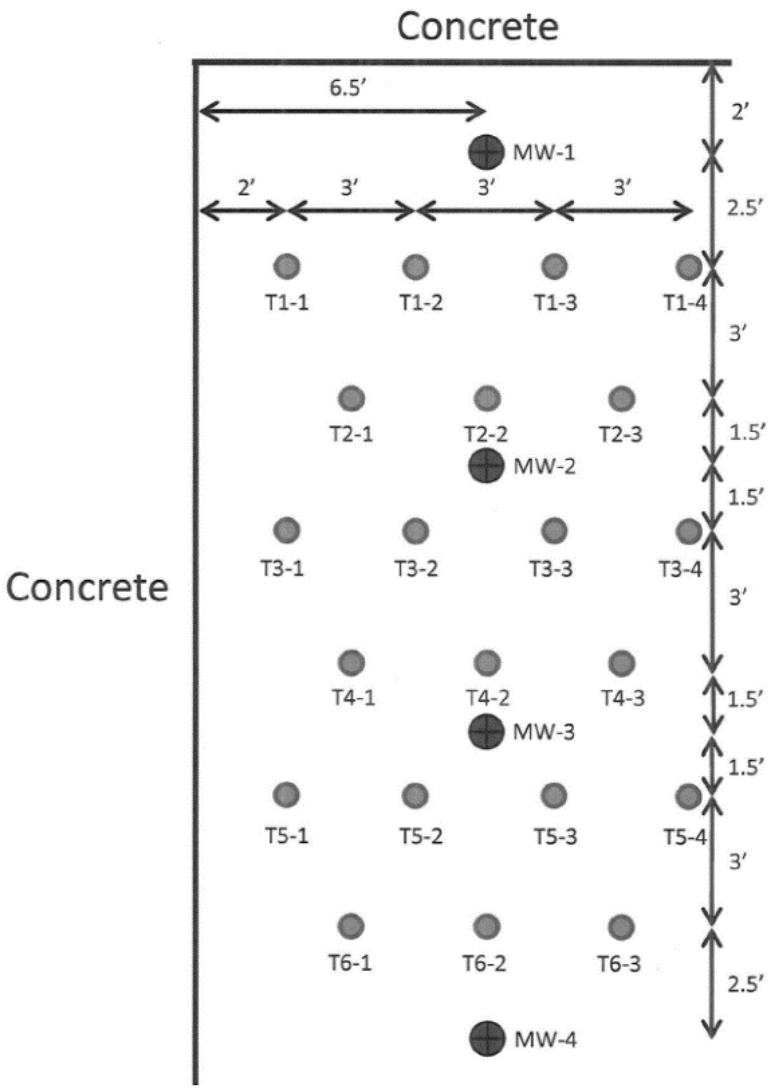

Figure 6. The treatment grid in the test area.

3.2. Lithology Model

Very little information was available on the soil properties of the site. Soil lithology information was first based on the well boring information. As illustrated in Figure 4, eight monitoring wells were installed across the site. During the well

installation, soil samples for each depth interval from the well boring were visually analyzed and classified. A limited soil profile for the monitoring well No. 1 was shown in Figure 7 as an example. Vertical soil profiles in eight monitoring wells mainly consist of two soil types, i.e. fat clay and fine sand.

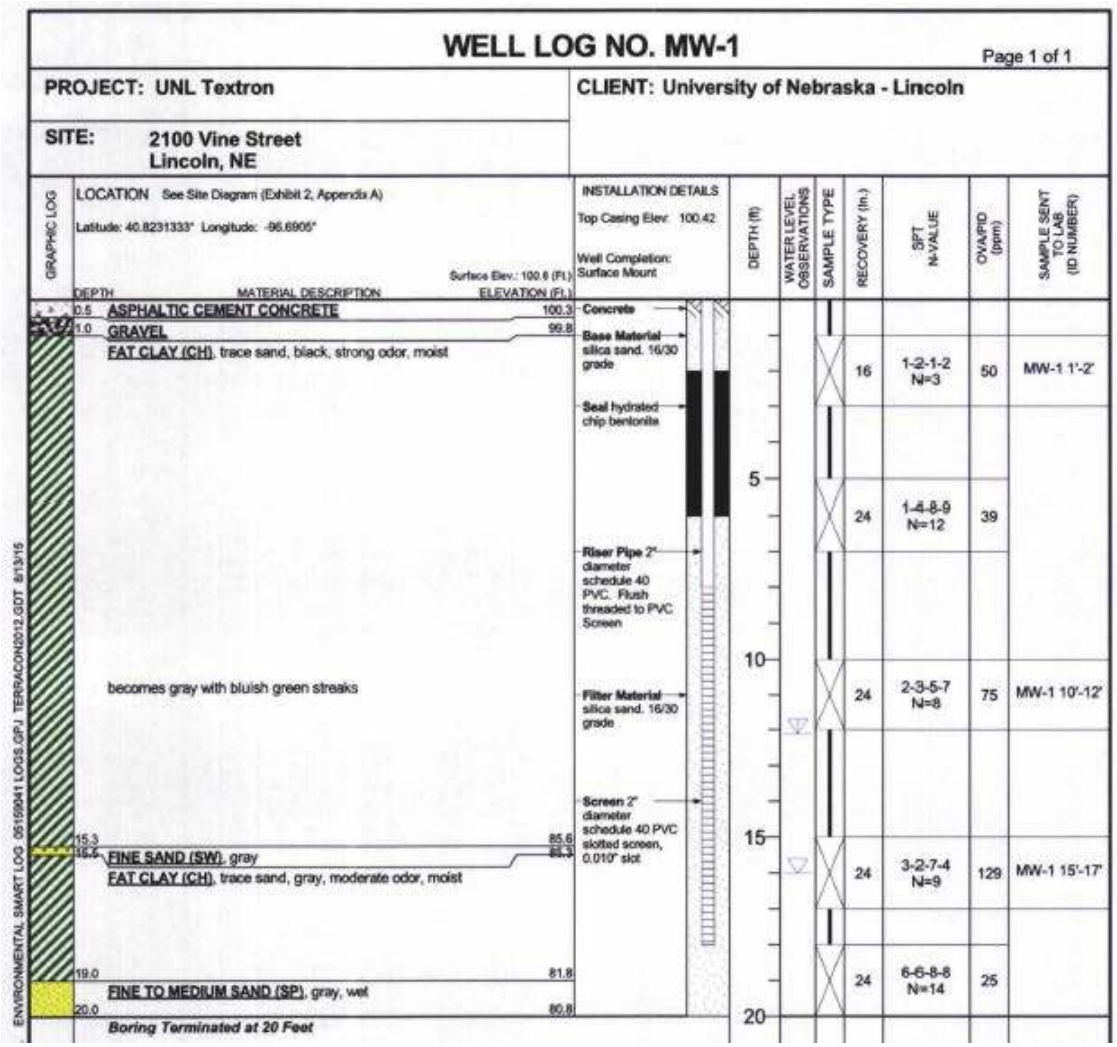

Figure 7. Limited soil profile for the monitoring well No. 1

Because the average depth of eight monitoring wells was about 20 ft below the ground surface, the vertical soil profiling was limited to the boring depth. To advance the

soil profile information, we need to determine the depth of the bedrock and the soil types between the bottom of borehole and the bedrock. According to *Soil and Groundwater Assessment Report*, additional three borings indicated the bedrock was approximately 85 ft below the ground surface(Terracon Consultants, 2016). To determine the soil types below 20 ft of the ground surface, we used the information from a test hole (i.e. No. 2-A-50) in the Nebraska Statewide Test-hole Database that is the closest to the site (Conservation and Survey Division, School of Natural Resources, & University of Nebraska, 2017). According to this test hole information, fine sand was the major soil type from 20 ft bgs (below ground surface) to 85 ft bgs. We assumed the extended soil profiling in the Textron site was same as that in the test hole.

A three-dimensional solid lithology model was developed using RockWorks 17, a widely used software program for creating logs and cross sections, geological models and general geology diagrams for the environmental, geotechnical, mining, and petroleum industries. Model dimensions were based on the horizontal geometry and the vertical soil profiling. The horizontal surface has the maximum dimension of 1100 ft and 1106 ft in the x and y direction, respectively. The vertical depth on the z direction was 85 ft. Figure 8 illustrated the final lithology model of the Textron site developed by Rockworks 17. As shown in the Figure 8, the site has a very distinctive two-layer soil lithology. The fat clay is located on the top of the fine sand, with an average depth of about 20 ft. The average depth of the fine sand layer is 65.5 ft, which is approximately five times of that of the fat clay. Each type of soil has its own typical hydraulic conductivities. According to Natural Resources Conservation Service, average hydraulic conductivity for fat clay is 9.14 E-7

m/s, and that for fine sand is 9.17×10^{-5} m/s (Natural Resources Conservation Service, n.d.). These typical values of hydraulic conductivity were associated with soil types in the lithology model.

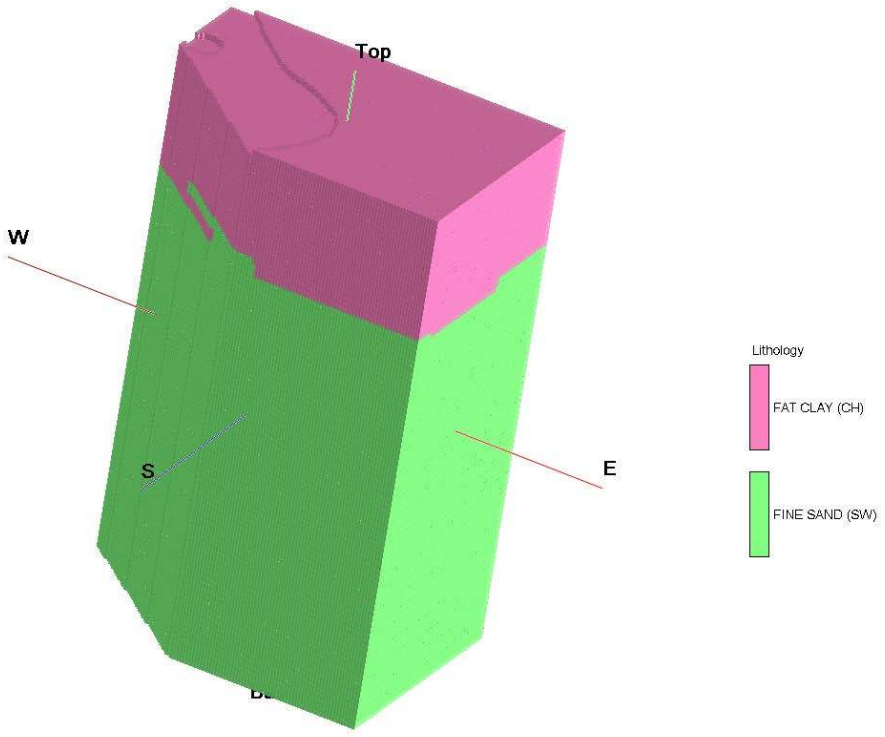

Figure 8. The lithology model of the Textron site.

3.3. Groundwater Level

To estimate the groundwater level in the test area, we used water level data from 4 recently installed monitoring wells in the test area together with the eight monitoring wells in the larger area. The groundwater level in the whole area was obtained by interpolating the 12 monitoring wells using a hybrid of inverse distance and kriging

algorithms in RockWorks 17. Figure 9 presented the groundwater table of the Textron site in a blue pentagon and that of the test area in a red rectangle. Figure 10 was a closer look of the groundwater elevation for the test area. As shown in the Figure 10, the groundwater level in the test area is relatively flat at around 87 ft.

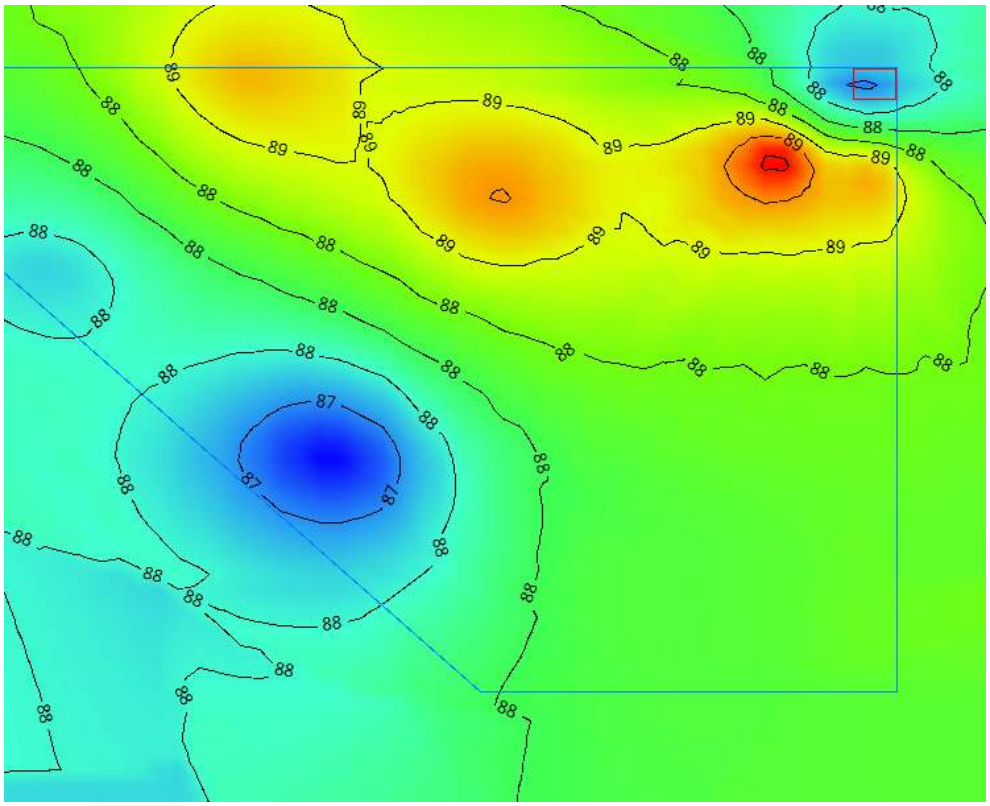

Figure 9. Groundwater table for the Textron site.

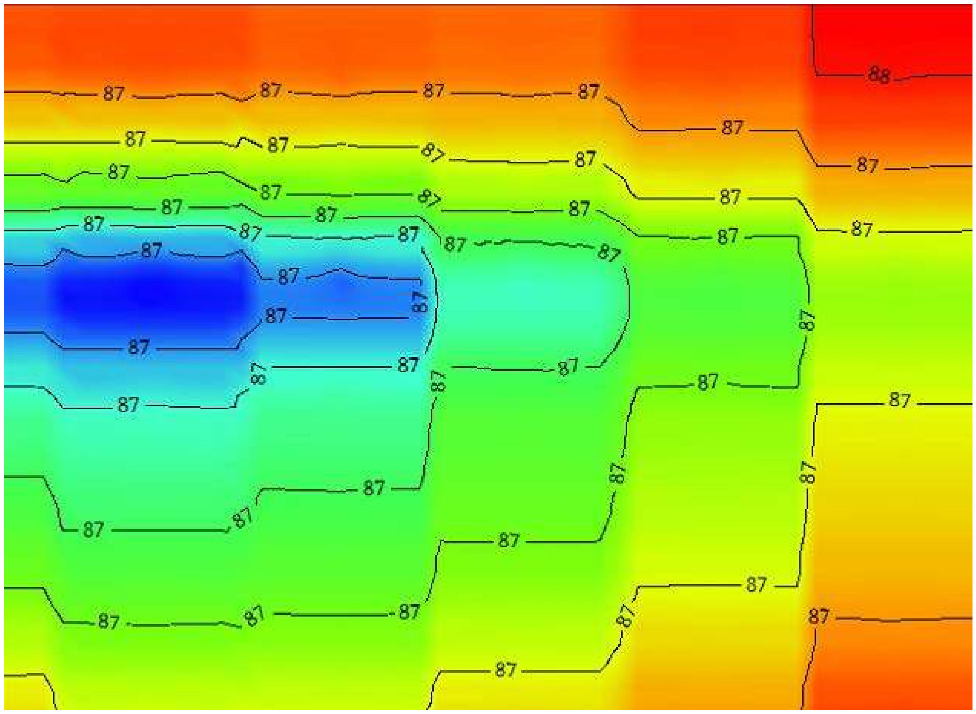

Figure 10. Groundwater table for the Test area.

3.4. Groundwater Velocity

Groundwater velocity is an essential and critical parameter for site characterization. Here we used AutoCAD Civil 3D and Excel to provide a rough estimation of groundwater velocity. A brief summary of Darcy velocity calculation procedure was presented below.

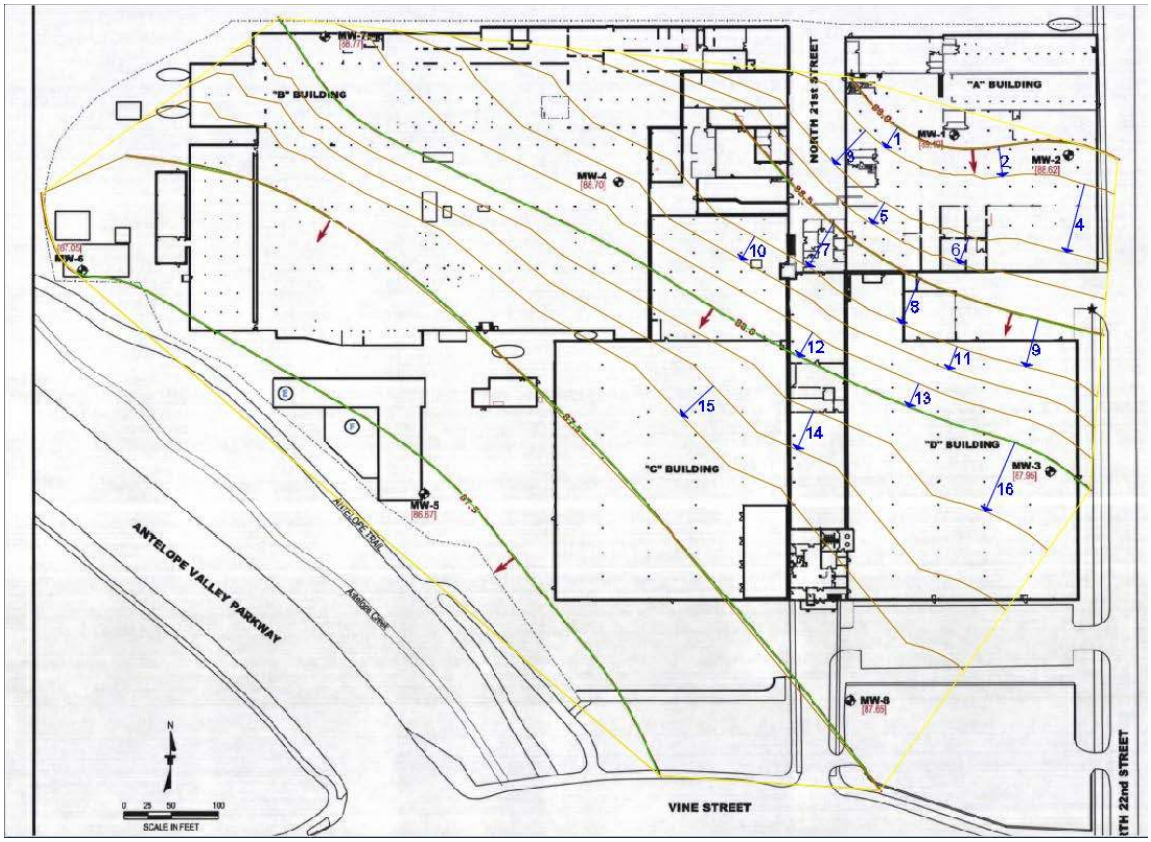

Figure 11. Groundwater surface (blue colored numbers denote the locations used for groundwater velocity calculation)

First, the groundwater elevation contour map from August 19, 2015, in the Terracon report was inserted into AutoCAD Civil 3D (Terracon Consultants, 2016). As shown in Figure 11, the area of analysis was noted by a light yellow polygon. Polylines were then drawn to match with existing contours, and values of groundwater elevation were assigned to each contour curve. Using the 'create a surface' function in AutoCAD Civil 3D, a groundwater surface can be created. A 3D view of the groundwater surface is provided in Figure 12. On this surface, location and water head data for each point can be

easily obtainable. New contours with smaller intervals were generated with higher accuracy.

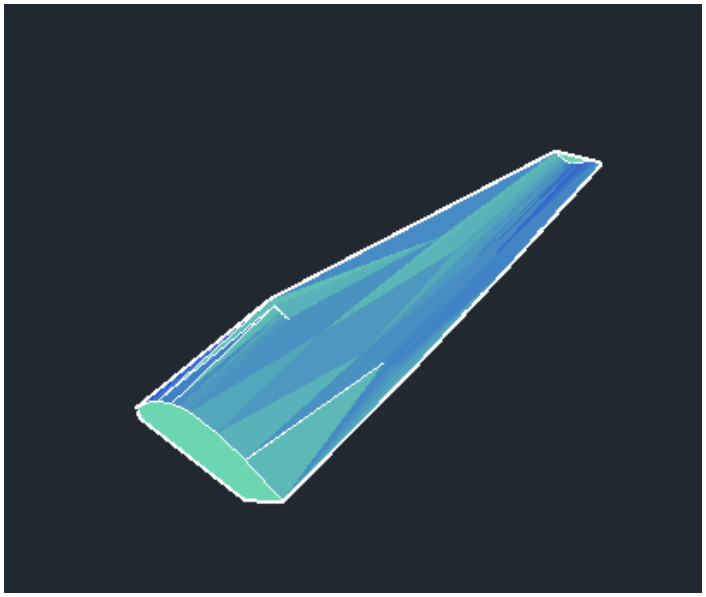

Figure 12. 3D Groundwater surface

Groundwater flow velocity estimation was focused on a smaller target zone in the upper right part of the site, where groundwater level contours are well established. Sixteen locations were chosen to calculate Darcy velocity in the target zone. The direction of groundwater velocity, which is perpendicular to water level contours, were denoted in the Figure 11 using blue arrows and numbers.

According to Darcy's law as expressed in Eq. 1, groundwater velocity is proportional to water head gradient along the travel distance.

$$q = -K\frac{\Delta h}{\Delta x} \qquad \text{(Eq. 1)}$$

Where, q is the Darcy velocity (m/s); K is the hydraulic conductivity (m/s); Δh is the head difference (m); Δx is the distance difference (m).

At each calculation point, head gradient was estimated as the ratio of head difference of two adjacent equipotential lines and the distance between them. According to the site characterization, fat sand was found in the target zone. Therefore, a hydraulic conductivity of 5 m/day was used based on the recommendation from Natural Resources Conservation Service (Natural Resources Conservation Service, n.d.). Based on the calculation, groundwater flow was generally very uniform. Darcy velocities at the sixteen locations of calculation are in the range of 0.260 – 0.262 ft/day. The average Darcy velocity in the target zone is around 0.2619 ft/day. Assuming a porosity of 0.3, the actual groundwater velocity of the site is about 0.87 ft/day.

References

Conservation and Survey Division, School of Natural Resources, & University of Nebraska. (2017). Nebraska Statewide Test-hole Database. Retrieved from http://snr.unl.edu/data/geologysoils/NebraskaTestHole/NebraskaTestHoleIntro.aspx

Natural Resources Conservation Service. (n.d.). Saturated Hydraulic Conductivity. Retrieved from https://www.nrcs.usda.gov/wps/portal/nrcs/detail/soils/survey/office/ssr10/tr/?cid=nrcs144p2_074846

Terracon Consultants. (2016). *Soil and Groundwater Assessment Report*.

Chapter 4

Quantifying Sodium Persulfate Release Kinetics

4.1. Conceptual Model

A sodium persulfate candle is a mixture of wax and sodium persulfate powder. The concentration of the sodium persulfate in the candle is much higher than the solubility of sodium persulfate in the water. In the flowing water system, the sodium persulfate candle gradually delivers sodium persulfate into water and keeps its original shape. Dissolution-diffusion is the main driving mechanism to release the sodium persulfate from the candle since various flowrates in the outside of candles result in similar longevity (Liang & Chen, 2017)

Assuming the sodium persulfate distributes homogeneously in the candle, and the diffusion coefficient is a constant; an analytical model developed by Roseman and Higuchi can be adapted to quantify the release kinetics of sodium persulfate (Roseman & Higuchi, 1970). A hypothetical diagram for the matrix-boundary diffusion model is shown in the Figure 13.

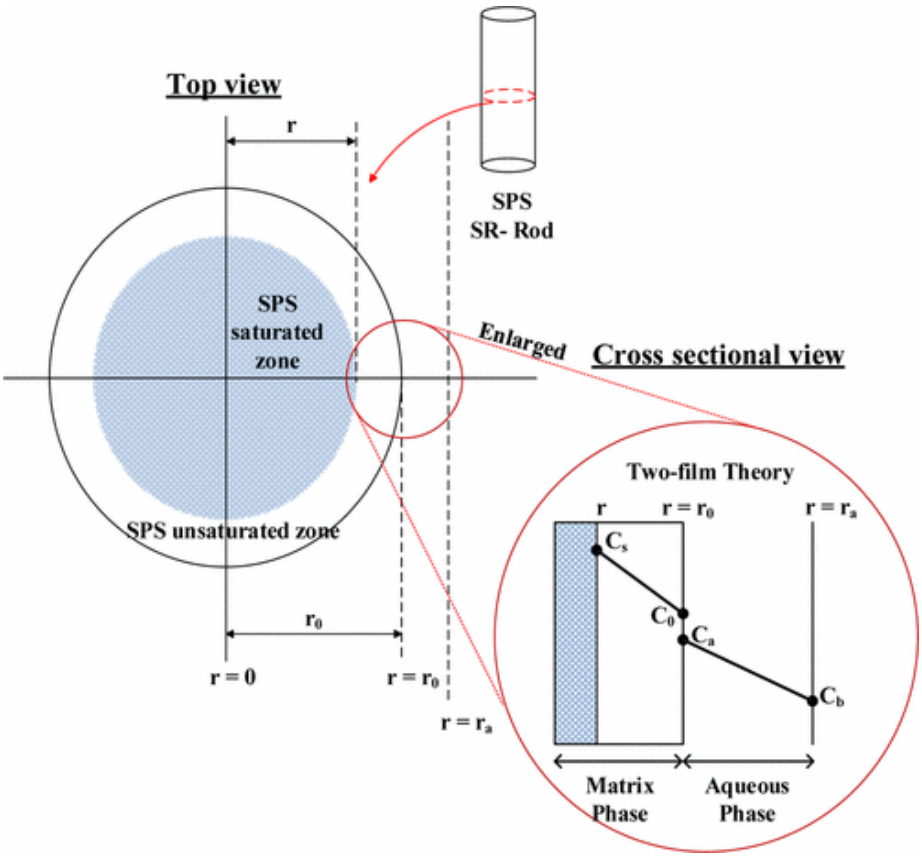

Figure 13. Hypothetical diagram for the matrix-boundary diffusion model for the release of SPS from the sodium persulfate candle.

From: **Characterization of a Sodium Persulfate Sustained Release Rod for in Situ Chemical Oxidation Groundwater Remediation**

In Figure 13, the shaded area represents the sodium persulfate saturated zone and the blank area represents depletion zone of sodium persulfate. Initially, the candle is fully sodium persulfate saturated and has a radius of r_0. When sodium persulfate gradually diffused through the candle, the radius of saturated zone (i.e. r) decreases until it reaches zero when all sodium persulfate is depleted. Assuming that the sodium persulfate in the

bulk fluid will be moved instantly due to advection, dispersion and reaction, the concentration of the sodium persulfate is zero (i.e.$C_b = 0$) at $r = r_a$.

The rate of sodium persulfate across the surface area of the cylinder is given by Fick's law,

$$\frac{dM}{dt} = 2\pi r h D_e \frac{dC}{dr} \quad \text{(Eq. 2)}$$

Where M is the mass of sodium persulfate depleted (g); t is the duration of the depletion (day); h is the height of the candle (cm); r is the radius of the saturated zone (cm); D_e is the effective diffusion coefficient (cm^2/day); C is the concentration of sodium persulfate in the aqueous phase (g/cm^3).

When Eq.2 satisfies boundary conditions, $C = C_s$ at r = r and $C = C_0$ at $r = r_0$ from Figure 13, the solution is:

$$\frac{D_e C_s t}{A} = \frac{r^2}{2} \ln \frac{r}{r_0} + \frac{1}{4}({r_0}^2 - r^2) \quad \text{(Eq. 3)}$$

and

$$M = \pi h A({r_0}^2 - r^2) \quad \text{(Eq. 4)}$$

Where C_s is the solubility of sodium persulfate in the water at 20 °C (556 g/L); r_0 is the initial radius of a candle (cm); A is the concentration of the persulfate in the matrix (g/cm^3).

Combining Eq.3 and Eq.4 yields a plot about accumulative mass of sodium persulfate over time. Release rate is then available by mass differences over small time periods.

4.2. Analyzing Lab and Field Data to Predict the Release Rate of Sodium Persulfate in the Field

4.2.1. Lab Data

To quantify persulfate release rates, Kambhu conducted a laboratory experiment with sodium persulfate candles(Kambhu, Comfort, Chokejaroenrat, & Sakulthaew, 2012). 0.5-inch diameter candles were submerged in 250-mL flasks containing 200 mL water. Sub-samples via pipette were collected intensively at the beginning and cursorily until the end and colormetrically analyzed. Accumulative mass of sodium persulfate over time data was recorded (Figure 14).

Roseman model (Eqs 3 and 4) was used fit the laboratory data by adjusting the effective diffusion coefficient (D_e). The criteria of fitting include (1) minimize the difference between simulated and measured mass release over time; and (2) minimize the difference between simulated and measured life time of the candle.

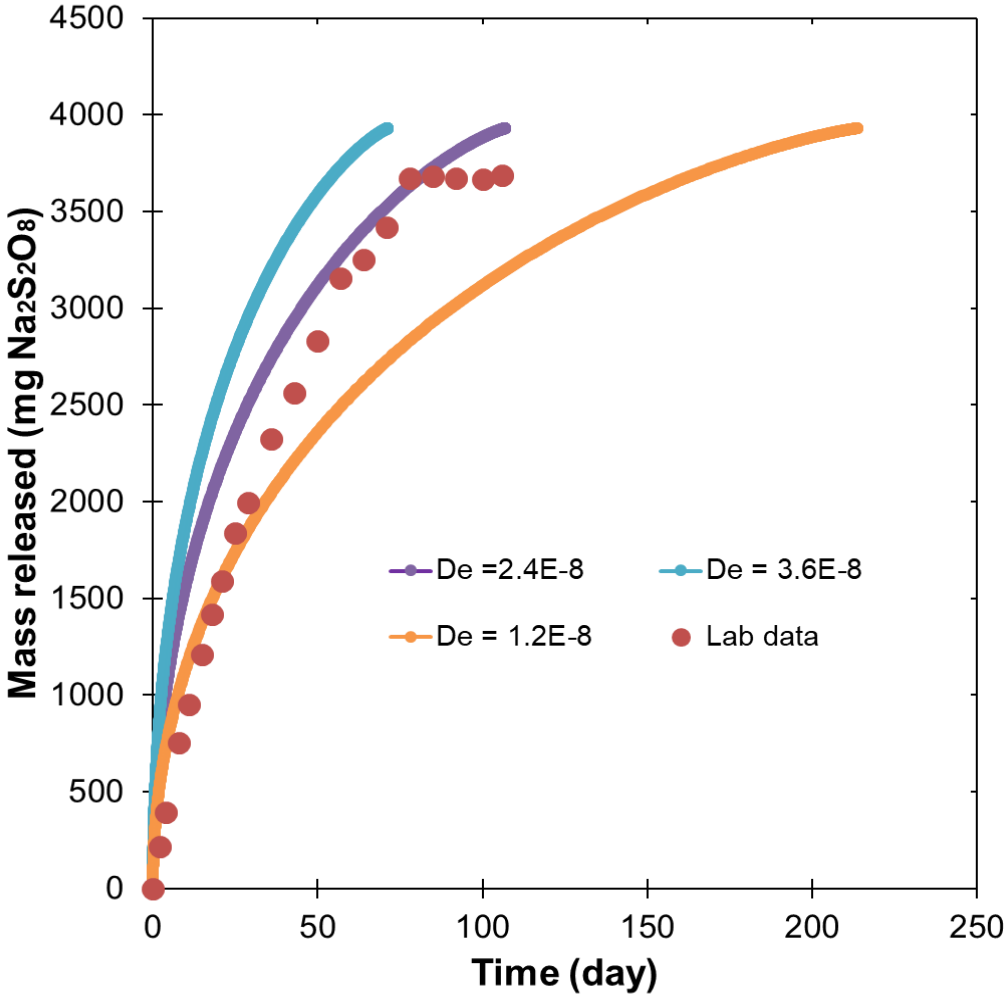

Figure 14. Cumulative Sodium persulfate mass release from lab experiment and simulations with different effective diffusion coefficient

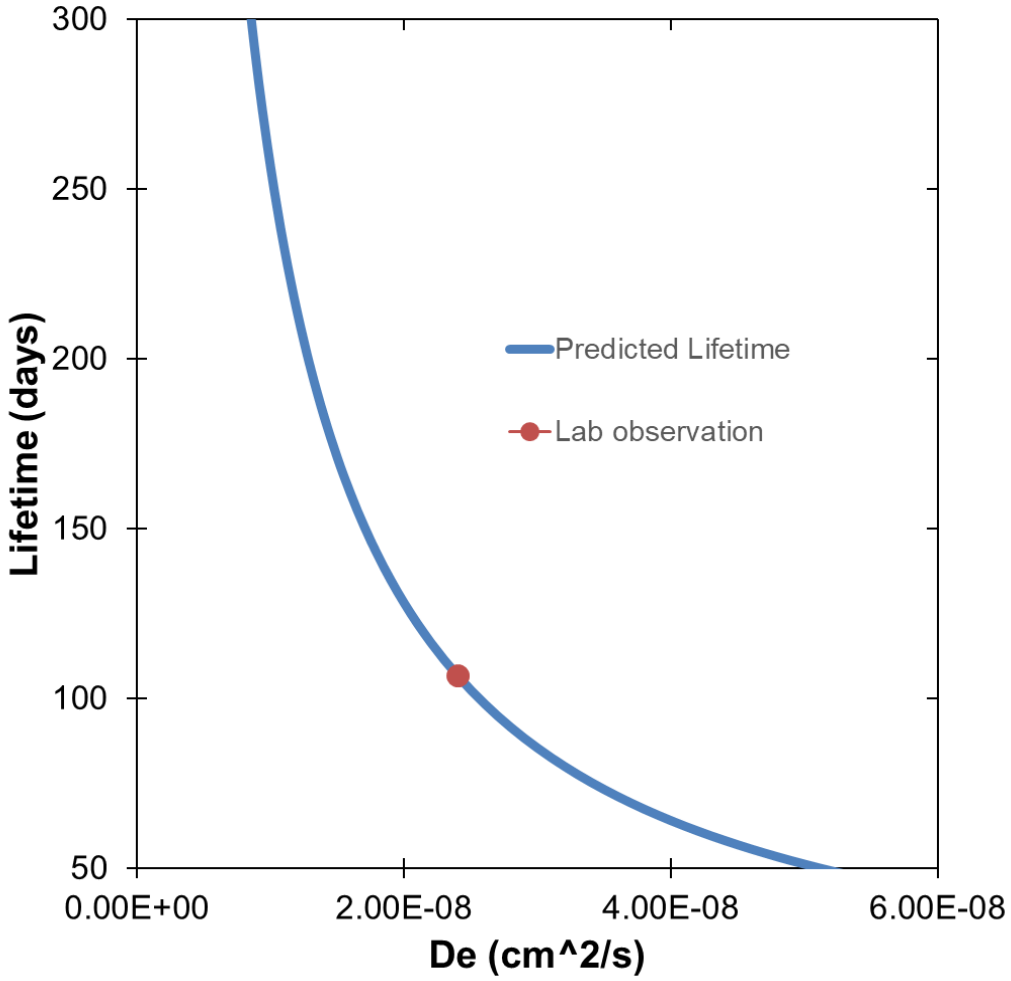

Figure 15. Predicted lifetime of lab candles with different diffusion coefficient

Simulated accumulative sodium persulfate mass over time with different effective diffusion coefficient and lab data were shown in Figure 14. Figure 15 presents simulated lifetime of lab candles as a function of effective diffusion coefficient. Figure 14 showed the sensitivity analysis of De. Lifetime of the candles decreases with the increasing effective diffusion coefficient. Since the mass of sodium persulfate is fixed, the release rates are proportional to the effective diffusion coefficient. As shown in Figure 14 and 15,

an effective diffusion coefficient of 2.4×10^{-8} cm^2/s provides reasonably match (i.e. R^2 = 0.9729) with both time series mass release data and the lifetime of candle.

4.2.2. Scaling from Lab to Field

Lab release data was obtained using 0.5-inch diameter candles with lengths of 1 inch. The sodium persulfate candle in the field was 1-inch diameter and 12 inch long. In the field, sodium persulfate candles and iron candles were packed on top of each other in candle casings, as shown in Figure 16. One inch long of iron candles were packed between every feet of persulfate candles. In a casing of 5 feet long, 53 inches of persulfate candles and 5 inches of iron candles were packed. Candles are located at 10 feet from the bottom of the casing, and the top casing is empty.

For simplification, we assumed persulfate is instantaneously fully activated by the iron and all candles are represented as a big candle. In converting the lab data to field data, we assume that diffusion coefficient obtained from the lab data was remained the same in the field. Eq.3 and Eq.4 with field candle characteristics (i.e. radius of the candle, mass of sodium persulfate, and height of the candle) yields the accumulative mass of sodium persulfate over time. Predicted release rate in the field is then available by mass differences over small time periods （Figure 17）. Assuming the release rate per surface area is same for the big candle and one field-size candle, the release rate over a big candle is then quantified.

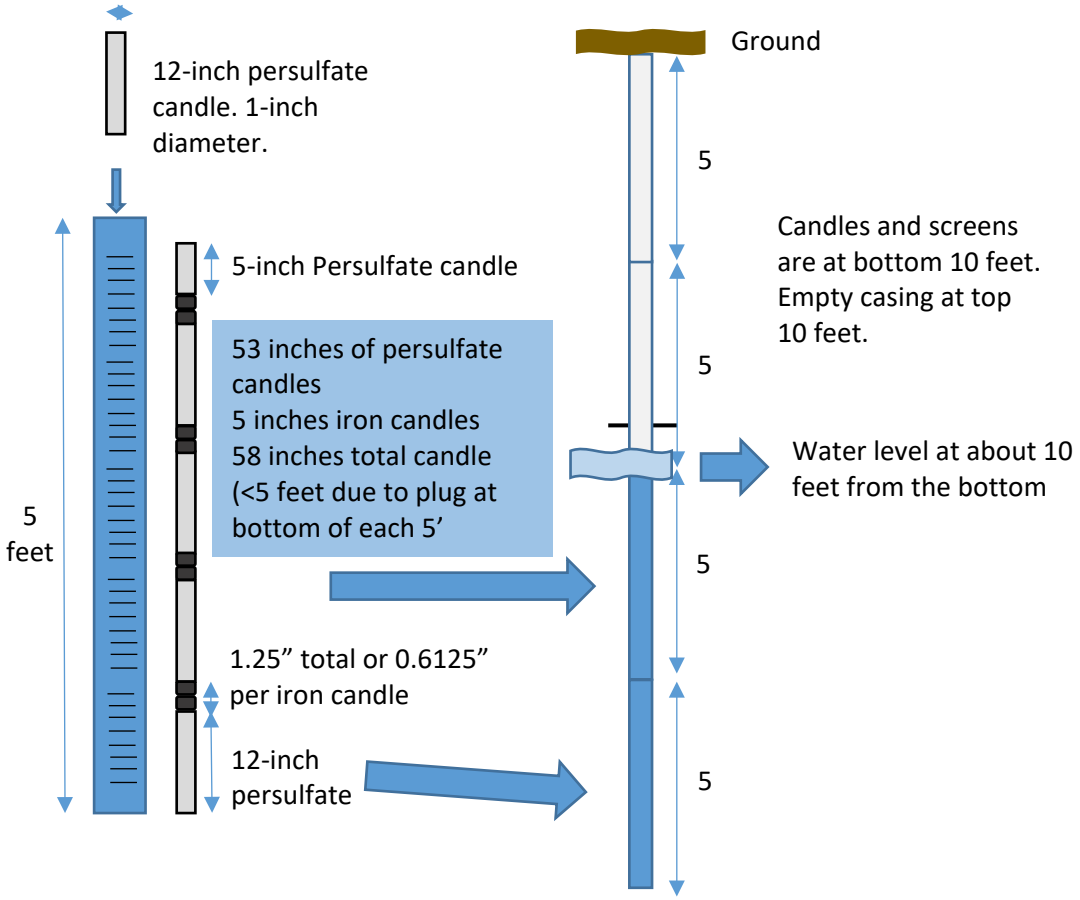

Figure 16. Diagram of field candles' settlement (provided by Airlift)

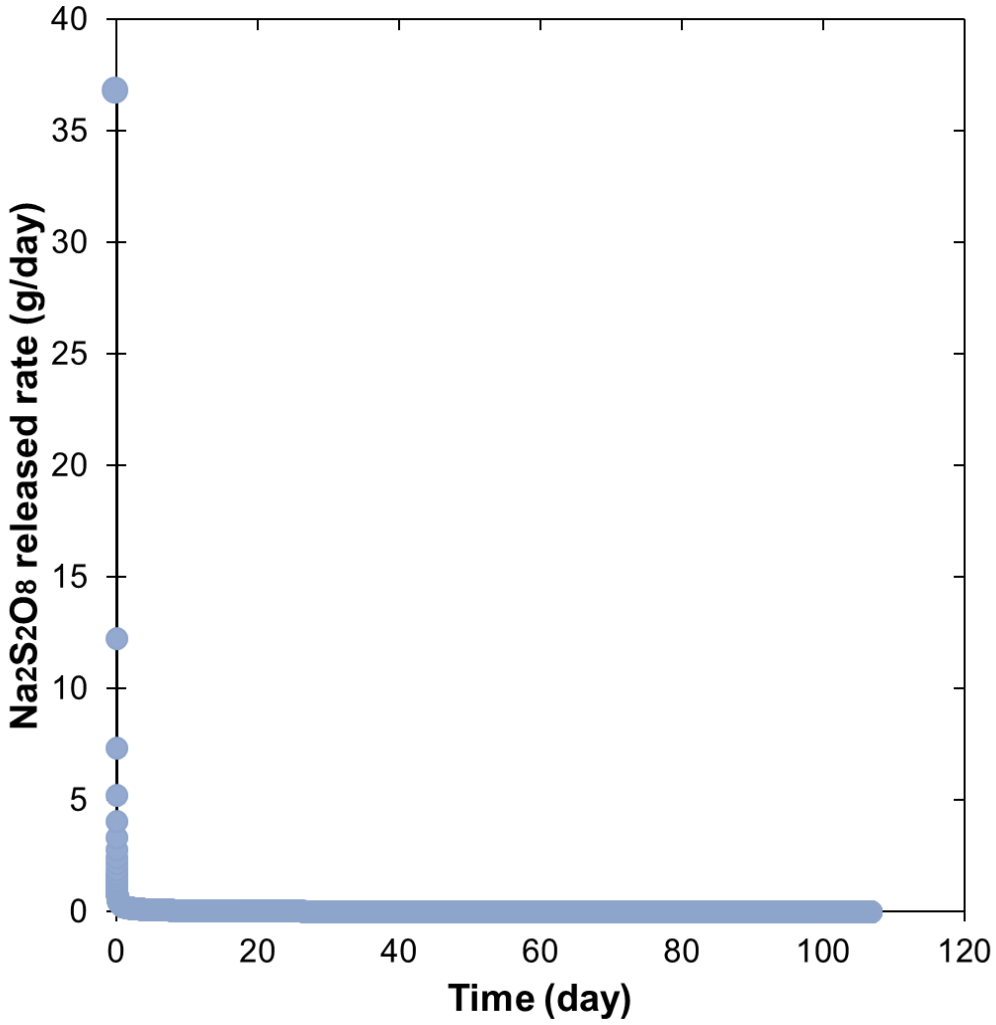

Figure 17. Simulated sodium persulfate release rate over time with an effective diffusion coefficient of $2.4 \times 10^{-8}\ cm^2/s$

4.3. Field Release Data

To remediate the targeted contaminants, 1-inch diameter sodium persulfate candles were placed in the Textron site in a same configuration as described in Figure 16. James Reece, an environmental restoration technician in the Airlift Corporation, weighted the mass of candles every two weeks at the first month after the placement of candles,

and approximately every month until the remaining lifetime of the candles. Figure 18 shows the remaining mass of candles each time as shown in yellow and a comparison with their initial mass as shown in blue.

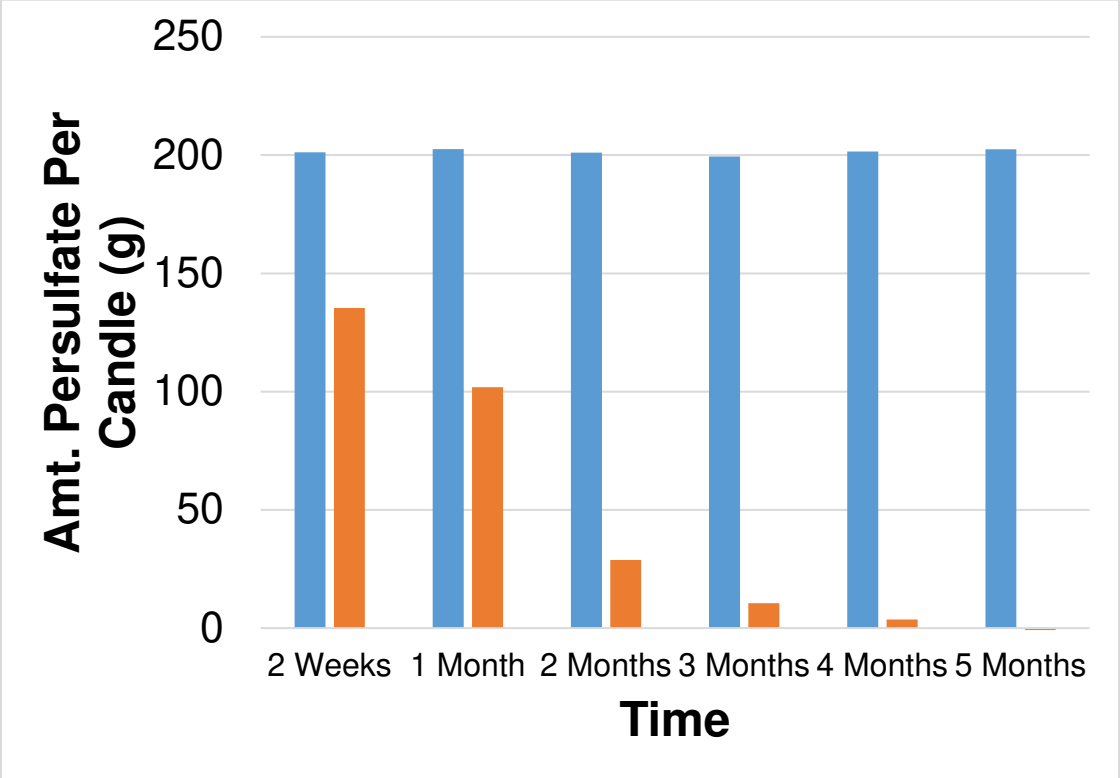

Figure 18. Sodium persulfate mass left in the Textron site over time (provided by Airlift)

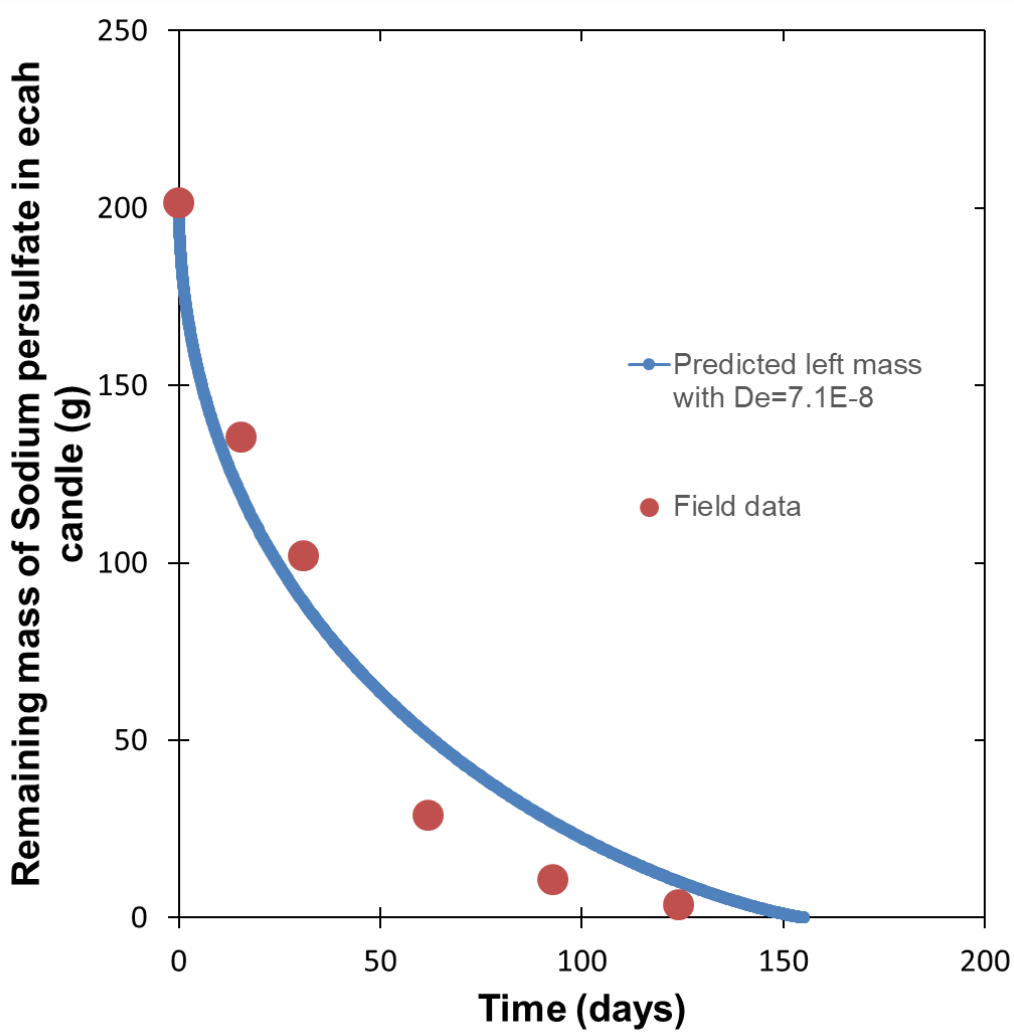

Figure 19. Simulated remaining mass of sodium persulfate over time with effective diffusion coefficient of 7.1×10^{-8} cm/s and field data

Roseman model (Eqs 3 and 4) was used fit the field data by adjusting the effective diffusion coefficient (D_e). The criteria of fitting include (1) minimize the difference between simulated and measured mass release over time; and (2) minimize the difference between simulated and measured life time of the candle. As shown in Figure 19, an effective diffusion coefficient of 7.1×10^{-8} cm^2/s provides reasonably match (i.e. R^2 =

0.9738) with field observation for both time series remaining mass data and the lifetime of candle.

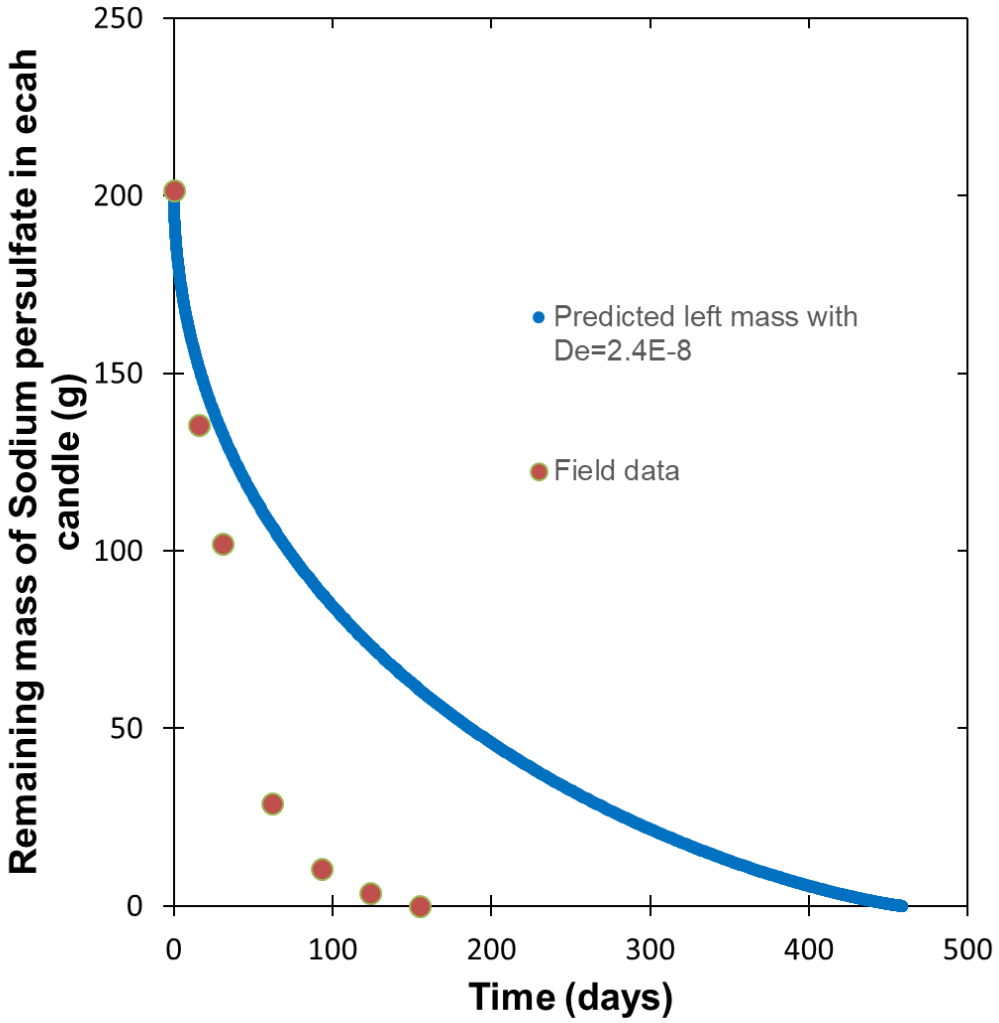

Figure 20. Simulated remaining mass of sodium persulfate over time based on lab data and field data

The field data was available at the beginning of the August in 2017. A comparison between the field data and a simulated prediction based on the lab data was analyzed for a more reasonable release rate. Figure 20 shows a difference between field data and release based on the lab data. The simulated lifetime is almost 2.5 times of the

reality and the simulated release rates are always much smaller than the field release rate on the time serious. The difference of release rate and longevity might be caused by the assumption that the effective diffusion coefficient of a 0.5-inch diameter candle is same as that of a 1.0-inch diameter candle and the complexity of the real site such as reaction and changing flow conditions over time. In addition, there was a potential influence from the tortuosity. Compared to a 0.5-inch diameter candle, 1-inch diameter candle has more available pore space (i.e. pathways) to deliver the oxidant. Lengthened potential pathways increase the delivering time and affect the release rate correspondingly.

Figure 19 and Figure 20 represents the simulated data based on the field observation has better fit with the field data than that based on the lab data. In the meantime, the simulated data based on the field observation provides reasonable prediction points on the time series. All in all, we decided to use the simulated release rate based on the field data.

References

Kambhu, A., Comfort, S., Chokejaroenrat, C., & Sakulthaew, C. (2012). Developing slow-release persulfate candles to treat BTEX contaminated groundwater. *Chemosphere*, *89*(6), 656–664. https://doi.org/10.1016/j.chemosphere.2012.06.004

Liang, C., & Chen, C. Y. (2017). Characterization of a Sodium Persulfate Sustained Release Rod for in Situ Chemical Oxidation Groundwater Remediation. *Industrial and Engineering Chemistry Research*, *56*(18), 5271–5276. https://doi.org/10.1021/acs.iecr.7b00082

Roseman, T. J., & Higuchi, W. I. (1970). Release of Medroxyprogesterone Acetate from a Silicone Polymer. *Journal of Pharmaceutical Sciences*, *59*(3), 353–357.

Chapter 5

Modeling Sodium Persulfate Release under Different Subsurface Flow Conditions

5.1. Model Description

To understand sodium persulfate release, transport, and reactions in the field site, we first develop a model to simulate sodium persulfate release and transport in a field site with simplified flow field. To build this physical-based model, COMSOL Multiphysics 5.3, a widely used finite element based simulation software provided by COMSOL Incorporation, is used. COMSOL was used for simulating electromagnetics, structural & acoustics, fluid & heat, and chemical physical systems.

This chapter describes the basic equations used in the simulation and analyzes the release of sodium persulfate under two subsurface flow conditions without aeration: I) Fine sand and clay media only; II) two layers with fine sand and clay media on top of the sand and gravel media.

5.1.1. Geometry

The simulation area was defined based on the simplified geometry of the Test area. As illustrated in Figure 21, the site is 52 ft long, 38 ft wide, and 72.4 ft deep. According to the field settlements, twenty-one big candles were placed in the North West corner of the domain. Figure 22 demonstrates the detailed arrangements of candles in blue points and four monitoring wells in red points. Groundwater flow direction is

assumed to be from north to south. A constant horizontal water table, which is 10 ft from the surface, is used in this simulation. The water table was defined based on limited field monitoring data.

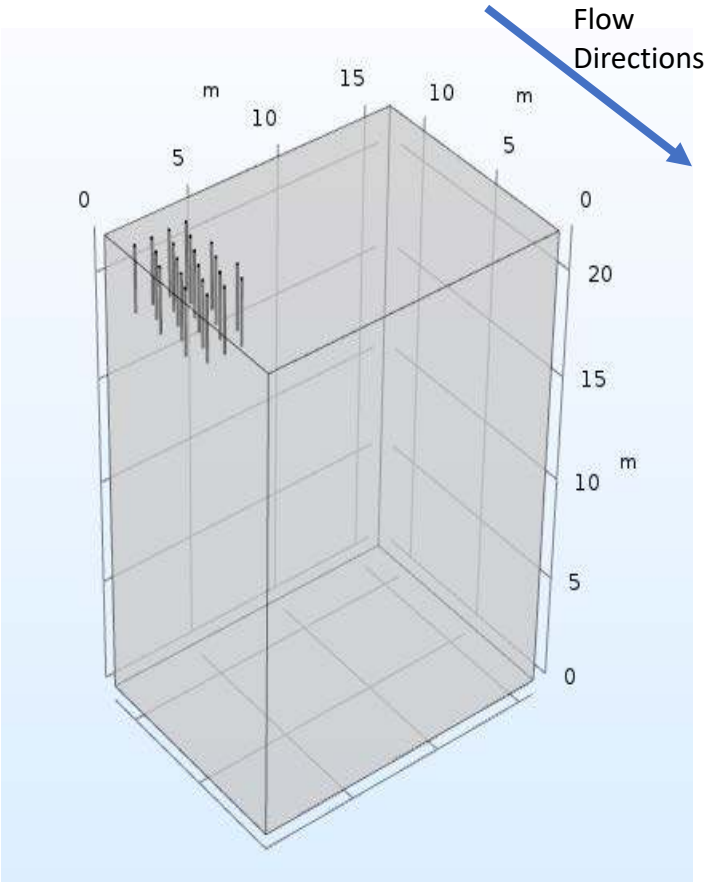

Figure 21. Basic geometry of the model

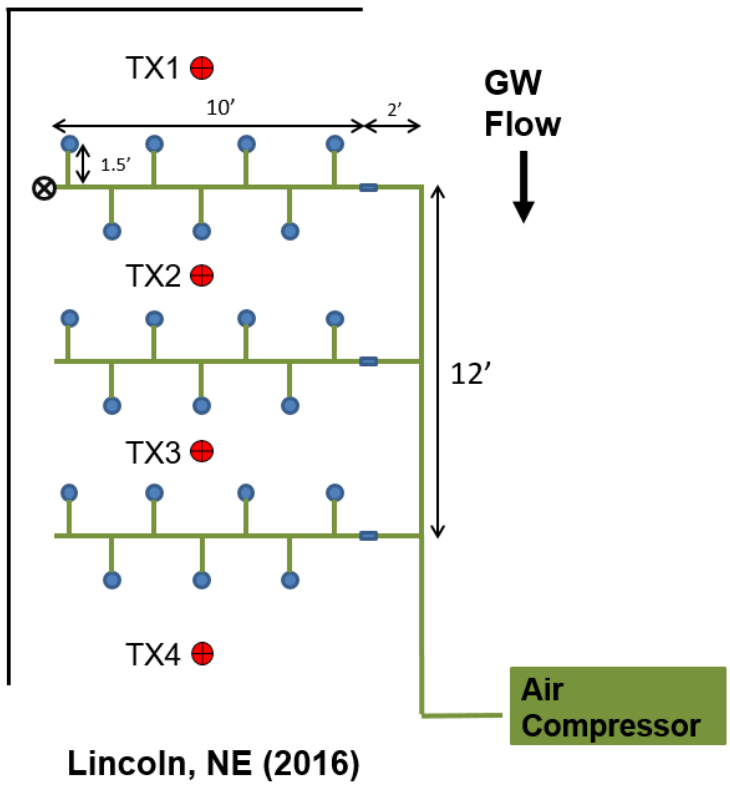

Figure 22. Candles placements in the Textron test area (provided by Airlift)

5.1.2. Governing Equations, Boundary and Initial Conditions

Advection and dispersion are the main driven mechanisms for persulfate release and transport, which can be described by a general mass balance equation (Eq.5).

$$\frac{\partial c_i}{\partial t} + \nabla(-\mathbf{D}\nabla c_i) + \mathbf{u}\nabla c_i = R_i + S_i \qquad \text{(Eq. 5)}$$

$$D = D_e + \mathbf{u}\alpha \qquad \text{(Eq. 6)}$$

Where c_i is the concentration of species i (mol/m^3); t is the simulation time (day); D is the mechanical dispersion coefficient (m^2/s); u is the velocity vector (m/s); R_i is the reaction

rate of species i (mol/m^3/s); S_i is the source/sink term of species i (mol/m^3/s); D_e is the diffusion coefficient in porous media (m^2/s); α is the dispersivity (m).

The release of persulfate from the candle was incorporated by defining a release flux of each big candle based on the release data described in the chapter 4. Because diffusion, dispersion, and advection are the main transport mechanisms in this case, the flux equation can be expressed as:

$$\mathbf{N_i} = (-\mathbf{D}c_i) + \mathbf{u}c_i \quad \text{(Eq. 7)}$$

Where $\mathbf{N_i}$ is the flux vector (mol/m^2/s). $\mathbf{N_i}$ is determined by dividing the release rate (g/day) obtained in Chapter 4 by the molar mass of 238.03 g/mol and the surface area of small candle (i.e. 0.0243 m^2). Because the release rate quickly reached a very sharp maximum during a very short period (i.e. 0.45 minutes), the numerical simulation had difficulty with convergence. In order to avoid this problem, an averaged release rate of 18.18 g/day was used during the first 1.525 day. This average release rate was calculated by considering the same amount of mass release during this period of time. Considering the longevity of the candle (i.e. 153 days), an approximation during the first 1.525 day should not have big impact on the final results. In the meantime, a step function starting from 0 and reaching 1 at 0.1 day multiplies the release rate and makes a smooth transition from zero to the maximum of the release rate. With these two adjustments, the numerical model was able to converge. Figure 23 illustrates the flux vector developed by the release rate. After 0.1 day, there is a smooth transition from zero to the maximum flux. The maximum flux lasted 1.425 days after it reached the peak. For the remaining time, flux

data was not adjusted and gradually decreased to zero until the end of the longevity of a candle.

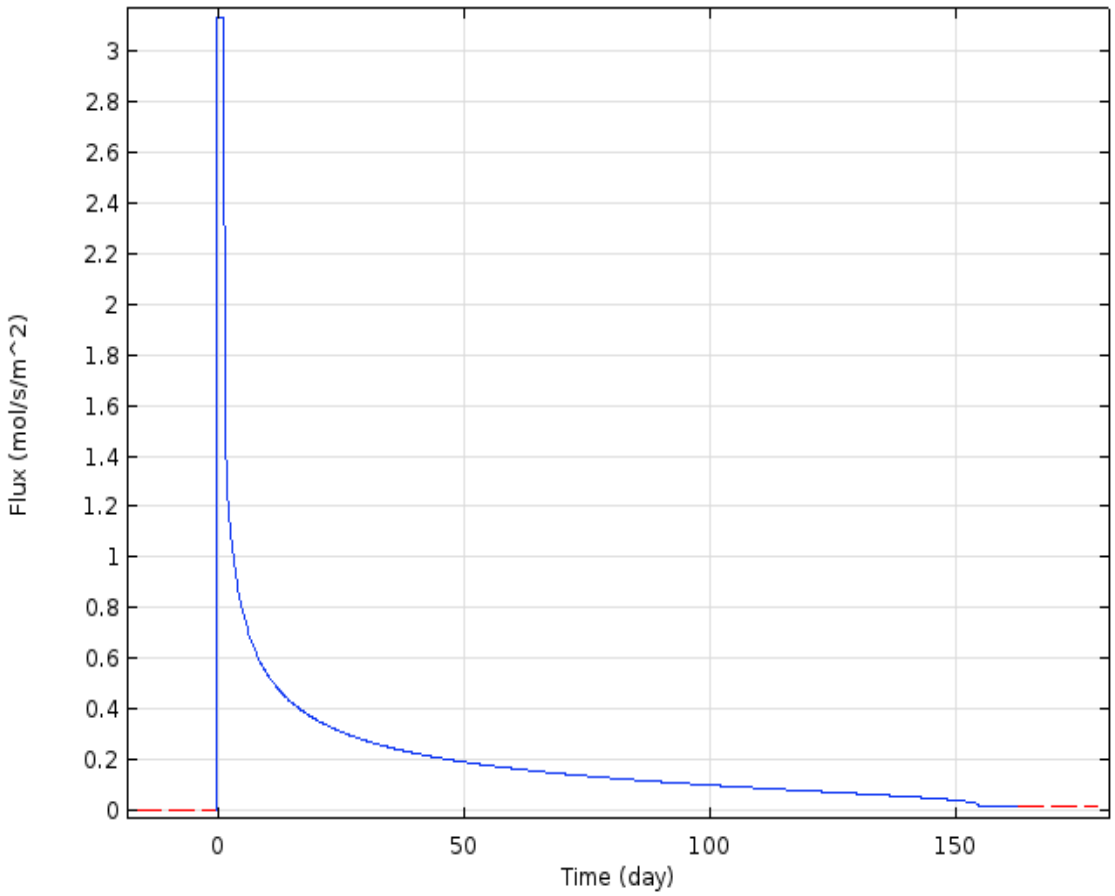

Figure 23. Flux vector yields from the release rate of the sodium persulfate

To respect the physics, inflow, outflow, no flux and flux boundary conditions were used. No flux boundary condition is a boundary where no mass flux flows in or out and it was assigned at the top and bottom surfaces as water could not pass the water table and the bedrock. Literally, inflow and outflow boundary conditions means the inlet and

outlet boundary where species could come in or out, respectively. As illustrated in Figure 21, the out surface, which is perpendicular to the groundwater flow direction and first encounters the water, was assigned as an inflow boundary. The remaining surfaces were assigned as outflow boundary conditions.

We assumed that the whole domain does not have any species (i.e. concentrations equal to zero) at time zero. After that, sodium persulfate was released from the candle and spread in the domain.

5.1.3. Mesh and Solver Settings

The mesh of the model was tetrahedral and predefined as extra fine. Boundary layers mesh was utilized to refine the mesh around the candles. There were 1292442 elements in the domain with average element quality of 0.6551.

To model the real time release and transport of sodium persulfate, the simulation was time dependent. In the time-dependent solver, implicit BDF time stepping method, generalized minimum residual (GMRES) iterative linear system solver, and Newton's nonlinear method with constant damping factor of 0.9 were used.

5.2. Simulation Scenarios and Results

According to the *Soil and Groundwater Assessment Report* provided by Terracon Consultants Incorporation, the major soil type in the test area of the Textron site are clay and fine sand. Persulfate release and transport were simulated in two aquifer scenarios, one homogenous aquifer with fine sand and clay and two-layer aquifer containing sand and clay on the top of the sand and gravel(Terracon Consultants, 2016).

5.2.1. Homogenous Aquifer with Fine Sand and Clay

5.2.1.1. Basic parameter setup

Natural Recourses Conservation Service provided a typical value of hydraulic conductivity for the fine sand as 9.174×10^{-5} m/s(Natural Resources Conservation Service, n.d.). In the meantime, Gelhar et al. reported that a similar site to the test area with "medium to fine sand interspersed with clay and silt", had a hydraulic conductivity of 5.1×10^{-4} m/s, effective porosity of 25%, dispersivity of 0.6 m, and velocity of 0.05 m/day (Gelhar, Welty, & Rehfeldt, 1992). The site is 6 m long, which is at the same scale as the width of the test area (i.e. 6.71 m). Therefore, basic parameters of the reported site, including groundwater velocity, dispersivity, and effective porosity, were adopted in this study.

5.2.1.2. Results

5.2.1.2.1. The Release of Sodium Persulfate over Time

Figure 24 presents a transverse cross section of simulated concentration distributions of sodium persulfate released (mol/m^3) from first row of candles at 20, 40, 100, 153 days. Again, those candles lasted 153 days. Figure 25 presents a closer look to the concentration of sodium persulfate over the length of the line. As shown in Figure 24, concentration of persulfate was the highest at the location adjacent to candles, and then gradually decreased as further away from the candle. From 20 day to 153 day, the overall persulfate concentration in the area was decreasing with time. A closer look at Figure 25 indicated that the concentration of sodium persulfate quickly increased to a

very high value from the beginning to day 1, then gradually reduced after that. At day 1, the highest concentration reached around 6.5 mol/m^3.

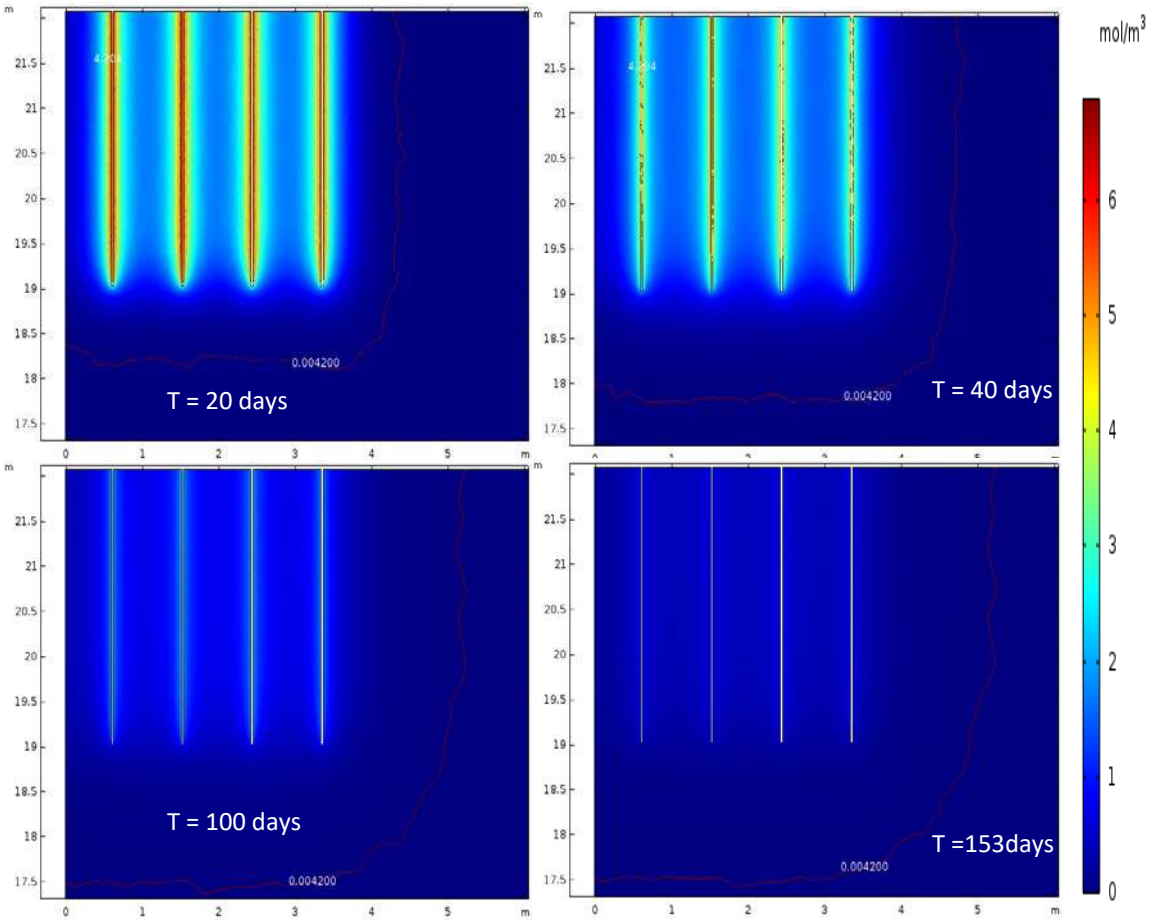

Figure 24. Simulated concentration of sodium persulfate from first row of candles at 20, 40, 100, 153 days (flow direction is out of the paper)

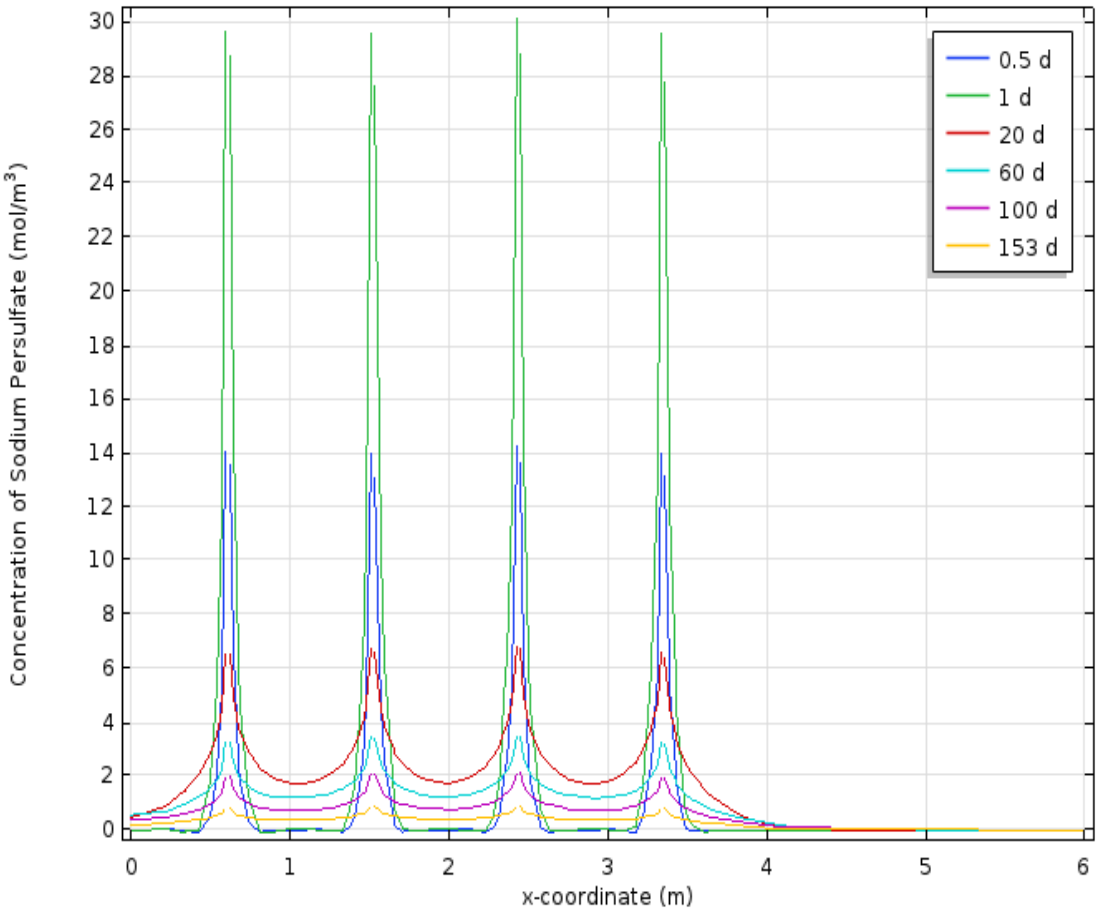

Figure 25. Concentration of sodium persulfate over first row of candles at various time

The sharp increase of concentration before day 1 and the gradual decrease of concentration after that were consistent with the release rate and relevant transport processes such as advection and dispersion. Because the flow velocity and dispersivity were constant, the accumulation/depletion of sodium persulfate depended on the magnitude of the release. As illustrated in Figure 23, the flux delivering the sodium persulfate into the surrounding area of candles quickly reached its maximum during the first 1.525 days and gradually diminished until the end of a candle. Initially there was no sodium persulfate in the site, the concentration of the sodium persulfate sharply increased

because the release rate was much higher than dispersion and advection. After that, the concentration of sodium persulfate decreased because the release rate was decreased so that dispersion and advection were able to transport more persulfate away than the amount of released.

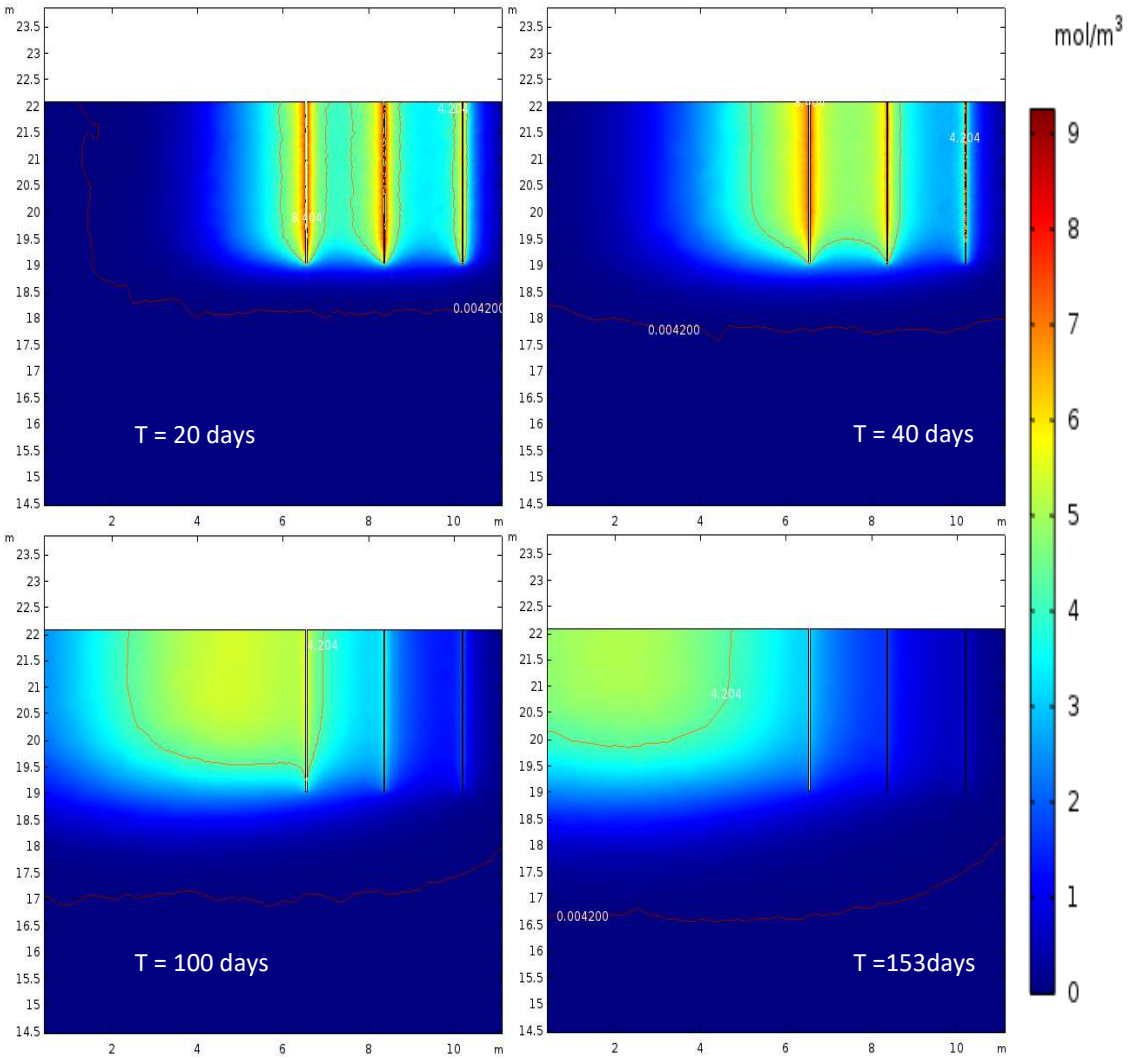

Figure 26. Simulated concentration of sodium persulfate from first column of candles at 20, 40, 100, 153 days (flow direction is from the right to left)

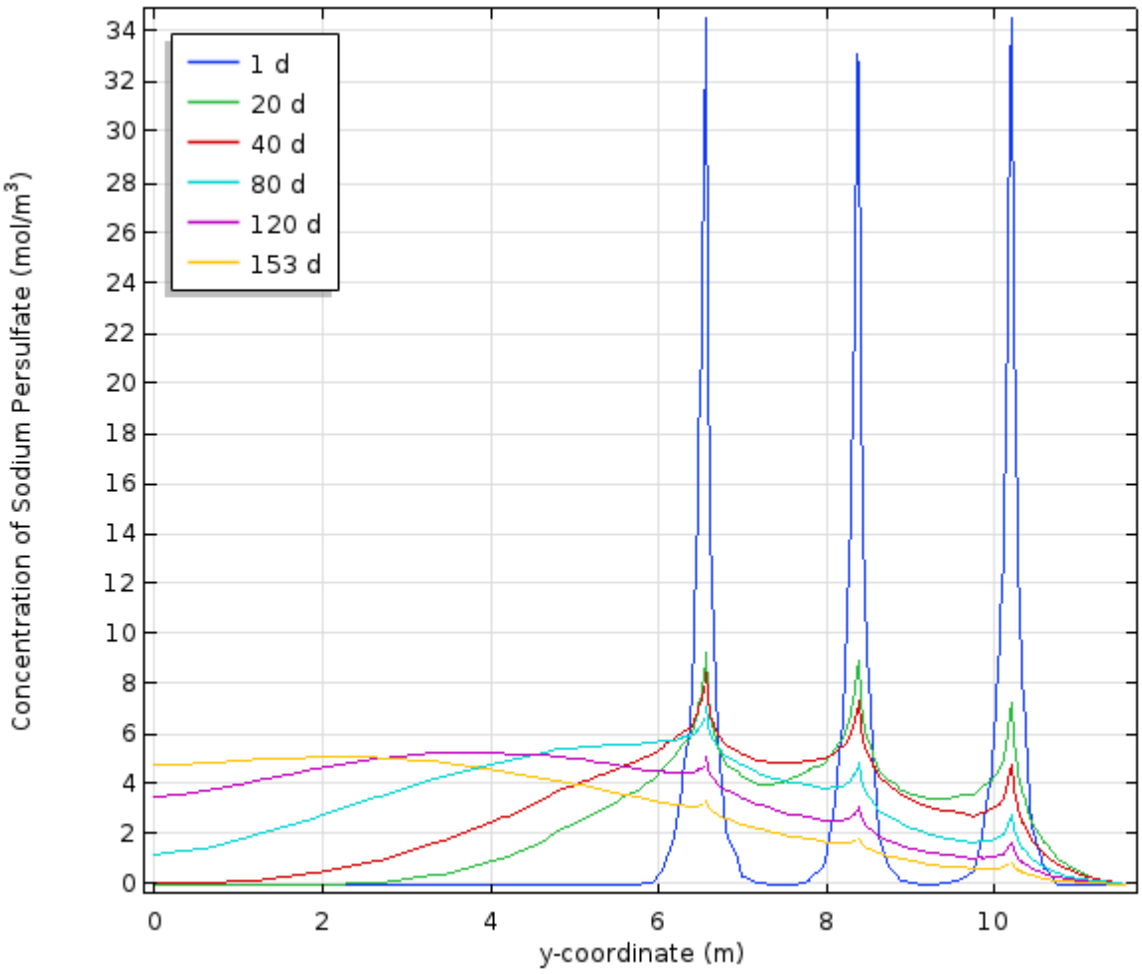

Figure 27. Concentration of sodium persulfate over first column of candles at various time

Figure 26 presents a longitudinal cross section of simulated concentration distributions of sodium persulfate released (mol/m^3) from first column of candles at 20, 40, 100, 153 days. Figure 27 presents a closer look to the concentration of sodium persulfate over the length of the line. As shown in Figure 26, initially, the highest concentration occurred at the location adjacent to candles and the concentration reduced with the distance from candles. From 20 days to 153 days, the center of the mass moved

down stream. Overall concentration at the downstream of candles increased with time while the concentration in the remaining positions decreased with time. A closer look at Figure 27 indicates that the highest concentration moved to the downstream of the candles after 80 days. In the meanwhile, the value of the maximum concentration decreased to 5 mol/m^3.

The movement of the center of the mass was consistent with the groundwater flow direction. The sodium persulfate released from the upstream candles were carried by the advection, dispersion, and diffusion to downstream, so that the concentration of persulfate in the downstream increased. During 80 to 120 days, the release rate from candles was smaller than the advection and dispersion and the center of the mass already passed through candles, so that the location of the maximum concentration moved downstream.

5.2.1.2.2. The Radius of Influence

To analyze the radius of influence of candles on the transverse direction with/without previous mass accumulation, two candles were chosen. Figure 28 demonstrates the location of two candles. The first one was on the right of the first row. The second one was on the downstream of the first one and located on the fifth row.

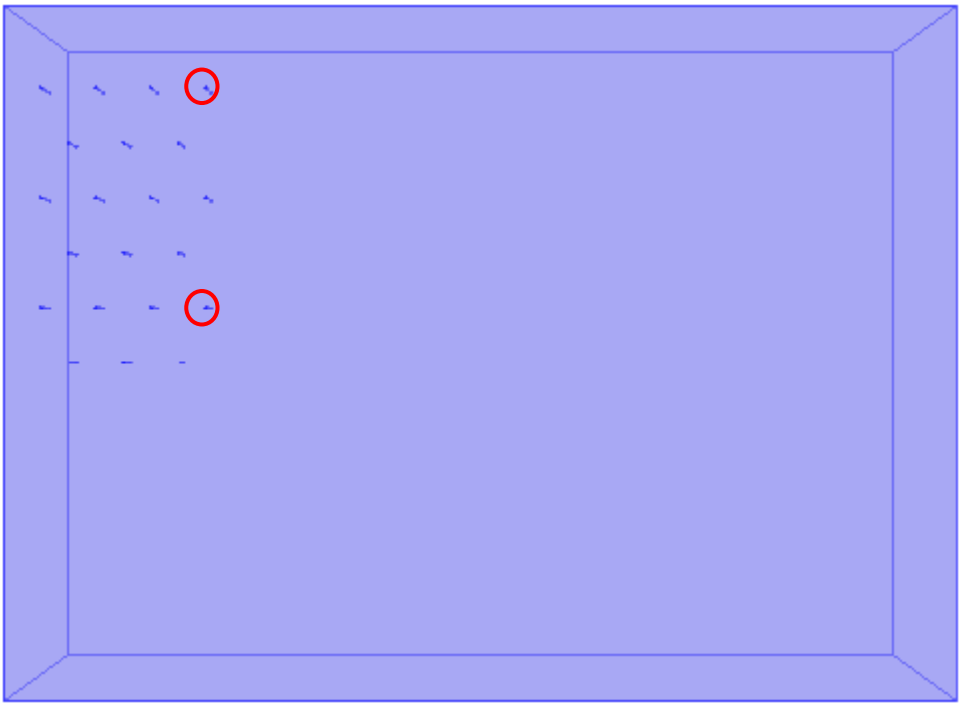

Figure 28. Locations of analyzed candles on the top view of domain

Figure 29 presents the radius of influence of a candle on the right of the first and fifth row in the transverse direction. Here, the radius of influence was defined as the distance of a certain concentration value (i.e. 1 mM, 5 mM, and 10 mM) from the center of the candle in the transverse direction. For all concentrations examined on the first row, the radius of influence increased at the early time range. After that, the radius of influence reduced with time. In addition, the decrease rate of the radius of influence was much smaller than the increase rate. As expected, smaller concentration influence further and lasted longer. For example, the radius of influence for 1 mM reached as high as 35 cm in the transverse direction at day 21. The maximum radium of influence for 5 mM was only 10 cm at a very early stage.

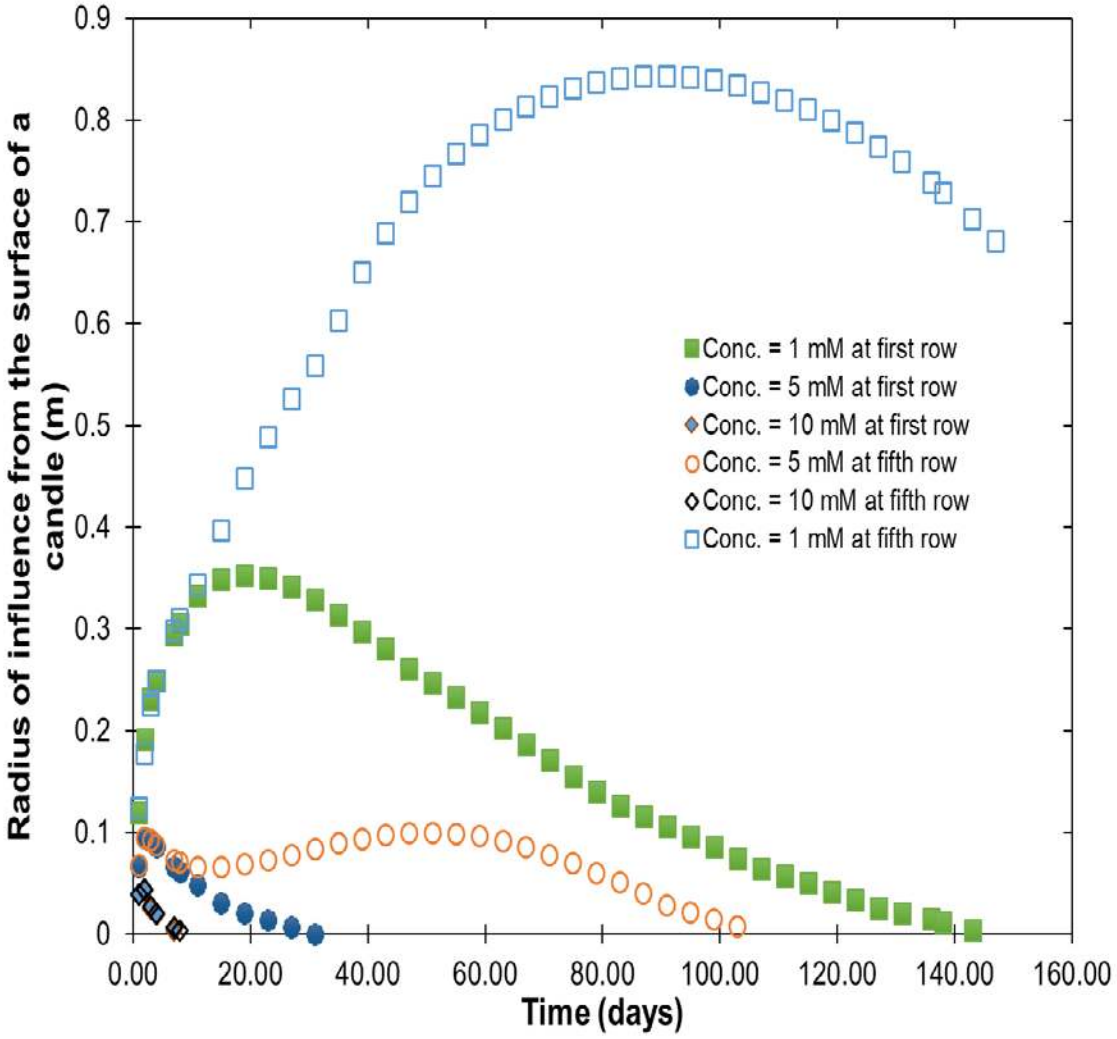

Figure 29. The radius of influence of a candle on the right of the first and fifth row in the transverse direction over time

The radius of influence in the fifth row was same as that of the first row at the early stage. After that, the radius of influence in the fifth row for each concentration deviated from that of the first row due to the arrival of sodium persulfate from the upstream. For 1 mM concentration, the radius of influence kept increase until a new peak of 0.843 m at day 90, which was almost 2.5 times further than the 1 mM radius of influence in the first row. For 5 mM concentration, the sodium persulfate mass from the

upstream sustained the radius of influence from decreasing to a trend of increase, such that the maximum radius of influence in the fifth row remained as high as 0.1 m until day 53. Finally, sodium persulfate concentration from upstream was not as high as 10 mM when it reached the fifth row. Because no influence from upstream for 10 mM, the radius of influence in the fifth row was same as that in the first row for the whole time period.

5.2.2. Two-Layer Aquifer

To evaluate the influence of aquifer heterogeneity on the release of sodium persulfate, simulation was conducted on a two-layer aquifer. Same as the Textron site, the top layer was composed of fine sand and clay with a thickness of 6.94 ft. The bottom layer was composed of sand and gravel with a thickness of 65.49 ft. The thickness of each layer was determined from the average thickness of the soil lithology model developed in Chapter 3. Figure 30 represents the geometry of two-layer model. Ten feet long big candles extended from the top of the first layer to 3.06 ft into the second layer.

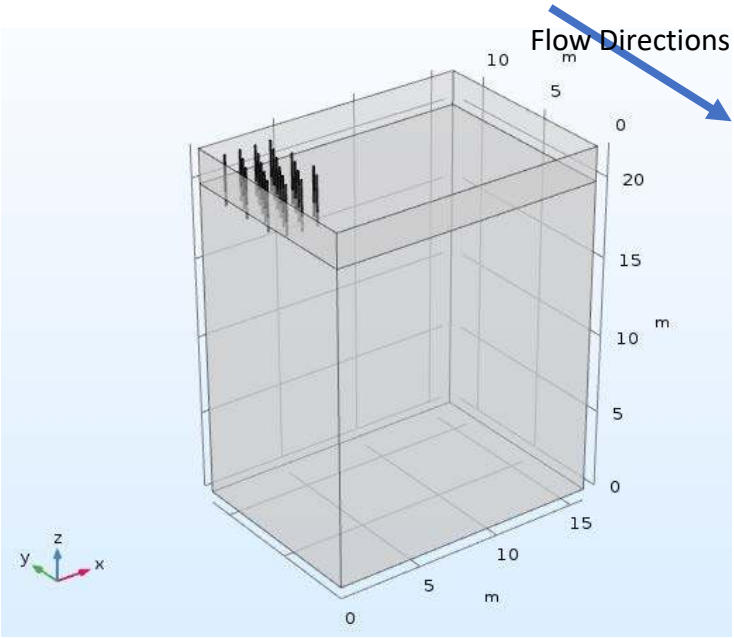

Figure 30. Geometry of the two-layer model

Parameters of aquifer materials were obtained from a similar site published by Gelhar et al. (Gelhar et al., 1992). For the fine sand and clay layer, dispersivity was 0.6 m; velocity was 0.05 m/day; effective porosity was 25%. For the sand and gravel aquifer the hydraulic conductivity was 6.5×10^{-3} m/s; dispersivity was 6.9 m; the velocity was 18 m/day; the effective porosity was 14% (Gelhar et al., 1992).

5.2.2.1. Results

Two cross-sectional views of the results are provided: I) four big candles in the first row on the transverse direction, and II) three big candles in the first column on the longitudinal direction.

Figure 31 represents simulated concentration of sodium persulfate released (mol/m^3) from first row of candles at 20, 40, 100, 153 days. Figure 33 and Figure 32 provided a closer look at the concentration over the length in the top and bottom layer, respectively. On the top layer, the trend of sodium persulfate release is just same as in the homogeneous aquifer. The sodium persulfate concentration was quickly increased to a very high value and then gradually reduced. The concentration of sodium persulfate in the sand and gravel layer was much smaller than that in the fine sand and clay layer. For example, the maximum concentration in the top layer at day 1 was around 32 mM, which was over 100 times that in the bottom layer as 0.0285 mM. The significantly lower persulfate concentration in the bottom layer is due to much higher velocity in this layer, which efficiently flushed the mass of sodium persulfate away as soon it released. The flow velocity in the second layer is 18 m/day, which is 360 times higher than the velocity in the top layer.

Figure 34 presents the concentration distribution along the longitudinal direction of the flow for the first column of the candles. Again, as for the homogeneous aquifer, the same accumulation of persulfate mass in the downstream due to contribution from upstream was observed for the top layer. Furthermore, the center of spread moved quicker in the bottom layer than that in the top layer as the vast magnitude difference of the groundwater velocity.

The striking difference of persulfate concentration in the two-layer aquifer has significant implication on the implementation of slow-release candle technology on a field site. Because a reasonable influence radius was formed in the sand and clay aquifer,

persulfate concentration in the sand and gravel aquifer is too low to achieve any contaminant removal if contaminant exists. Therefore, slow-release candle may not be suitable for aquifer with very high hydraulic conductivity.

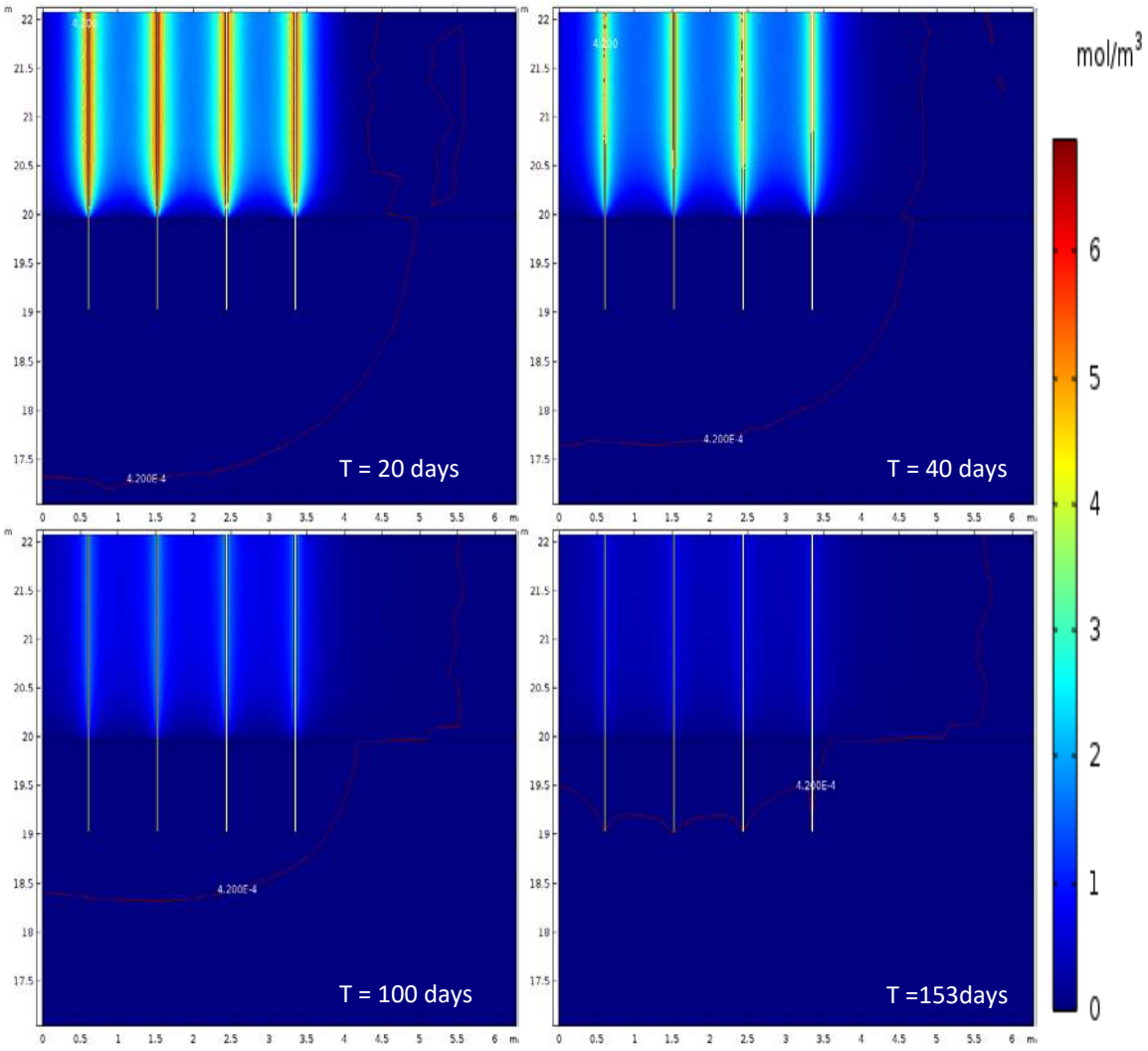

Figure 31. Simulated concentration of sodium persulfate from first row of candles at 20, 40, 100, 153 days in the two-layer model (flow direction is out of the paper)

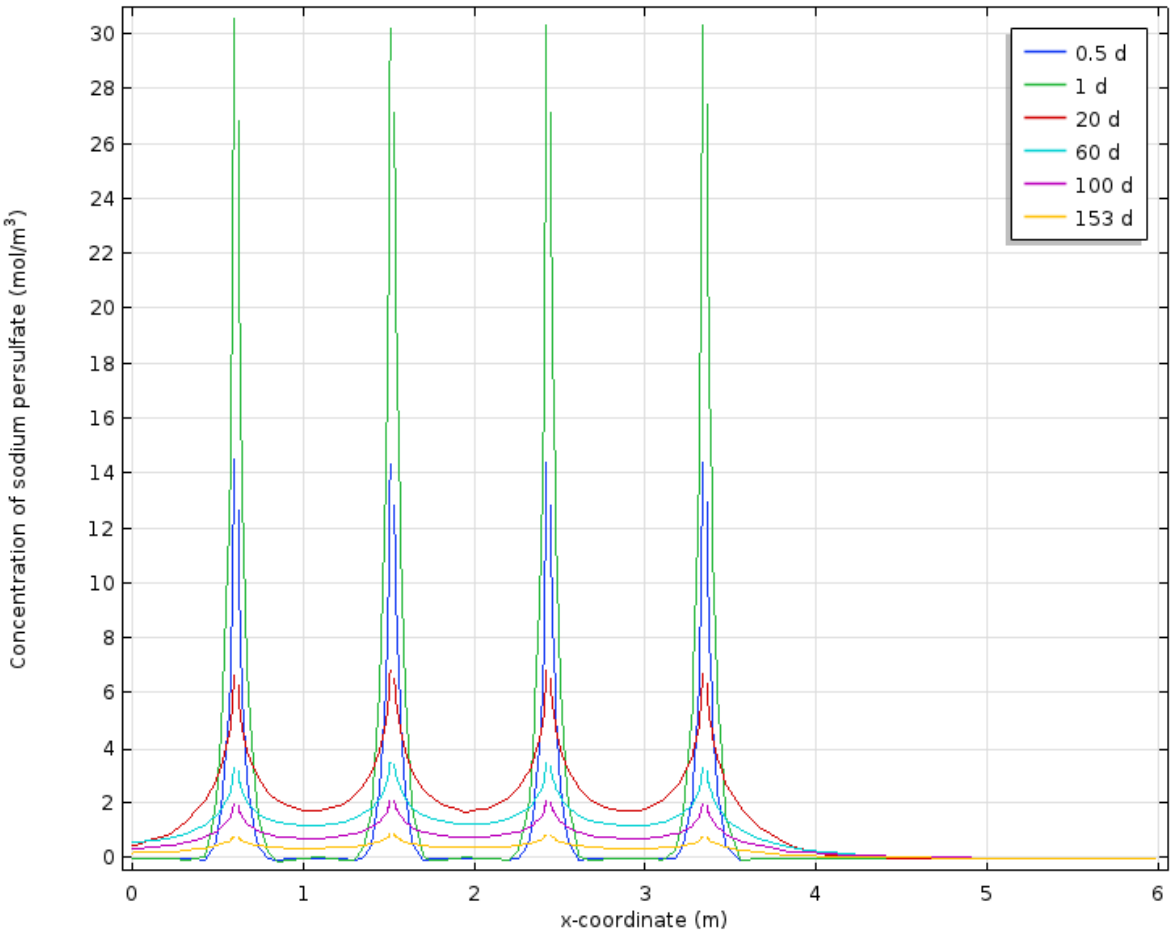

Figure 32. Concentration of sodium persulfate over first row of candles at various time in the bottom layer

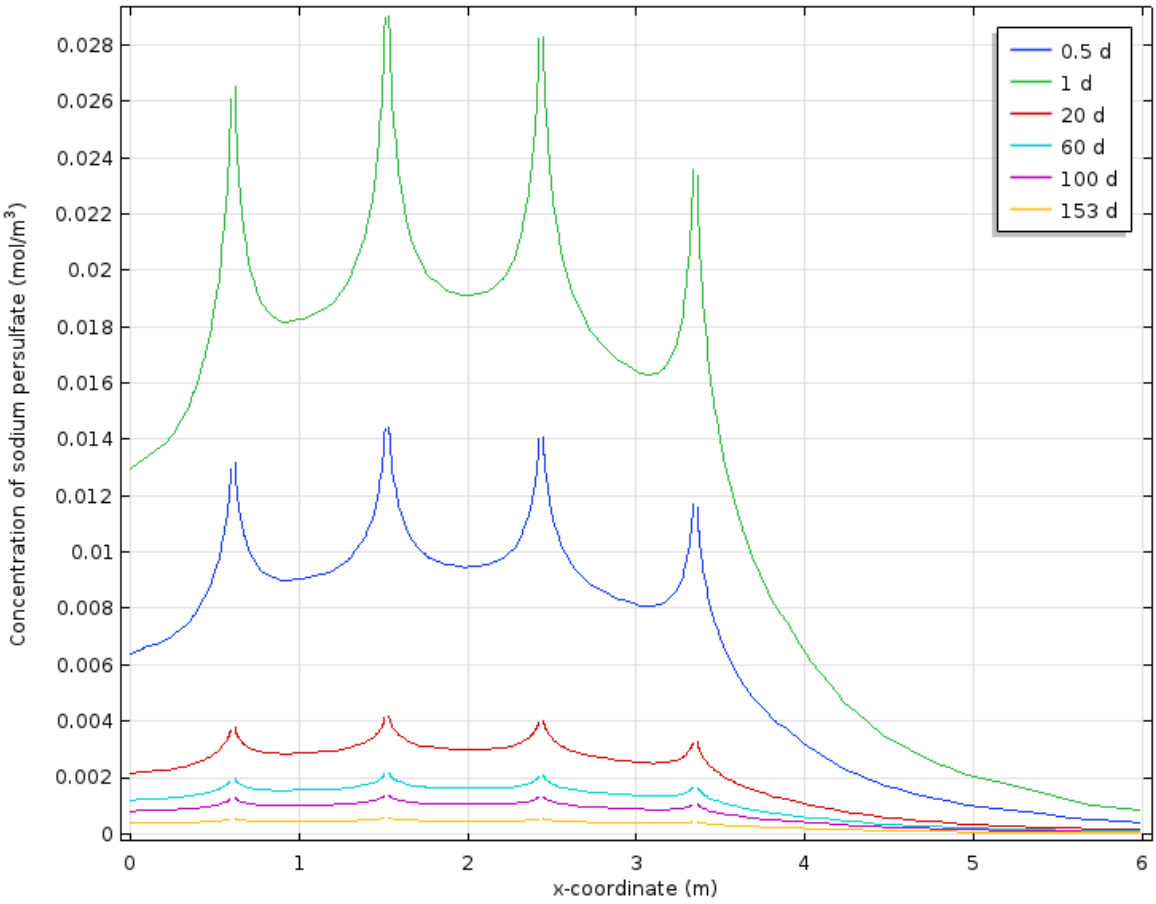

Figure 33. Concentration of sodium persulfate over first row of candles at various time in the top layer

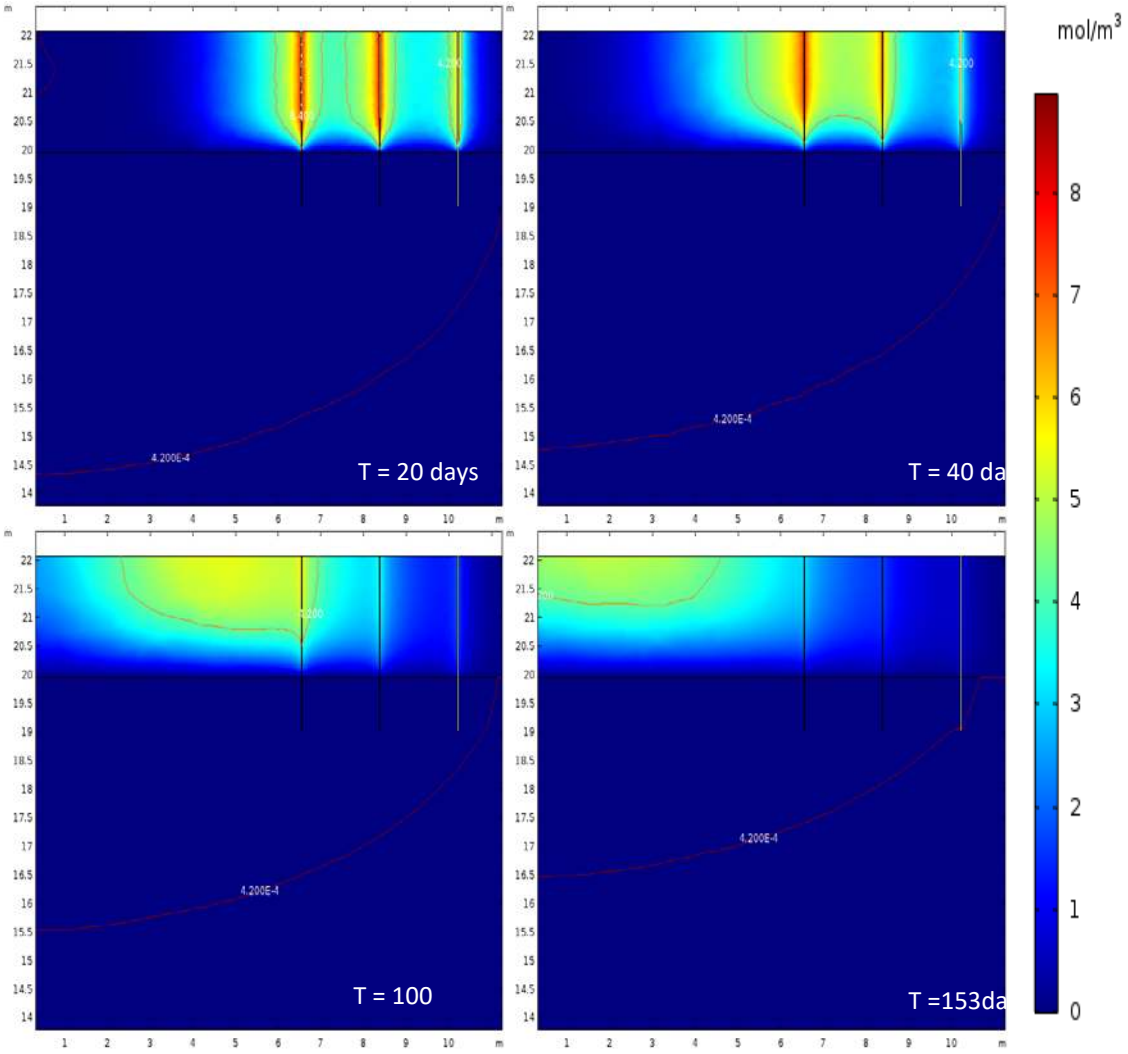

Figure 34. Simulated concentration of sodium persulfate from first column of candles at 20, 40, 100, 153 days in the two-layer model (flow direction is from the right to left)

5.3. Conclusion

To understand sodium persulfate release and transport in the field site, COMSOL Multiphysics 5.3 was used to develop a model under two scenarios: I) Homogeneous fine

sand and clay aquifer; II) two layer aquifer with fine sand and clay media on top of the sand and gravel media.

Simulated results from both conditions were consistent with basic theories and expectations. For the concentration distribution, the relative contribution of advection and the release rate of the sodium persulfate from a candle determined the accumulation/depletion of sodium persulfate. In the sand and clay aquifer, sodium persulfate was able to accumulate around the candle and the concentration of it proved its capability to remove the contaminants in the aqueous phase based on the basic stoichiometry. In the sand and gravel aquifer, groundwater velocity played a dominant role in the distribution of sodium persulfate. When sodium persulfate was released out, it would be immediately flushed away and leave almost nothing for the remediation. That indicated controlled release candle might not be suitable for high flow rate area like the sand and gravel aquifer. However, contaminants typically retained in the low permeability zone in the nature, we might not need to apply this technology in the high flow rate area.

For the radius of influence in the sand and clay aquifer, higher the required concentration of the sodium persulfate, smaller the radius of influence was. If 1 mM was the basic concentration requirement for the remediation, 0.66 m was the minimum radius of influence except the initial phase and the spacing of candles of 0.91 m was big enough to capture the incoming contaminants (i.e. $0.66\ \mathrm{m} \times 2 = 1.32\ \mathrm{m} > 0.91\ \mathrm{m}$). In the meanwhile, increasing the spacing of the later rows or decreasing the amount of sodium persulfate in the candle was suggested in the economical wise consideration. If the

amount of sodium persulfate was same, the spacing could be change to 2.64 m (i.e. $0.66\ \text{m} \times 4 = 2.64\ \text{m}$) instead of 0.91 m with the present of next row to fix the gap. Based on that, implication of controlled release candles were applicable in the field. For the sand and clay aquifer, the radius of influence was not considerate as mentioned before.

Finally, the performance of two-layer model demonstrated the capacity to handle wide range of soil properties where field site properties locate. The model is ready to be associated with aeration or reaction in the further steps.

References

Gelhar, L. W., Welty, C., & Rehfeldt, K. R. (1992). A Critical Review of Data on Field-Scale Dispersin in Aquifers. *Water Resources Research*, *28*(7), 1955–1974. https://doi.org/10.1029/92WR00607

Natural Resources Conservation Service. (n.d.). Saturated Hydraulic Conductivity. Retrieved from https://www.nrcs.usda.gov/wps/portal/nrcs/detail/soils/survey/office/ssr10/tr/?cid=nrcs144p2_074846

Terracon Consultants. (2016). *Soil and Groundwater Assessment Report*.

Chapter 6

Modeling Remediation Using Sodium Persulfate Candles

6.1. Model Description

In this chapter, a model coupled with reaction in the field-scale was developed. In the model, transient persulfate release, transport and reactions with benzene under the flow condition in the field site were simulated. A space-dependent reaction module in COMSOL Multiphysics 5.3 was used to simulate reaction. This chapter first describes basic reactions used in the simulation, and then analyzes the efficacy/radius of influence of sodium persulfate under different remediation scenarios.

6.1.1. Modeling Domain

In this chapter, the simulation domain focuses on the North-West corner of the original site where candles were installed (Figure 35). The simulation domain is 38 ft long, 14.76 ft wide, and 22.97 ft deep. Twenty-one big candles were placed in the same arrangement as implemented in the Textron site (Chapter 3). Contaminated groundwater flow direction was assumed to be from north to south. A constant horizontal water table, which was 10 ft below the ground surface, was accounted as the top surface of the simulation domain. The water table was defined based on the limited field monitoring data. Coupling reactions in a transport model led to a sharp increase on the computational demand. In order to make the computational time feasible, candles were simulated as line sources. The actual diameter of a candle 1 inch, which is only 1/177 of the width of the

field (14.76 ft). The details of the candle geometry should not impact overall simulation results.

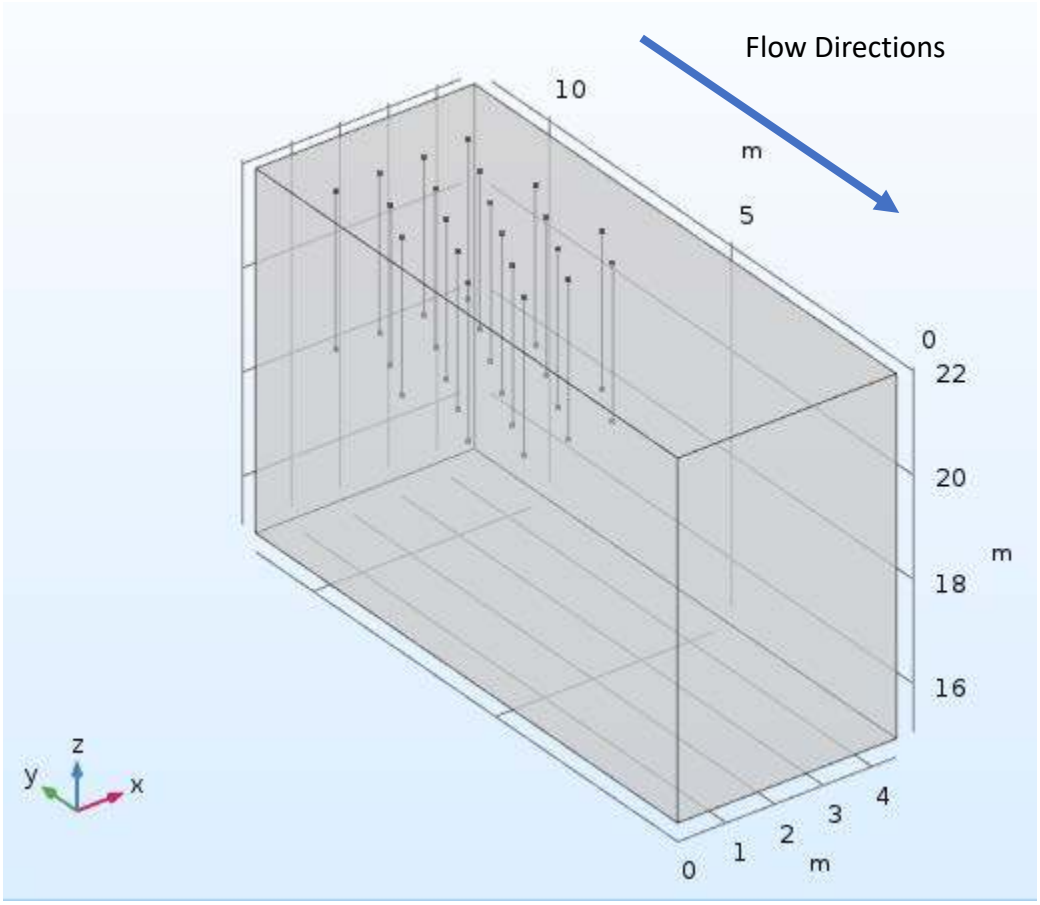

Figure 35. Basic geometry of the model

6.1.2. Governing Equations, Boundary and Initial Conditions

Persulfate release, transport, and reaction can be described by the advection-dispersion –reaction equation (Eq.5 – 7):

$$\frac{\partial c_i}{\partial t} + \nabla(-\mathbf{D}\nabla c_i) + \mathbf{u}\nabla c_i = R_i + S_i \quad \text{(Eq. 5)}$$

$$D = D_e + \mathbf{u}\alpha \quad \text{(Eq. 6)}$$

$$\mathbf{N_i} = (-\mathbf{D}c_i) + \mathbf{u}c_i \quad \text{(Eq. 7)}$$

Where c_i is the concentration of species i (mol/m^3); t is the simulation time (day); D is the mechanical dispersion coefficient (m^2/s); u is the velocity vector (m/s); R_i is the reaction rate of species i (mol/m^3/s); S_i is the source/sink term of species i (mol/m^3/s); D_e is the diffusion coefficient in porous media (m^2/s); α is the dispersivity (m); N_i is the flux vector (mol/m^2/s).

Different from the models in Chapter 5, R_i, reaction rate of species i, is calculated based on the reaction kinetics, as detailed below. Persulfate candles were simulated as mass line sources for reactive transport. Sodium persulfate release rate, in the unit of mol/m/s, was determined by dividing the small candle mass release rate(g/day) obtained in Chapter 4 by the molar mass of sodium persulfate (238.03 g/mol) and the length of small candle(i.e. 0.3048m). To avoid the converge problem, similar methods (i.e. early stage average and smooth function) applied in Chapter 5 were utilized to develop the

source strength.

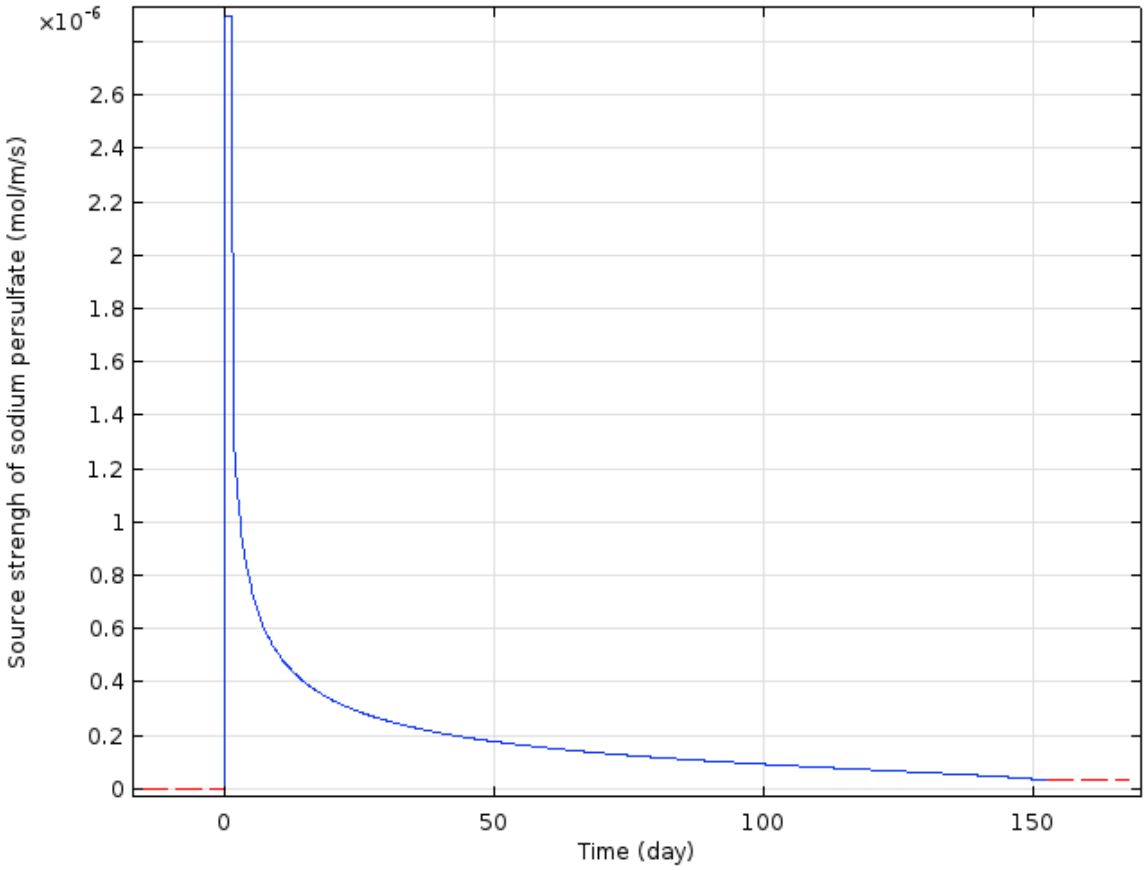

Figure 36. Source strength of sodium persulfate over time

Figure 36 illustrated the source strength of sodium persulfate over time developed by the release rate. After 0.1 day, there is a smooth transition from zero to the maximum flux, which lasted for 1.425 days. After that, mass flux gradually decreased to zero until the end of the longevity of a candle.

Additional boundary conditions including inflow, outflow, no flux boundary conditions were used in the model. No flux boundary condition is a boundary condition to consider no mass flux flows in or out of the boundary. No flux boundary condition was

assigned at the top and bottom surfaces because water could not pass the water table and the bedrock. Inflow and outflow boundary conditions assume that species could come in or out of the boundary. , respectively. As illustrated in Figure 35, the upstream surface, which was perpendicular to the groundwater flow, was assigned as an inflow boundary. We assumed there was an unknown source zone of benzene in the upstream, and a constant benzene concentration boundary condition was assigned at the upstream surface. The remaining surfaces were assigned as outflow boundary conditions. We also assumed that the whole domain was initially homogeneously contaminated by benzene (i.e. constant concentration of benzene and zero concentration of other species). After that, sodium persulfate was released from the candle, fully activated, spread and reacted with benzene in the domain.

6.1.3. Determination of Reaction Rates

Activation of persulfate was demonstrated to be a much more efficient way to treat contaminants than persulfate itself. Activation is a process to transform persulfate ($S_2O_8{}^{2-}$) into sulfate radical($SO_4^{\bullet 2-}$), which has higher oxidation-reduction potential in the presence of activator. Zero-valent iron (Fe^0) was a source to slowly release activator (Fe^{2+}) and the activation process with persulfate can be expressed as(Hussain, Zhang, Huang, & Du, 2012):

$$Fe^0 + 2S_2O_8{}^{2-} \rightarrow Fe^{2+} + 2SO_4^{2-} + 2SO_4^{\bullet 2-} \quad \text{(Eq. 8)}$$

$$Fe^{2+} + S_2O_8{}^{2-} \rightarrow Fe^{3+} + SO_4^{\bullet 2-} + SO_4^{2-} \quad \text{(Eq. 9)}$$

The reaction between sulfate radical and benzene is complicated and could be site dependent. In this work, we used degradation rates quantified by the laboratory experiments. Kambhu and co-workers (Kambhu, Comfor t, Chokejaroenrat, & Sakulthaew, 2012) conducted a series of experiments to measure the degradation of benzene by persulfate and zero-valent iron. Figure 37 and Figure 38 illustrated experimental data for benzene (0.5 and 1 mM initial concentration) reaction with persulfate and zero valent iron. Figure 39 presents 0.1 mM benzene degradation with aged persulfate candle. As shown in the figure, a first-order reaction was able to sufficiently simulate the degradation of benzene for both new and aged candles with $R^2 \geq 0.9781$. The reaction rate constants of benzene in Figure 37, Figure 38, and Figure 39 were in the range of 2×10^{-5} s^{-1} to 7×10^{-5} s^{-1} with the average of 3.8×10^{-5} s^{-1}. In the transport model, a first order reaction was used to simulate benzene degradation. The reaction rate of benzene was assigned as 3×10^{-5} s^{-1} multiplied by the concentration of benzene (mM) as shown in Eq. 10.

$$R_i(\frac{\text{mol}}{\text{m}^3 \cdot \text{s}}) = 3 \times 10^{-5}\ (s^{-1}) \cdot c_i(\frac{mol}{m^3}) \qquad \text{(Eq. 10)}$$

Liu proposed several pathways for the oxidation of benzene by sulfate radical and each pathway consumed only one sulfate radical(Liu et al., 2016). We assumed the natural oxidant demands of soil was negligible and all sulfate radicals were consumed by benzene. Based on that and Eq. 8-9, the stoichiometry of persulfate, sulfate radical, benzene was assumed as 1:1:1. Therefore, the reaction rate for persulfate was same in the magnitude as that for benzene in the reaction model, but with a negative sign.

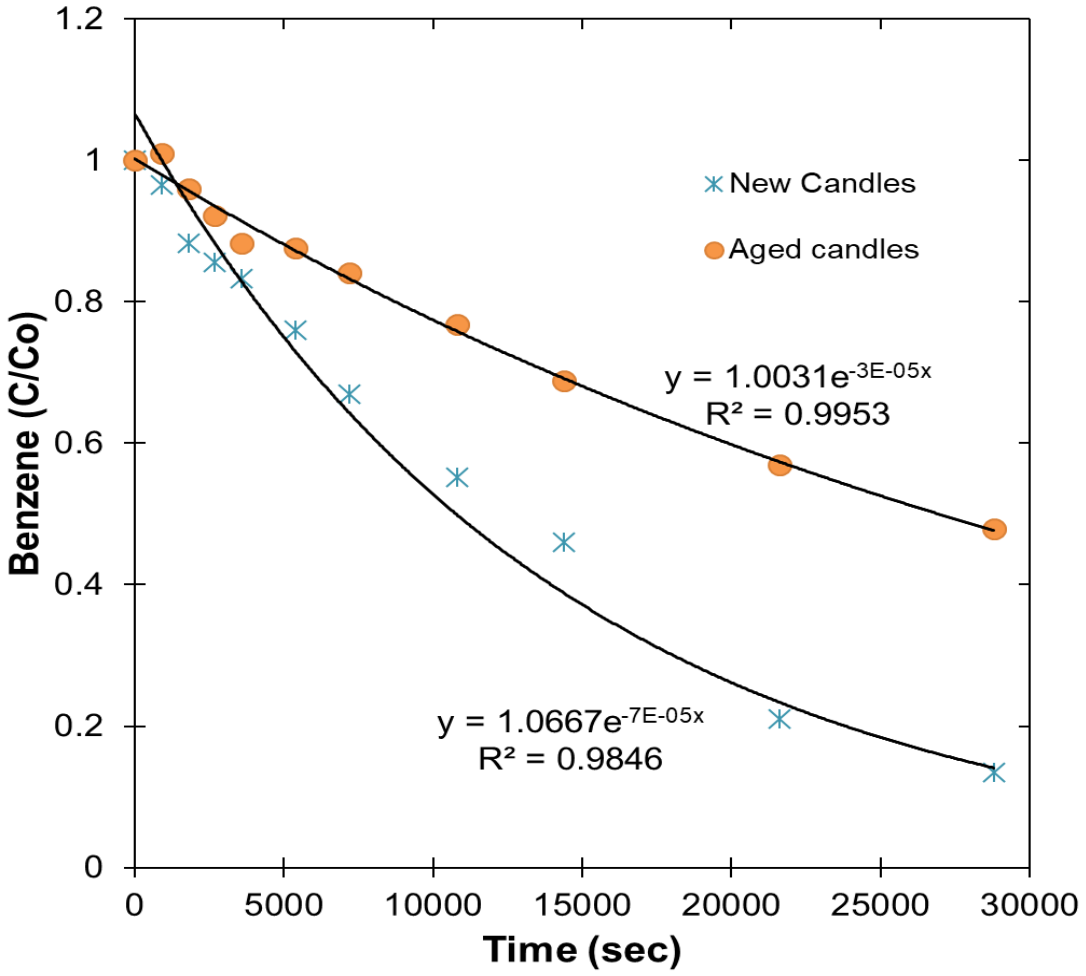

Figure 37. Benzene concentrations (Co = 0.5 mM) over time with new and 48-hr aged persulfate and zero-valent iron candles

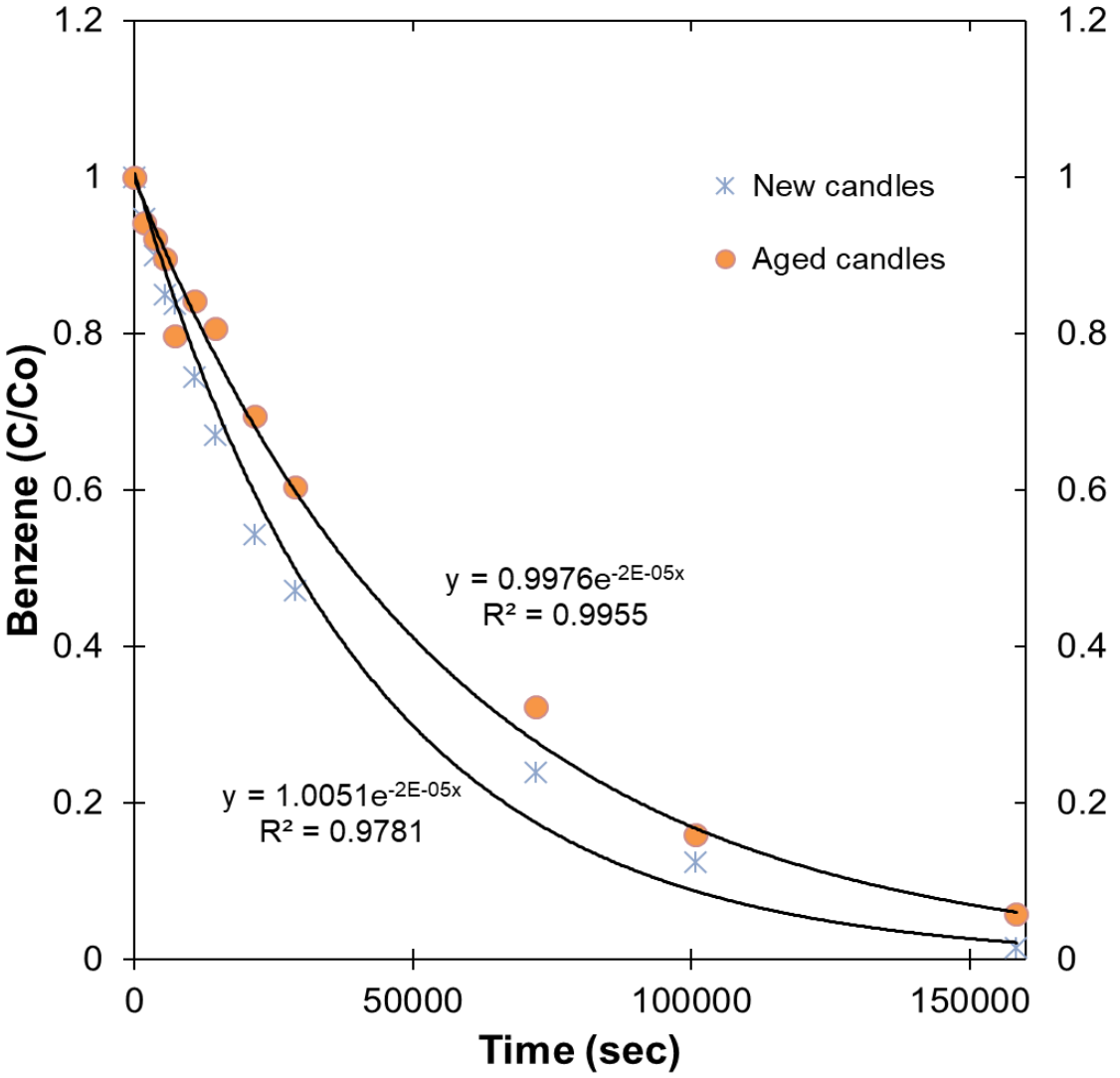

Figure 38. Benzene concentrations (Co = 1 mM) over time with new and 48-hr aged persulfate and zero-valent iron candles

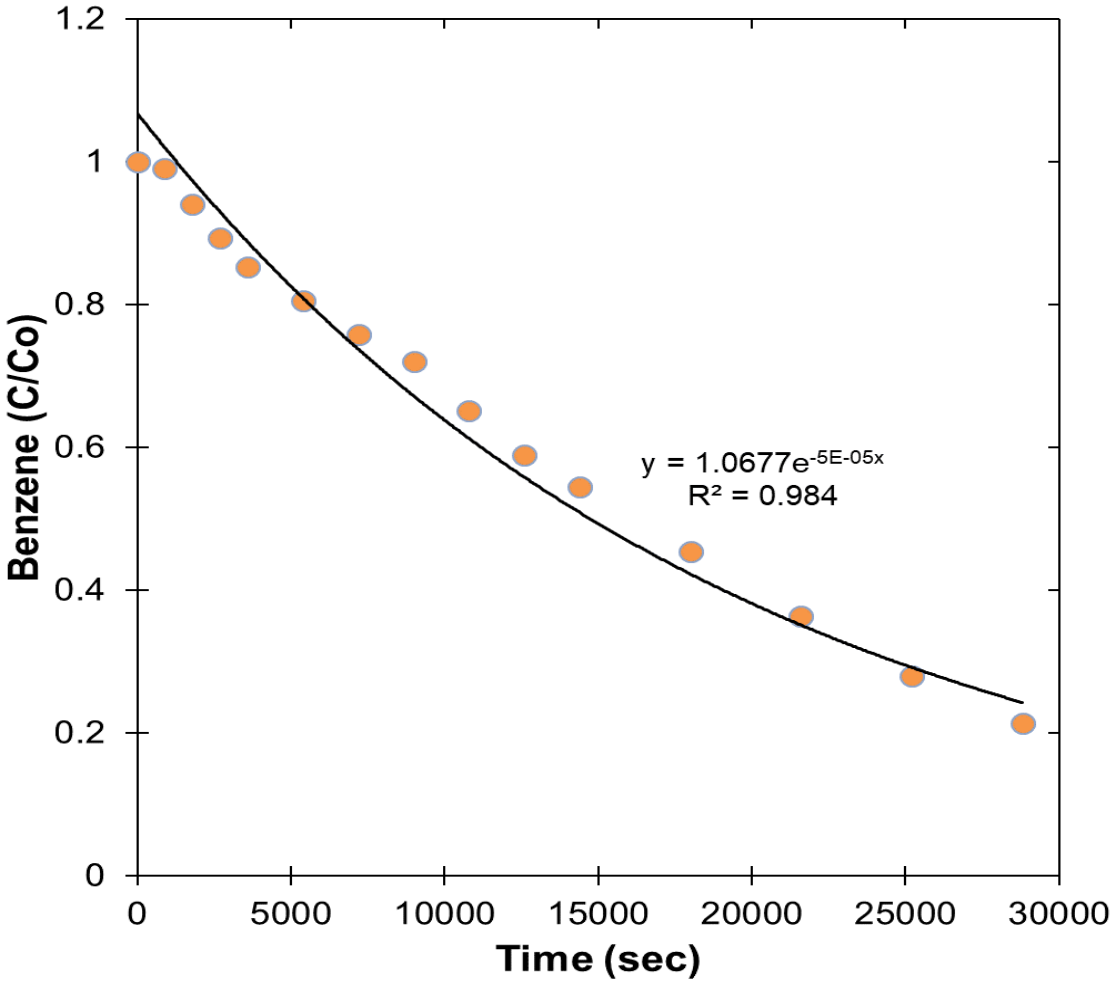

Figure 39. Benzene concentrations (Co = 0.1 mM) over time with 48-hr aged persulfate and zero-valent iron candles

6.1.4. Mesh and Solver Settings

The mesh of the model was tetrahedral and predefined as finer. There were 23143 elements in the domain with average element quality of 0.6646.

To model the real time release, transport, and reaction of sodium persulfate, the simulation was time dependent. In the time-dependent solver, implicit BDF time stepping

method, generalized minimum residual (GMRES) iterative linear system solver, and Newton's nonlinear method with constant damping factor of 0.9 were used. Before the optimization of mesh and solver settings, each model typical consumed 2 weeks to complete a simulation on a computer and only one simulation was capable run in the same time. After the optimization, typically computation time for a simulation was around 3 days in the range of 1 day to 2 weeks.

6.2. Simulation Scenarios

A basic set of simulation was conducted to investigate the influence of reaction on the radius of influence under three incoming concentration of benzene. We hypothesize the influential radius of persulfate is dependent on the concentration of contaminants in the field. A series of three incoming concentration, i.e. 0.02 mM, 1 mM, and 5 mM, was chosen. Particularly on the Textron site, the concentration of benzene was measured as around 0.02 mM in the area of slow-release candle implementation.

The second set of simulation was conducted to investigate the influence of groundwater flow velocity on the radius of influence under reaction condition. In this set of simulation, groundwater velocity was reduced to 1/10 of the groundwater velocity in the basic set of simulation. The same series of incoming benzene concentration, i.e. 0.02 mM, 1 mM, and 5 mM, was simulated.

The third set of simulation aimed to investigate the effect of increased mixing on the radius of influence due to aeration. In order to achieve better mixing and spreading, an aerator was installed at the bottom of the candle to blow air bubble and create a well-mixed flow condition surrounding the candle. Kambhu has conducted sand tank

experiments to evaluate the influence of aeration rates on the mixing. In that experiment, a permanganate candle with 6 inches high and 0.5 in diameter was installed in a tank filled with fine sand. As shown in Figure 40, when air flow rate increased from 3 mL/min to 5.3 mL/min, the transverse spreading of the permanganate increased from 7.5 cm to 10.2 cm at the location of candle after 24 hours of the release.

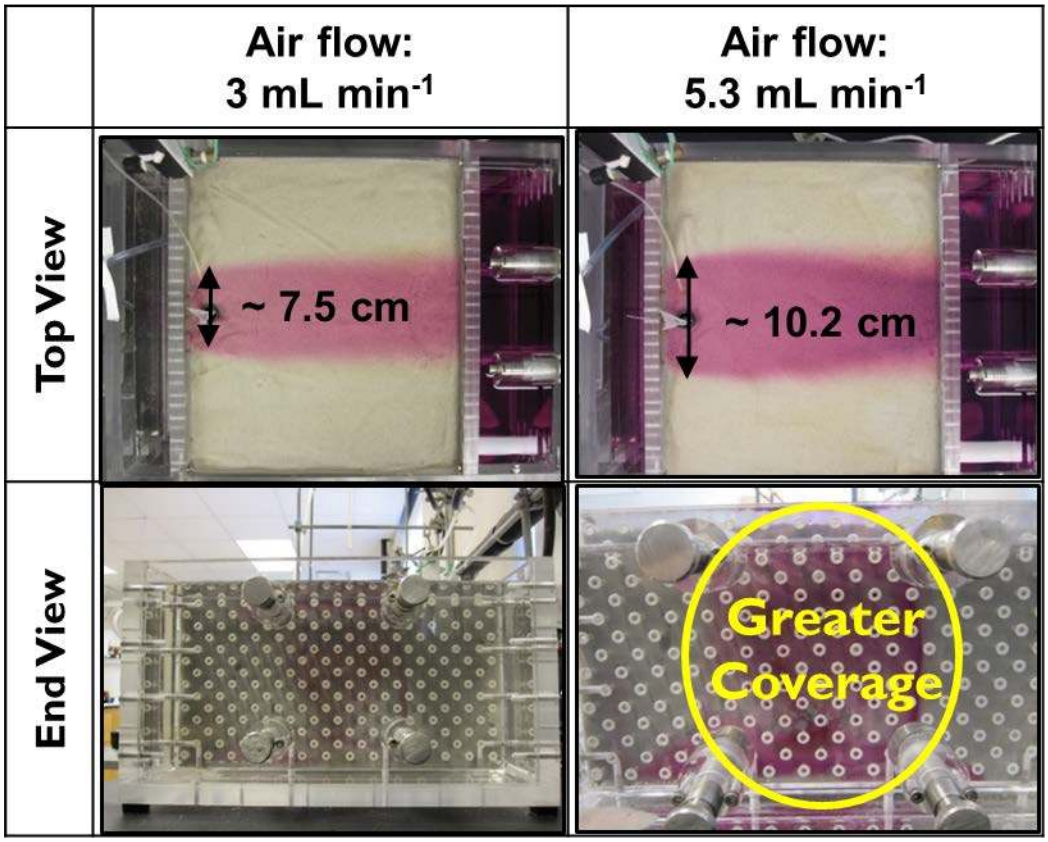

Figure 40. Influence of air rate on the lateral spreading

While a rigorous numerical model is still under development, a simplified approach was used to take into account the additional mixing created by aeration. Particularly, we assume that the aeration processes created additional mixing around the candle, which can be described by an enhanced dispersion in the area. To quantify a

dispersion enhance factor, we first examine the laboratory experiments conducted by Kambhu in Figure 40. For the release of a unit amount of solute in a two dimensional domain, the concentration distribution can be estimated as:

$$C(x,y,t) = \frac{1}{4\pi t(D_L D_T)^{0.5}} \exp\left[-\frac{(x-vt)^2}{4D_L t} - \frac{y^2}{4D_T t}\right] \quad \text{(Eq. 11)}$$

Where, $C(x,y,t)$ is the concentration at a point (x, y) at time t; D_L is the coefficient of longitudinal hydrodynamic dispersion (m^2/s); D_T is the coefficient of transverse hydrodynamic dispersion (m^2/s); v is the average linear velocity (m/s).

The standard deviation of concentration distribution started from the source can be described as:

$$\sigma_y = \sqrt{2D_T t} \quad \text{(Eq. 12)}$$

Assuming that plume dimension measured by the pictures in Figure 40 accounted for 95% of the mass, which related to two standard deviation away from the center. Based on equation 12, a transverse dispersion coefficient can be estimated as 8.07×10^{-9} m^2/s and 1.15×10^{-9} m^2/s for aeration rates of 3 mL/min and 5.3 mL/min, respectively. Typically, transverse dispersion is assumed to be 1/10 of the longitudinal dispersion. Therefore, under a groundwater flow velocity of about 3.94×10^{-6} m/s in the experiment, the longitudinal dispersivity values around the candle in the tank were estimated as 0.02 m and 0.038 m for aeration rates of 3 mL/min and 5.3 mL/min, respectively. The dispersivity measured by a tracer test conducted in the same tank using

same type of sand, however, was about 0.005m. Therefore, it is estimated that the aeration rate of 3 mL/min led to about 4 times higher mixing in the longitudinal direction in the area adjacent to the candle.

In this set of simulation, we increased the dispersivity to reflect the mixing created by the candle. Particularly, the longitudinal dispersivity of 1.2 m is used, which is 4 times of the original dispersivity used in the basic setting. Because the aerator created a well-mixed area surrounding the candle, it is reasonable to assume that the mixing in the transverse direction is now same as in the longitudinal direction, instead of typically assumed 1/10 of the longitudinal dispersivity. Therefore, a transverse dispersivity of 1.2 m is used.

6.3. Results

6.3.1 Basic Set

Figure 41 presents a top view of the simulated sodium persulfate concentration distribution at days 40, 80, 120, and 153 when no benzene is present. In comparison, Figure 42, 43, and 44 represent a top view of the simulated sodium persulfate and benzene concentration distributions (mol/m^3) at days 40, 80, 120, and 153 under different initial and incoming benzene concentration (i.e. 0 mM, 0.02 mM, 1 mM, and 5 mM). In all the conditions, sodium persulfate gradually released from the candles. Carried by the groundwater flow, the center of the sodium persulfate plume moved towards the downstream of the flow. Correspondingly, benzene was removed via the reaction with sodium persulfate.

As shown in Figure 41-44, the maximum concentration of persulfate decreased with the increase of initial and incoming benzene concentration. For example, the maximum concentration were around 6.5 mM, 6.4 mM, 6.1 mM, and 2 mM at 153 days under 0 mM, 0.02 mM, 1 mM, and 5 mM benzene, respectively. In addition, increased initial and incoming concentration of benzene decreased the distribution area of persulfate in both longitudinal and transverse directions. For example, persulfate plume at 153 days almost reached the entire domain with 0.02 mM benzene while it spread only 1/6 of the domain with 5 mM benzene. The change of the maximum persulfate concentration and the distribution area were consistent with the benzene concentration, relevant reaction and transport processes. Because the flow velocity and dispersivity were constant, the accumulation/depletion of sodium persulfate depended on the magnitude of the reaction. Persulfate and benzene reaction was simulated as a first order reaction (i.e. Eqs. 10), where the reaction rate was linked with the concentration of benzene. An increased concentration of benzene led to increased reaction rate, more sodium persulfate consumption, and reduced mass of persulfate left in the field.

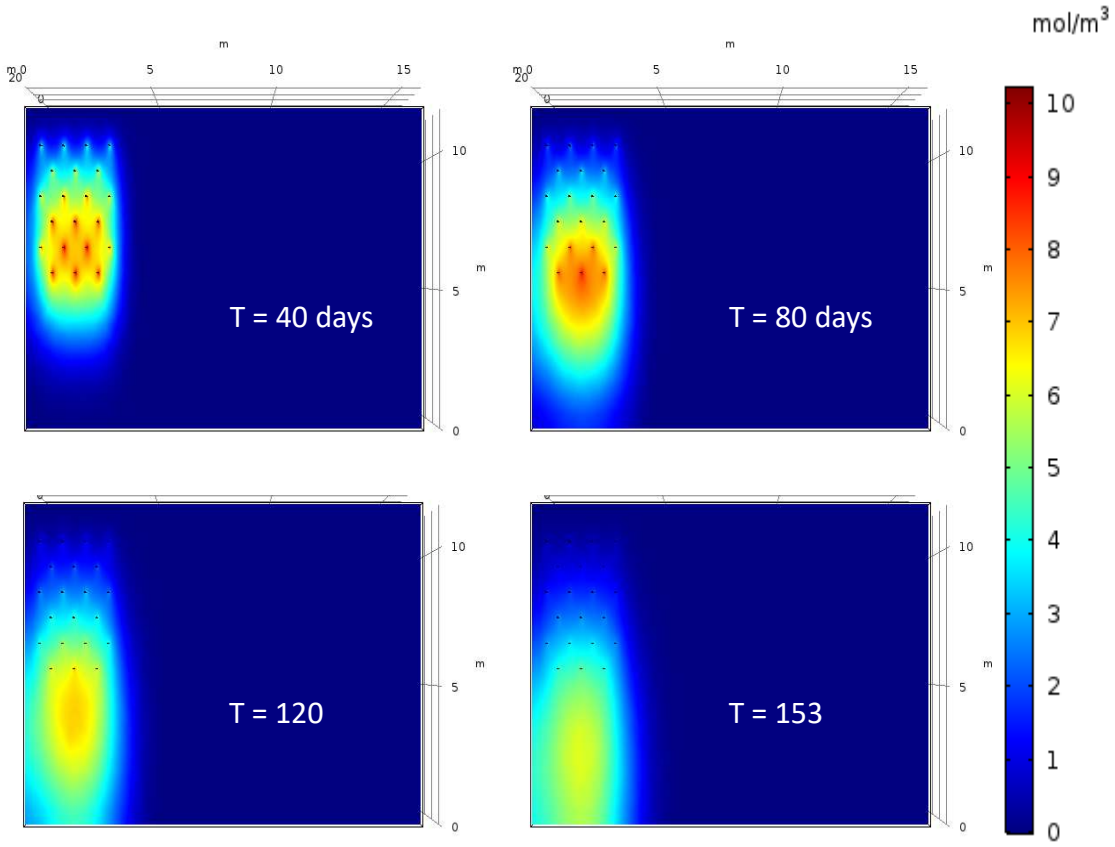

Figure 41. Concentration of sodium persulfate at day 40, 80, 120, and 153 without benzene (flow direction is from top to the bottom)

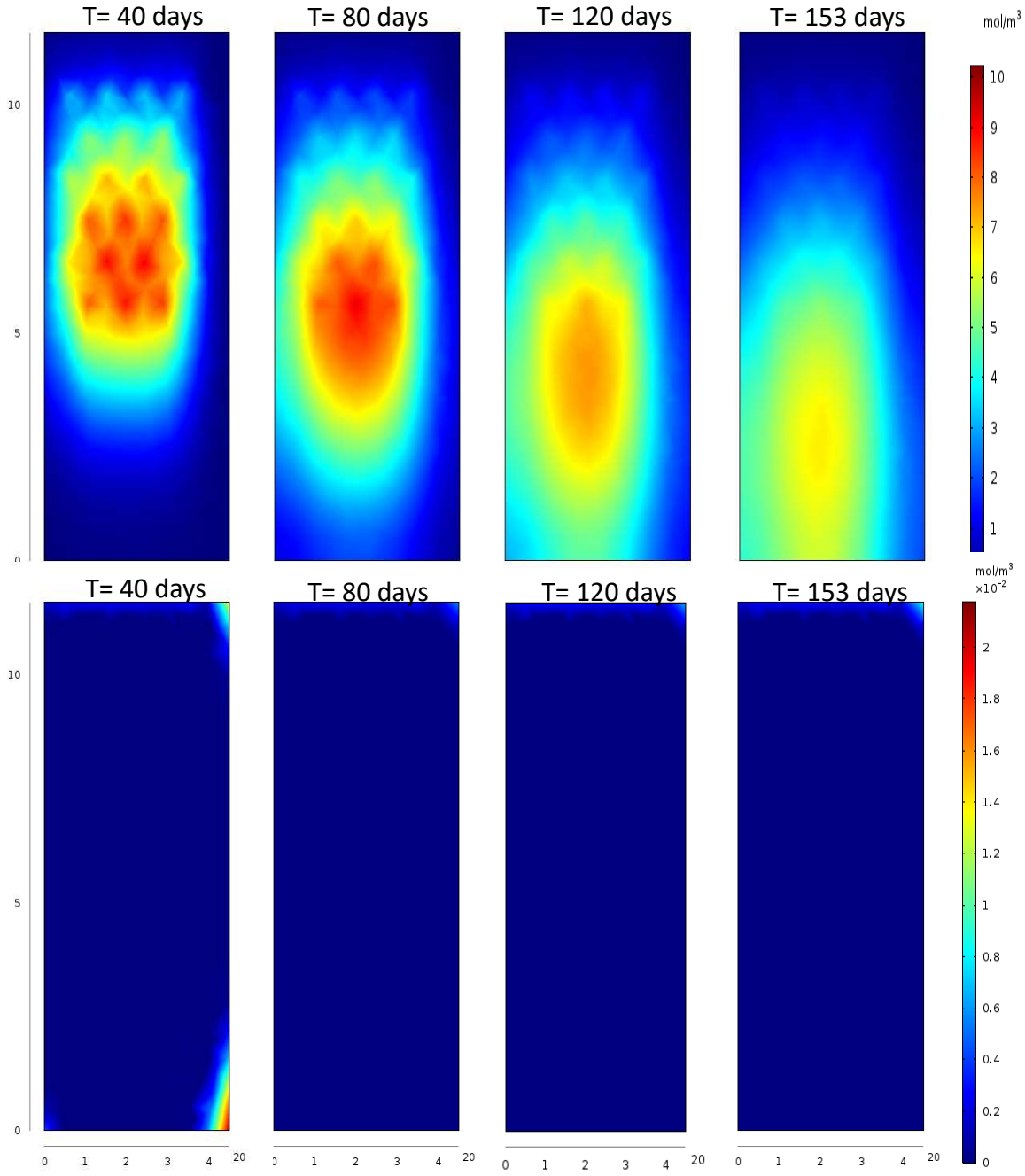

Figure 42. Basic set: First row shows concentration of persulfate at day 40, 80, 120, and 153 with 0.02 mM initial and incoming concentration of benzene. Second row shows concentration of benzene at days 40, 80, 120, and 153 (flow direction is from top to the bottom)

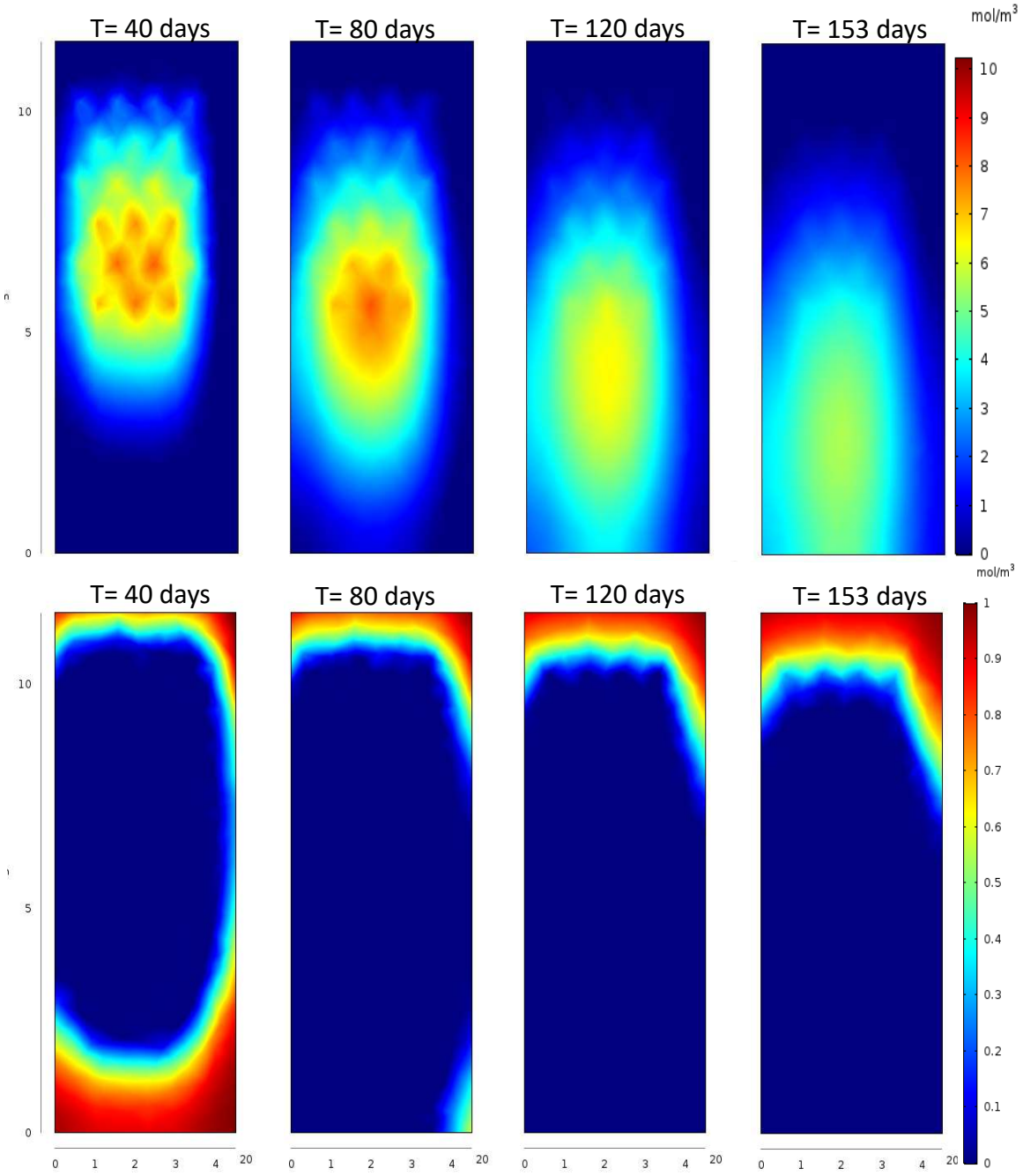

Figure 43. Basic set: First row shows concentration of persulfate at day 40, 80, 120, and 153 with 1 mM initial and incoming concentration of benzene. Second row shows concentration of benzene at days 40, 80, 120, and 153 (flow direction is from top to the bottom)

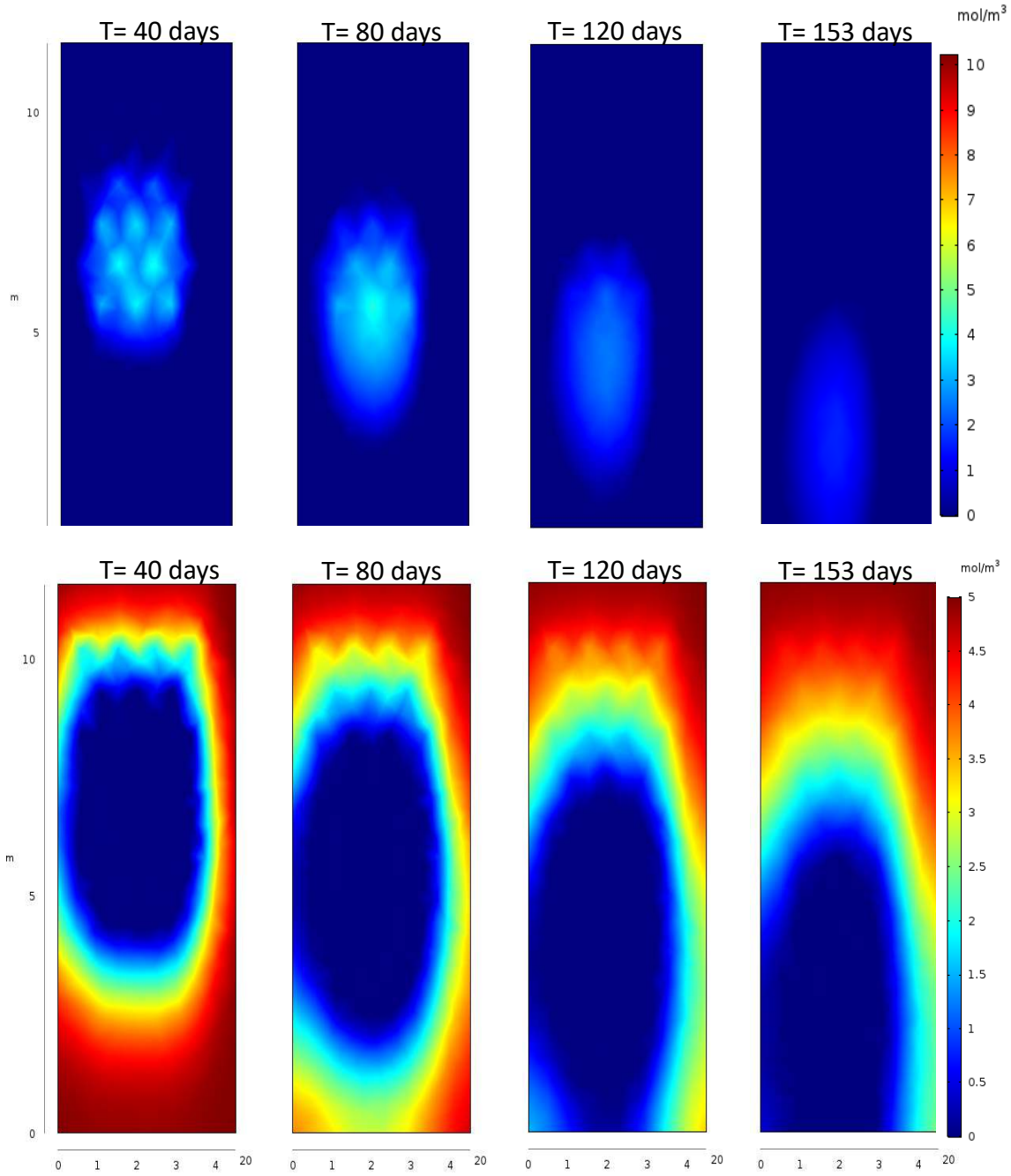

Figure 44. Basic set: First row shows simulated concentration of persulfate at day 40, 80, 120, and 153 with 5 mM initial and incoming concentration of benzene. Second row shows concentration of benzene at days 40, 80, 120, and 153 (flow direction is from top to the bottom)

Figure 45 and Figure 46 present radius of influence of a candle on the right most position of the first and fifth rows, respectively. Here, the radius of influence was defined as the distance between the center of candle and the location that sodium persulfate concentration is 1 mM in the transverse direction. Various examined concentrations have different results about radius of influence. However, the trend of change is predictable. To better analyze the data in this chapter, an arbitrary number, 1 mM, was chosen. As expected, the radius of influence reduced with increase of concentration of benzene. Under the smaller concentration of benzene, less amount of persulfate released from candle was consumed; therefore, it can be transported further in the domain. For example, the radius of influence on the first row with 0.02 mM benzene reached as high as 35 cm in the transverse direction around day 20. The maximum radium of influence on the first row with 1 mM was only 10.8 cm at day 10. When the benzene concentration was 5 mM, all persulfate released from the candle was consumed right away.

In the first row (Figure 45), the radius of influence for the candle in the first row always sharply reached a maximum and then quickly reduced. For initial benzene concentrations of 0, 0.02 mM, and 1 mM, some persulfate that was not consumed by benzene in the first several rows moved downstream. Therefore, the radius of influence of the candle showed a longer increasing trend before it started to reduce and more benzene downstream can be removed. As shown in Figure 46, until 150 days, the concentration of persulfate is higher than 1 mM within 0.45 m away from the candle when incoming benzene concentration is 0.02 mM. For the incoming benzene concentration of 1 mM, the highest radius of influence is 0.36 m after 60 days in the fifth

row. Considering a distance of about 1 meter between two candles, there is a gap between the two candles that has a persulfate concentration lower than 1 mM. For initial benzene concentration of 5 mM, however, all persulfate was consumed as soon as it was released. Therefore, the persulfate concentration is lower than 1 mM everywhere between the two candles in the fifth row. This analysis indicated that the effectiveness of candle based on the current position strategy is dependent on the incoming contaminant concentration.

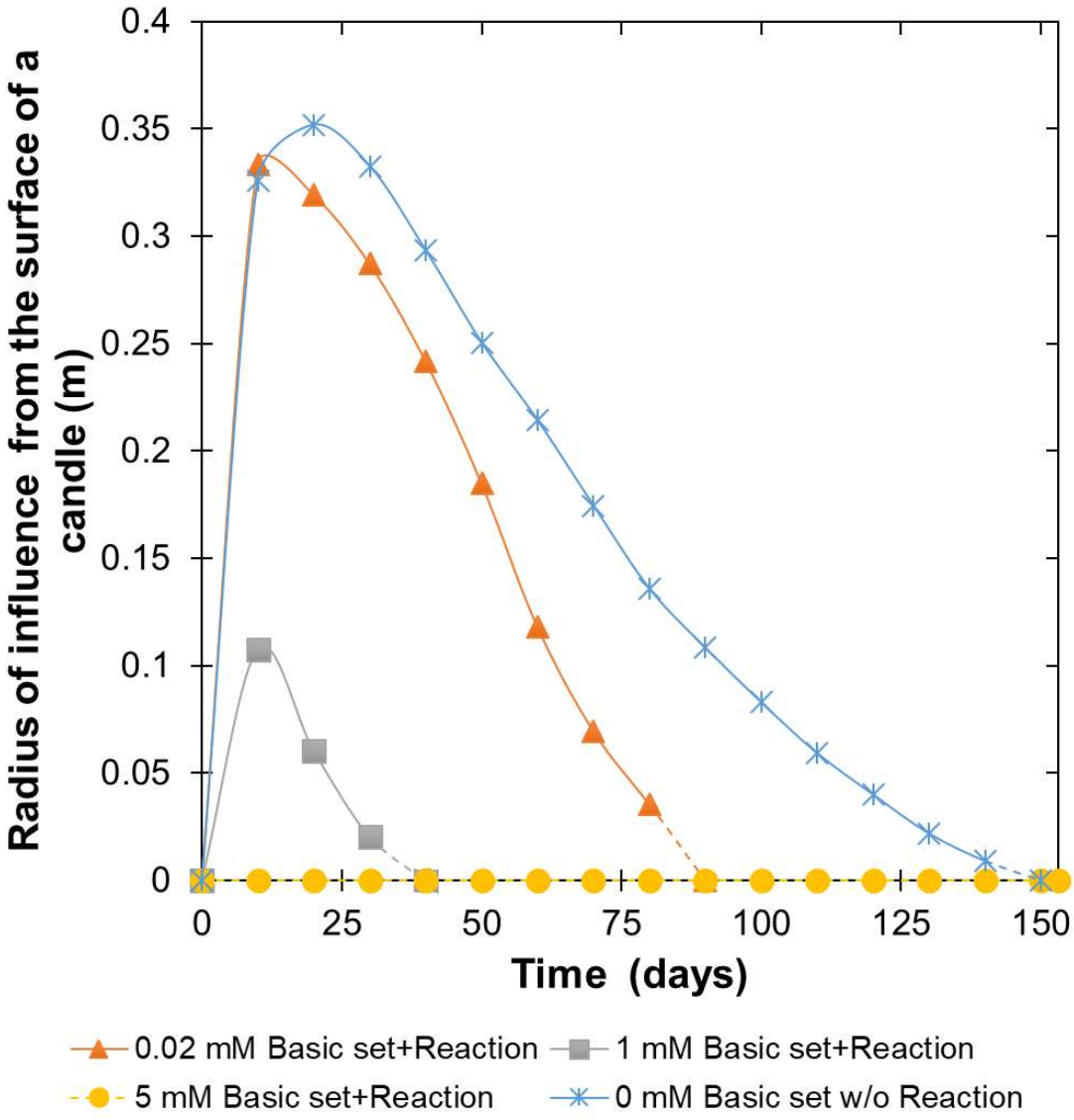

Figure 45. Basic set: The radius of influence of a candle on the right of the first row in the transverse direction over time via various concentration of benzene

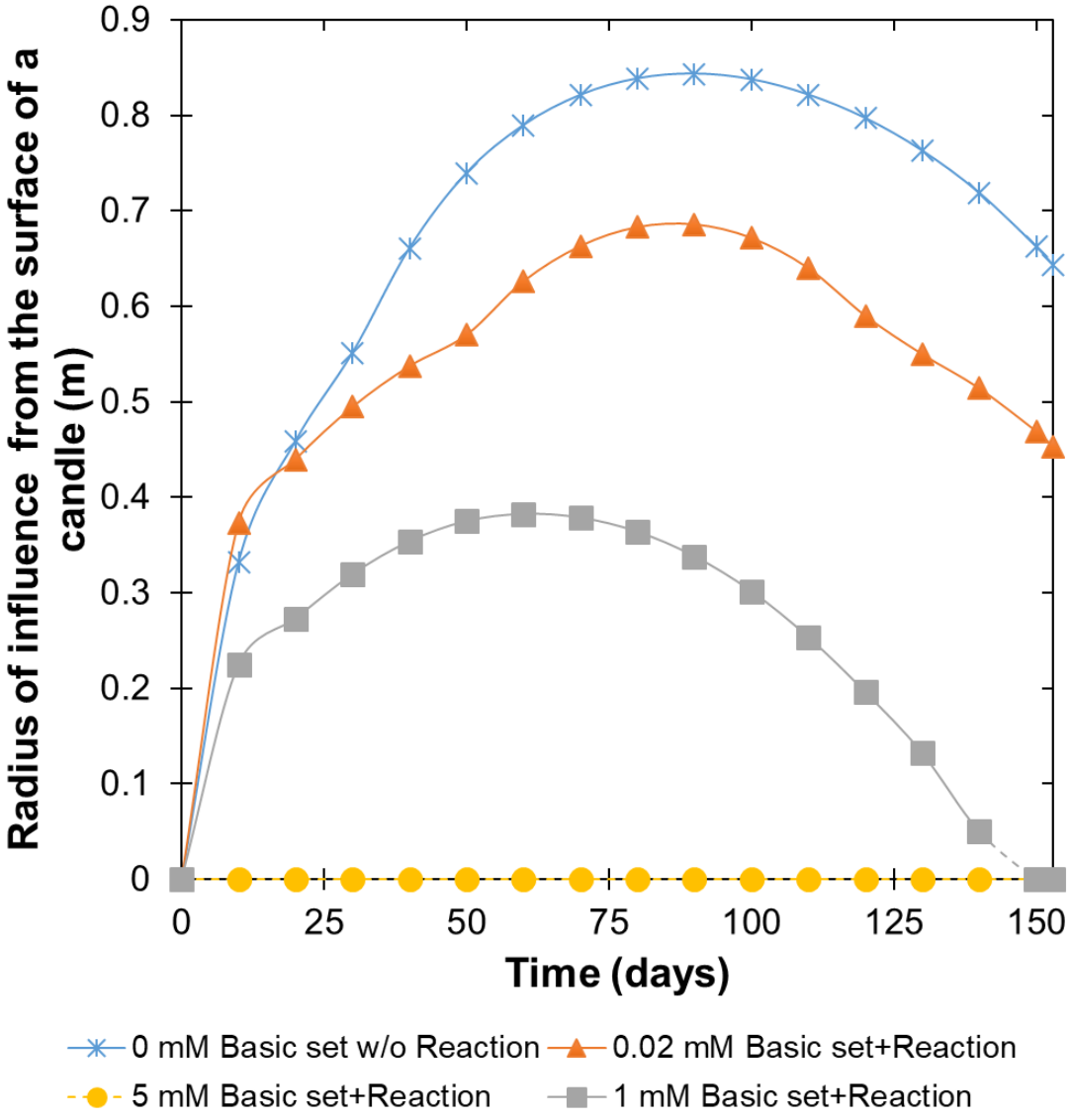

Figure 46. Basic set: The radius of influence of a candle on the right of the fifth row in the transverse direction over time via various concentration of benzene

6.3.2 Reduced Velocity Scenarios

Figure 47, Figure 48, and Figure 49 present a top view of simulated sodium persulfate and benzene concentration distributions (mol/m^3) under a lower groundwater (1/10 of the basic set), at days 40, 80, 120, and 153 with different initial and incoming benzene concentration (i.e. 0.02 mM, 1 mM, and 5 mM). As expected, increased concentration of benzene consumed more released persulfate, and led to reduced persulfate concentration in the field. Due to the reduced groundwater velocity, the plumes of persulfate did not move towards downstream as fast as the basic set of simulation (Figure 42, 43, and 44). In addition, we observed that the sodium persulfate plume at day 153 reached the upstream boundary and removed incoming 0.02 mM benzene (Figure 47). The concentration of persulfate moved to the adjacent upstream of the field was due to the dispersion effect, which is relatively more important under 10 times lower groundwater velocity. However, the amount of persulfate dispersed to the upstream was not able to remove the incoming benzene with a 5 mM initial concentration (Figure 49).

Figure 50 presents the radius of influence of a candle on the right of the first row in the transverse direction over time under various benzene concentrations for both the basic set and the reduced velocity set. For each examined benzene concentration, the radius of influence on the first row was higher under the lower velocity than that in the basic set. Particularly for the scenario with 5 mM incoming benzene concentration, the radius of influence was zero under the basic set. Under the lower velocity condition, the radius of influence reached as high as 0.2 m after about 20 day when incoming benzene concentration was 5 mM. This is consistent with the magnitude of the groundwater

velocity. Decreased groundwater velocity reduced the mass of persulfate carried by the advection and enhanced the lateral spreading. Correspondingly, the radius of influences were constantly increasing until 150 days of the implementation for scenarios with lower incoming concentrations of 0.02 mM and 1 mM, indicating that the all areas between candles in the first row kept a higher than 1 mM persulfate concentration. Obviously, the slow-release system was a more efficient and economic-wisely way to treat the contaminants in the low-permeable zone.

Figure 51 represents the radius of influence of a candle on the right of the fifth row in the transverse direction over time via various concentration of benzene for both the basic and reduced velocity sets. As explained previously, the radius of influence on the fifth row was expected to be higher than that of the first row due to the accumulation of the amount of persulfate not consumed by benzene from upstream. The radius of influence of the candle in the fifth row was higher than that in the basic set with 1 or 5 mM incoming benzene concentration. However, it is smaller than the basic set with 0.02 mM incoming benzene concentration up until 130 days. That is because it would take longer for extra amount of unconsumed benzene to move downstream under lower velocity conditions.

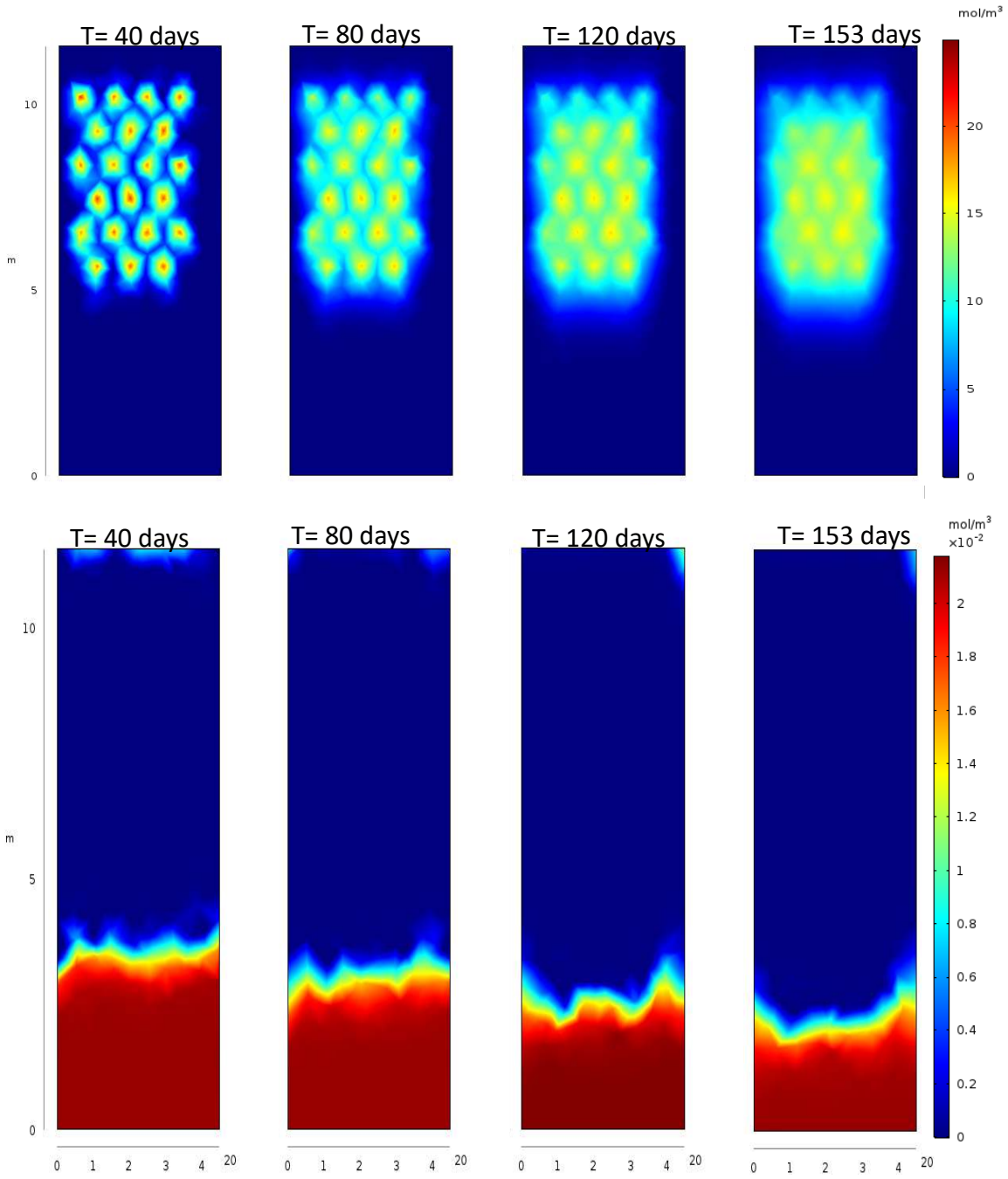

Figure 47. Velocity set: First row shows concentration of persulfate at days 40, 80, 120, and 153 with 0.02 mM initial and incoming concentration of benzene. Second row shows concentration of benzene at day 40, 80, 120, and 153 (flow direction is from top to the bottom)

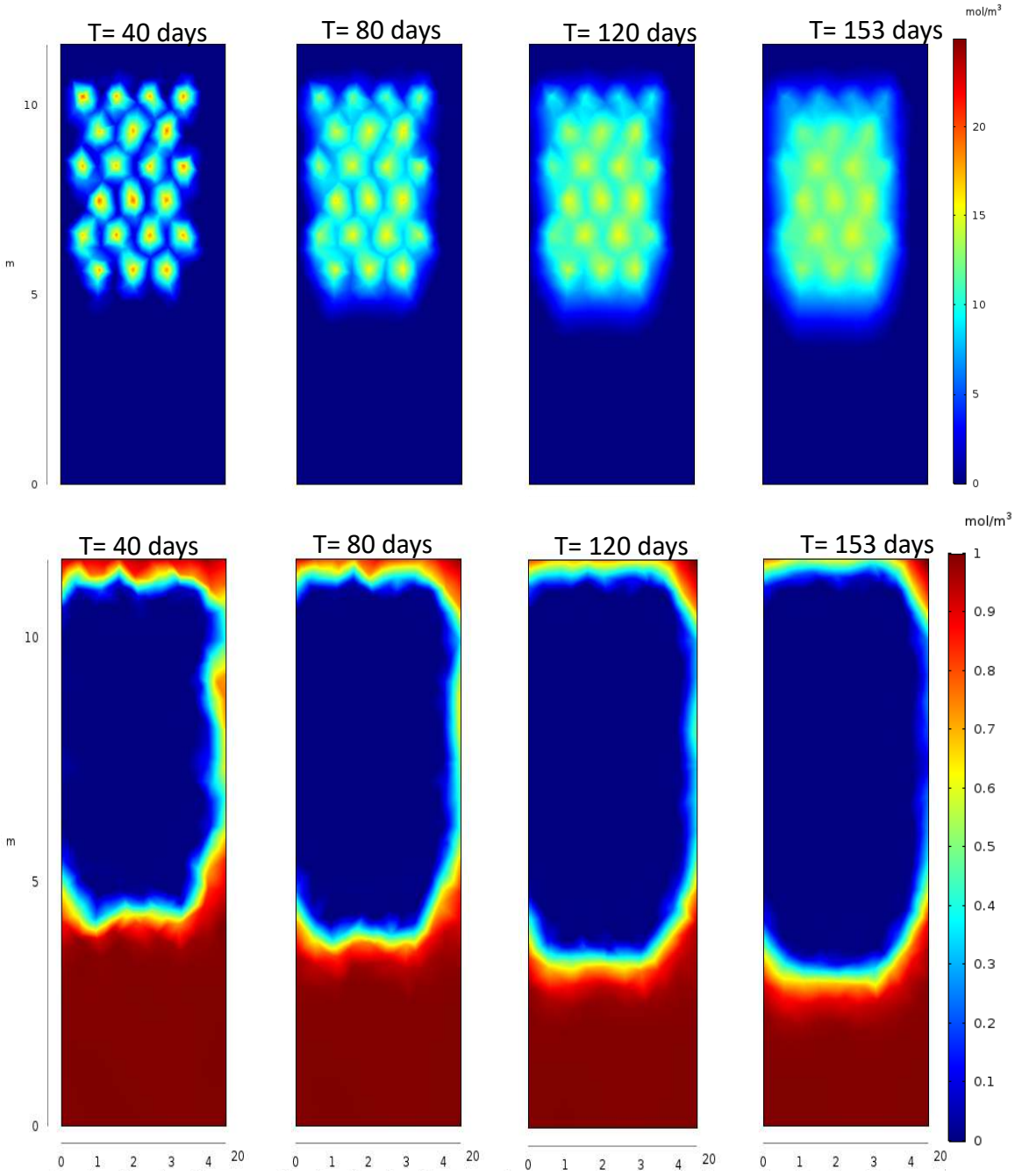

Figure 48. Velocity set: First row shows concentration of persulfate at days 40, 80, 120, and 153 with 1 mM initial and incoming concentration of benzene. Second row shows concentration of benzene at day 40, 80, 120, and 153 (flow direction is from top to the bottom)

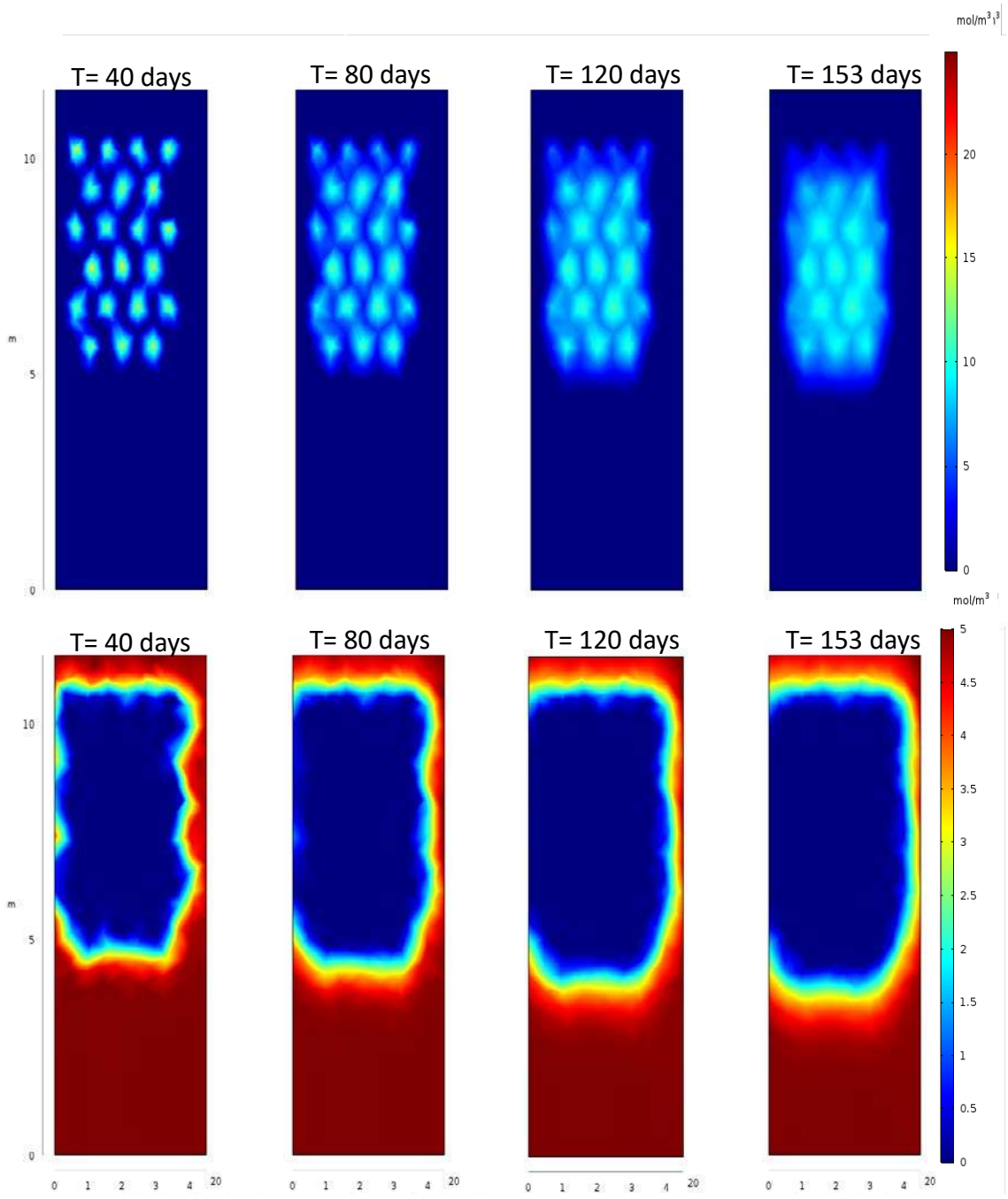

Figure 49. Velocity set: First row shows concentration of persulfate at days 40, 80, 120, and 153 with 5 mM initial and incoming concentration of benzene. Second row shows concentration of benzene at day 40, 80, 120, and 153 (flow direction is from top to the bottom)

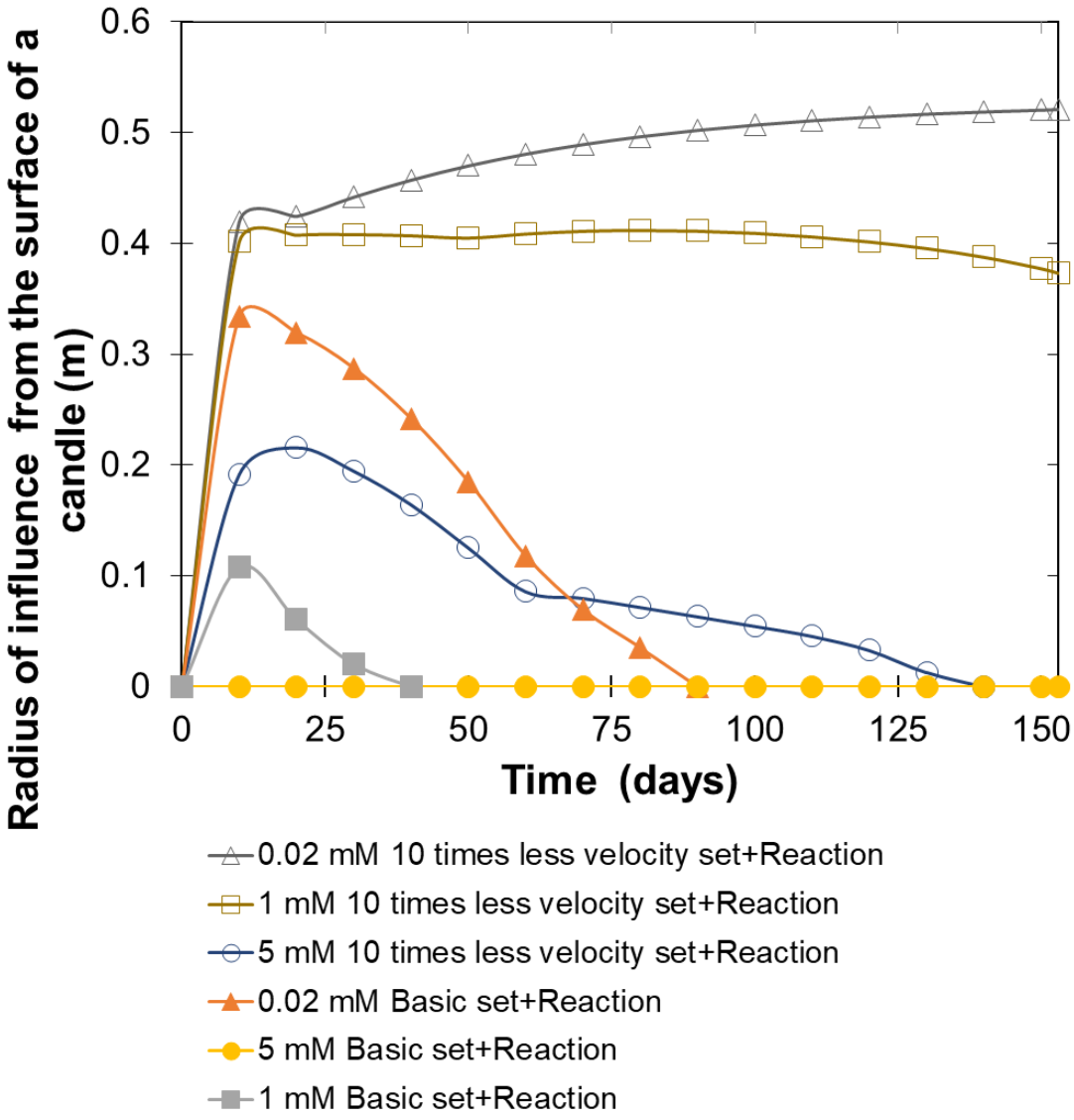

Figure 50. Velocity & Basic set: The radius of influence of a candle on the right of the first row in the transverse direction over time via various concentration of benzene

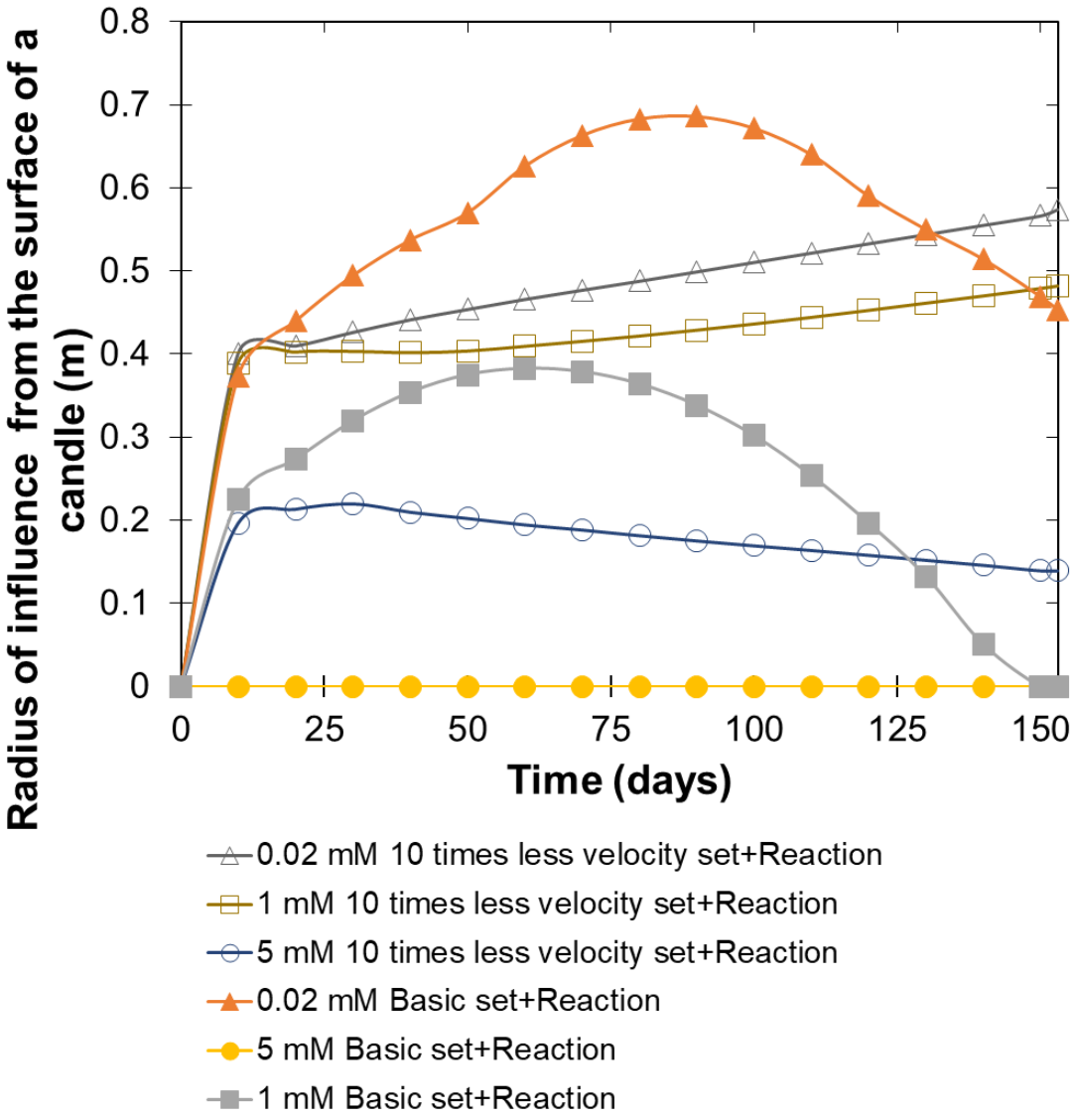

Figure 51. Velocity & Basic set: The radius of influence of a candle on the right of the fifth row in the transverse direction over time via various concentration of benzene

6.3.3 Enhanced Aeration Scenarios

Figure 52 and Figure 53 present a top view of sodium persulfate and benzene concentration distributions at days 40, 80, 120, and 153 under enhanced aeration condition with different initial and incoming concentration of benzene (i.e. 0.02 mM and 1 mM). As expected, increased concentration of benzene consumed more released persulfate, and led to reduced persulfate concentration in the field. In this set, the mixing due to aeration was simulated by an increased dispersion coefficient in both longitudinal and transverse directions. As a result, sodium persulfate quickly mixed with water adjacent to the candles as soon as they were released. Compared with the basic set (Figure 42, and 43), sodium persulfate is much better dispersed with lower concentration in the area. In the basic set (Figure 42, 43, and 44), the maximum concentrations were around 6.4 mM, 6.1 mM, and 2 mM at 153 days under 0.02 mM, 1 mM, and 5 mM benzene, respectively. In the enhanced aeration set, the maximum concentrations were 3.8 mM, 2.5 mM. In addition, due to enhanced dispersion/mixing, a small amount of persulfate dispersed to the upstream boundary, which was able to remove incoming benzene at the boundary when concentration is 0.02 mM.

Figure 54 presents the radius of influence of a candle on the right of the first row in the transverse direction over time via various concentration of benzene under both the basic and the aeration sets. Surprisingly, the radius of influence for 1 mM incoming benzene concentration under the aeration scenario was zero from the beginning to the end of simulation. This indicates that the concentration of persulfate was constantly lower than 1 mM in the transverse direction of the candle. As soon as persulfate was released

from the candle, it reacted with benzene in the field. Due to the enhanced mixing, the persulfate concentration was lower than the basic set. After reacting with 1 mM concentration benzene, the concentration of persulfate was reduced to less than 1 mM. Therefore, the radius of influence, by its definition, was reduced to zero. For 0.02 mM incoming benzene concentration in the aeration set, removal of the benzene did not consume as much of persulfate. The radius of influence on the first row extended out of the simulation domain, or at least 1.15 m, which was at least 3 times higher than that in the basic set (i.e. 0.33 m). It took about 110 days for the radius of influence reduce to zero, corresponding to 90 days for the basic set under the same incoming benzene concentration.

Figure 55 presents the radius of influence of a candle on the right of the fifth row in the transverse direction over time via various concentration of benzene under both the basic and the aeration sets. As explained previously, the radius of influence on the fifth row was expected to be higher than that of the first row due to the accumulation of the amount of persulfate not consumed by benzene from upstream. For an instance, after about 10 days of operation, the radius of influence in the fifth row for 0.02 mM benzene in the aeration set were generally extended out of the domain, or at least 1.15 m, which was at least 1.67 times bigger than that in the basic set (i.e. 0.33 m). It is important to point out that, the aeration resulted in lower concentration in the area. When incoming benzene concentration is relatively high (e.g. 1 mM), reacting with benzene will further reduce the concentration of persulfate, which could lead to a delay of persulfate mass accumulation in the fifth row and a decrease of the influential radius. For example, it took

about 20 more days to establish the radius of influence in the fifth row, and the radius of influence lasted only until about 100 days. After that, the concentration of persulfate adjacent to the candle in the fifth row reduced to less than 1 mM. In comparison, the radius of influence in the fifth row lasted for about 150 days in the basic set with 1 mM incoming benzene concentration.

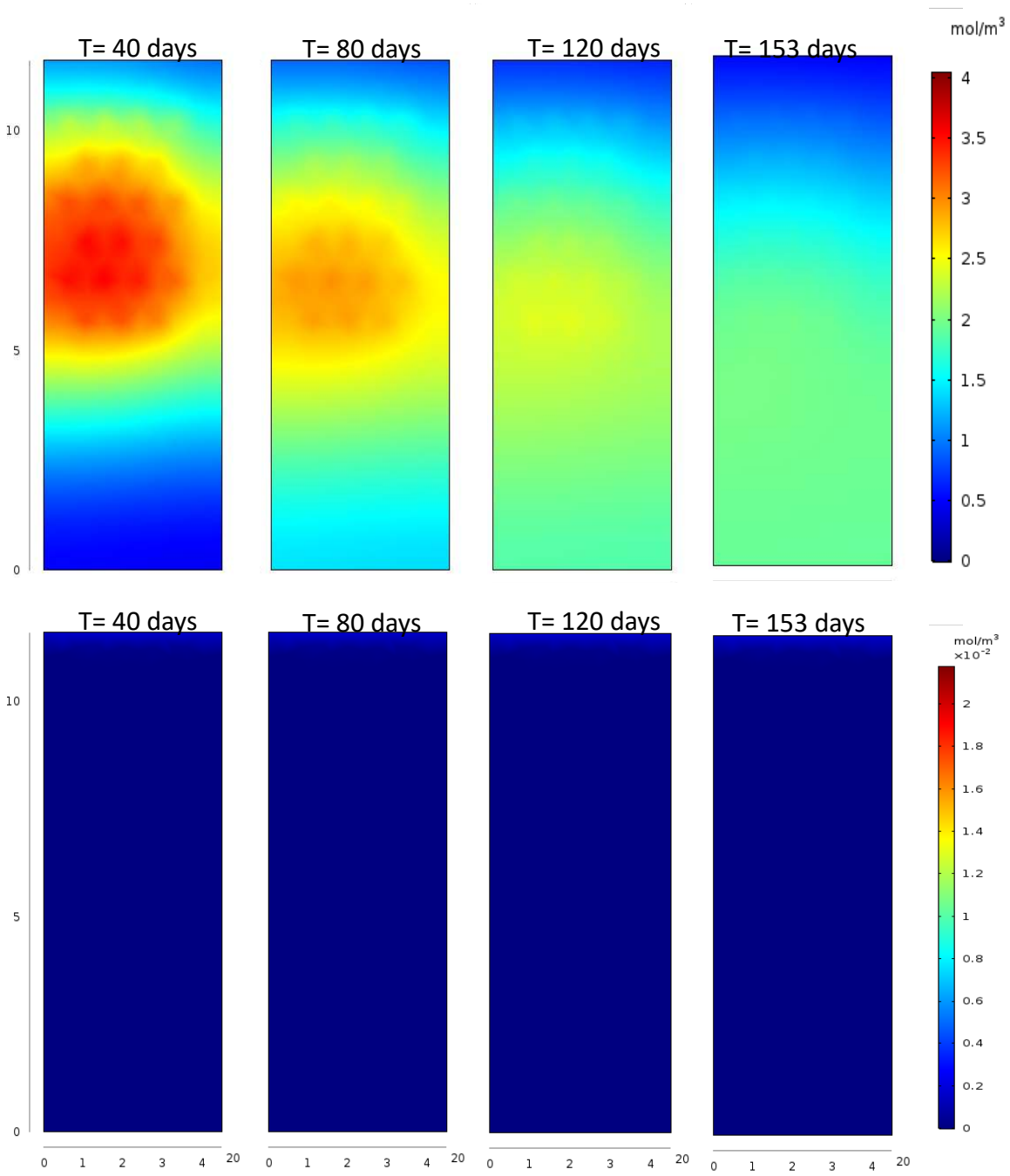

Figure 52. Aeration set: First row shows concentration of persulfate at day 40, 80, 120, and 153 with 0.02 mM initial and incoming concentration of benzene. Second row shows concentration of benzene at day 40, 80, 120, and 153 (flow direction is from top to the bottom)

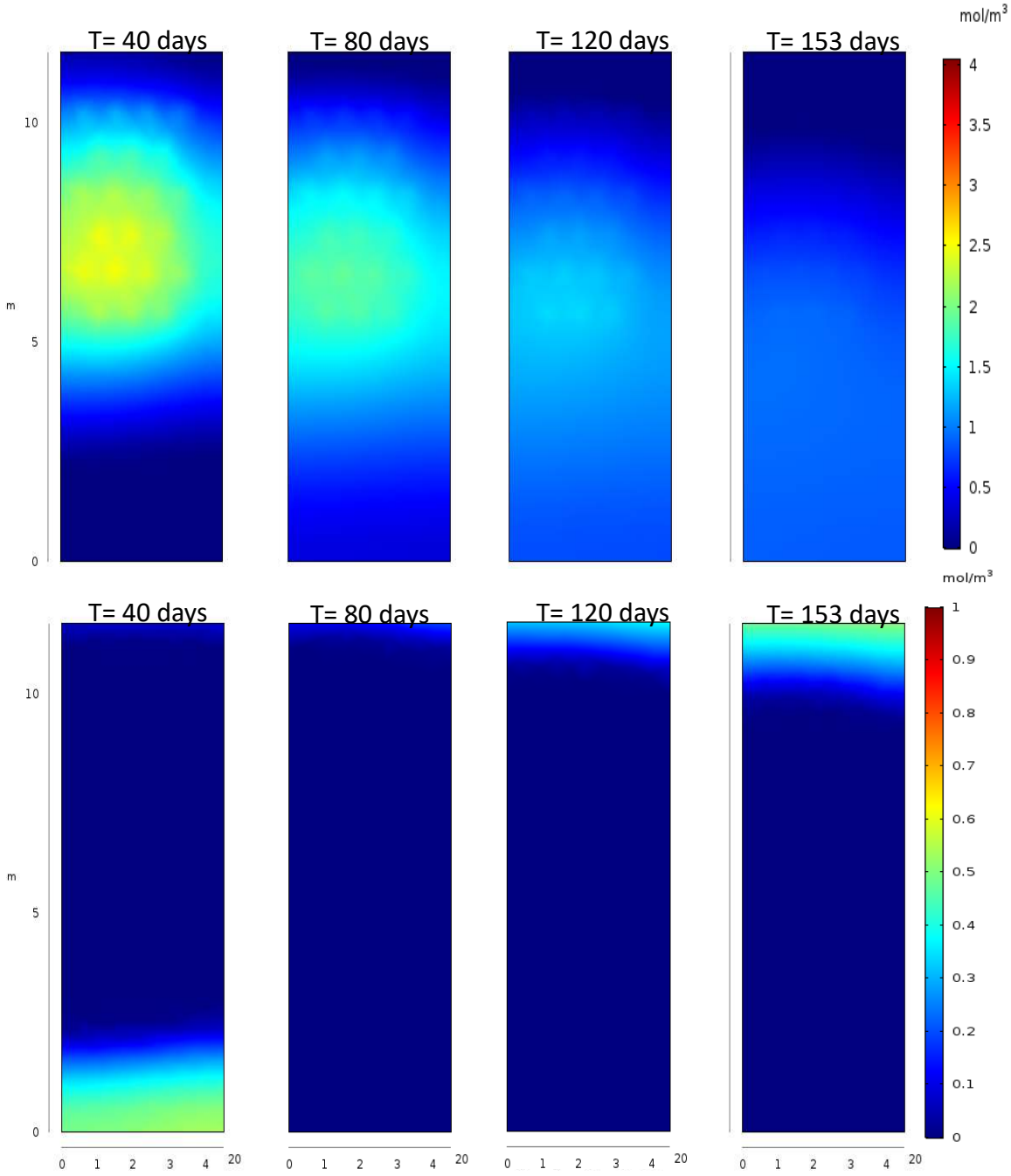

Figure 53. Aeration set: First row shows concentration of persulfate at day 40, 80, 120, and 153 with 0.02 mM initial and incoming concentration of benzene. Second row shows concentration of benzene at day 40, 80, 120, and 153 (flow direction is from top to the bottom)

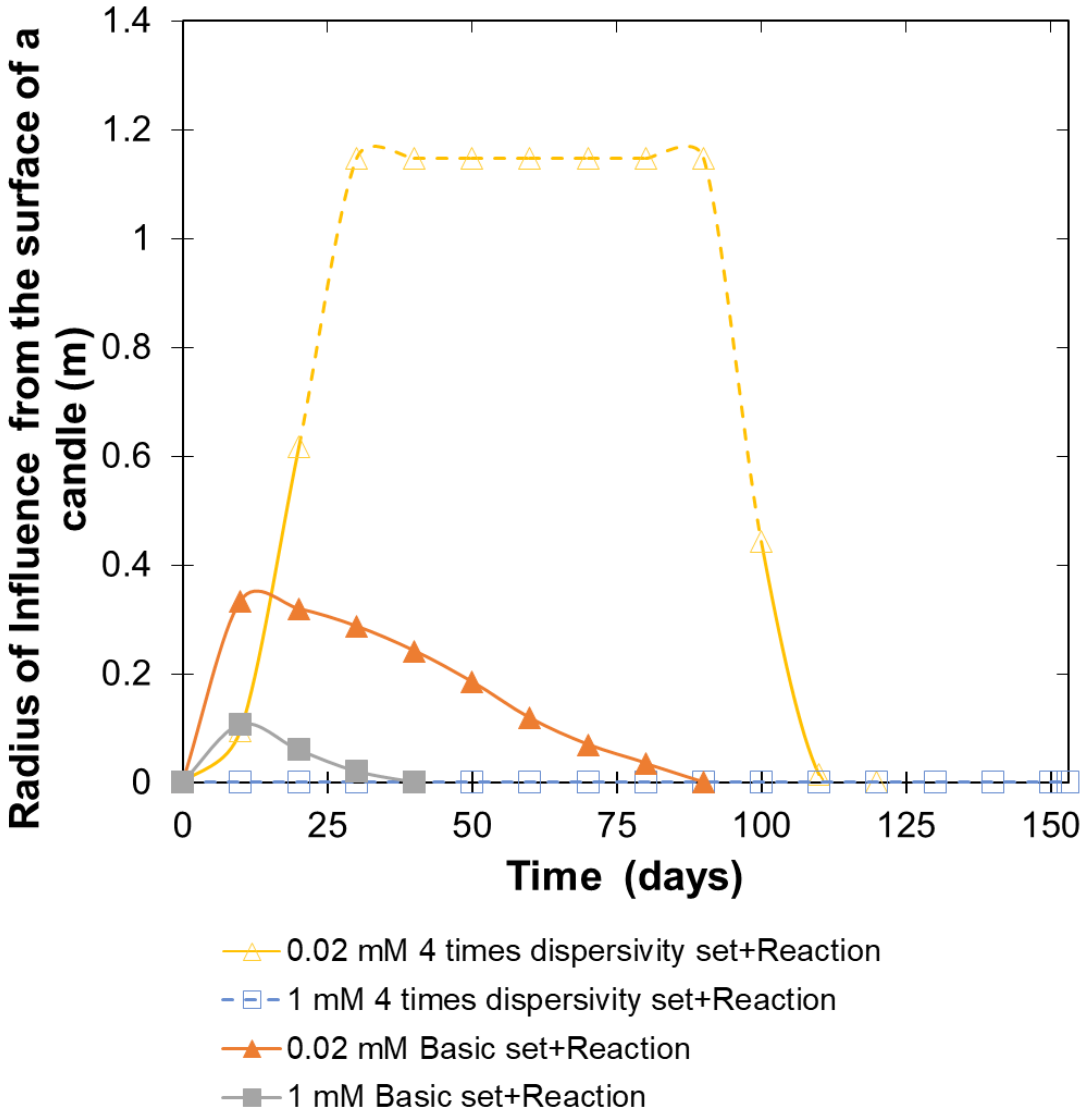

Figure 54. Aeration & Basic set: The radius of influence of a candle on the right of the first row in the transverse direction over time via various concentration of benzene. Dash lines meant the connection had artificial data point where the radius of influence was zero or its maximum was out of the simulation domain.

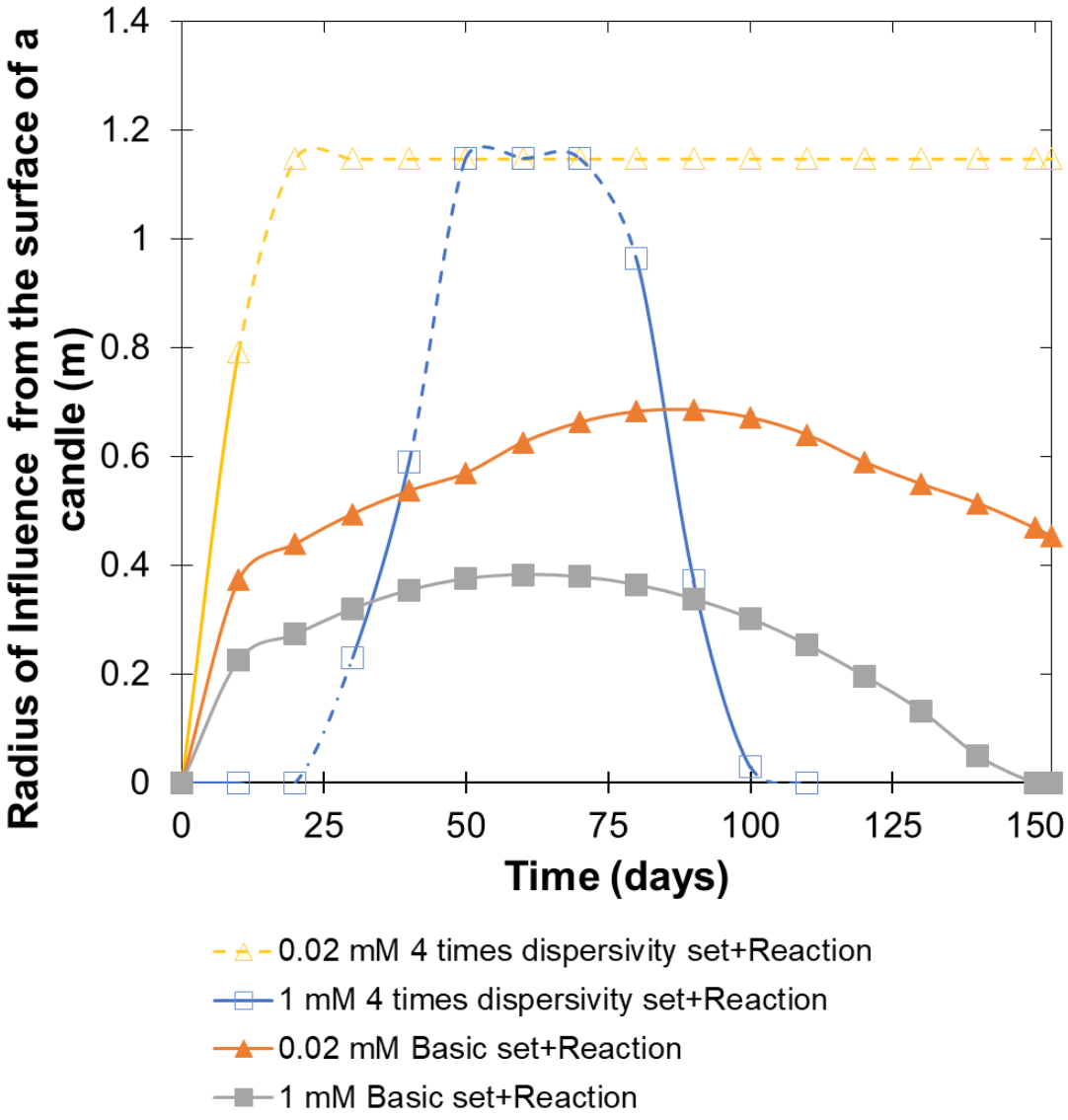

Figure 55. Aeration & Basic set: The radius of influence of a candle on the right of the first row in the transverse direction over time via various concentration of benzene. Dash lines meant the connection had artificial data point where the radius of influence was zero or its maximum was out of the simulation domain.

6.4. Conclusion

To understand sodium persulfate release and transport in the field site, COMSOL Multiphysics 5.3 was used to develop a model under three scenarios: I) three incoming concentrations of benzene; II) 10 times slower groundwater velocity scenarios; III) enhanced aeration scenarios.

Simulation results from all conditions were consistent with basic theories and expectations. The relative contribution of reaction and transport processes (i.e. advection and dispersion) determined the accumulation/depletion of sodium persulfate. In the basic set with various incoming concentrations, the reaction between persulfate and incoming benzene largely determined the mass and distribution of persulfate in the field. However, in the groundwater velocity set and the aeration set, advection and dispersion played a dominant role. In the reduced velocity set, the radius of influence of a candle was higher than the basic set, and they kept relatively constant at a high value for both 0.02 mM and 1 mM benzene. This indicates that it is possible to optimize the system to use less rows of candles and/or increase the distance between candles in the low permeability zone. In the comparison with basic and aeration sets, enhanced aeration could increase or decrease the radius of influence of a candle, dependent on the incoming contaminant concentration. When incoming contaminant concentration is not very high, enhanced aeration greatly increased the radius of influences, so that distances between the candles can be increased. When incoming contaminant concentration is very high, enhanced aeration rate could reduce the concentration of the persulfate, and reduce the radius of influences. Double checking the sufficient mass left for later spreading was a key to determine the

remediation efficacy or control the aeration rate in a suitable range. In the slow-release system design, if extra supply of oxidant in a candle was considered and suitable aeration rates was designed, the demand of boring and labor work could be greatly reduced by using larger interval distances. The effective duration time could also be increased.

To apply this model to offer rough spacing suggestions in a new site, initial and incoming contaminants concentration, groundwater velocity, and air flow rate were the key factors. Based on the contaminants concentration and stoichiometry of oxidants and contaminants, required mass of oxidants could be calculated. If we coupled that with typical diffusion coefficient of a candle, release model could yield optimized release rate. After inputting release rates and remaining key factors in COMSOL, radius of influence could be obtained to optimize the slow-release candles design.

References

Hussain, I., Zhang, Y., Huang, S., & Du, X. (2012). Degradation of 2,4-chloroaniline by persulfate activated with zero-valent iron. *Chemical Engineering Journal*, *203*(16), 269–276. https://doi.org/10.1016/j.cej.2012.06.120

Kambhu, A., Comfort, S., Chokejaroenrat, C., & Sakulthaew, C. (2012). Developing slow-release persulfate candles to treat BTEX contaminated groundwater. *Chemosphere*, *89*(6), 656–664. https://doi.org/10.1016/j.chemosphere.2012.06.004

Liu, H., Bruton, T. A., Li, W., Buren, J. Van, Prasse, C., Doyle, F. M., & Sedlak, D. L. (2016). Oxidation of Benzene by Persulfate in the Presence of Fe(III)- and Mn(IV)-Containing Oxides: Stoichiometric Efficiency and Transformation Products. *Environmental Science and Technology*, *50*(2), 890–898. https://doi.org/10.1021/acs.est.5b04815

Chapter 7

Summary and Conclusions

Although Lee's model (Lee, Liu, Schwartz, Kim, & Ibaraki, 2008) provided a way to investigate the slow-release system with basic physics (i.e. 2D simulation, constant oxidant release, w/o dispersion, and constant decay as reaction rate), some over simplifications could lead to bad judgments. In this work, a much more comprehensive model, considering realistic release kinetics, reactions, aquifer properties, and/or aeration was developed using COMSOL Multiphysics 5.3.

Following main tasks were accomplished in this thesis:

I. Developed an approach to simulate realistic release kinetics of sodium persulfate in the field;
II. Incorporated benzene and sodium persulfate reaction with the transport model ;
III. Evaluated the influence of aquifer properties (i.e. sand and clay and sand and gravel media) on the radius of influence of slow-release persulfate candles;
IV. Evaluated the influence of concentration of contaminants in the field on radius of influence of slow-release persulfate candles;
V. Evaluated the influence of groundwater velocity on radius of influence of slow-release persulfate candles;

VI. Evaluated the influence of aeration on radius of influence of slow-release persulfate candles.

Simulated results from both conditions were consistent with basic theories and expectations. Correspondingly, there were seven conclusions and suggestions:

I. In the sand and gravel aquifer with high groundwater velocity, sodium persulfate would be quickly flushed away immediately after release, which leaves almost nothing for remediation. That indicates that controlled release candles are not suitable for aquifer with high flow rate, such as sand and gravel aquifer;

II. For the radius of influence in the sand and clay aquifer, higher the required concentration of the sodium persulfate, smaller the radius of influence was.

III. When the spacing between a row is smaller than required radius of influence, increasing the spacing of the later rows or decreasing the amount of sodium persulfate in the candle was suggested in the economical wise consideration;

IV. In the basic set with various incoming concentrations, the reaction between persulfate and incoming benzene largely determined the mass and distribution of persulfate in the field;

V. In the reduced velocity set, the radius of influence of a candle was higher than the basic set, and they kept relatively constant at a high value for both 0.02 mM and 1 mM benzene. This indicates that it is possible to optimize

the system to use less rows of candles and/or increase the distance between candles in the low permeability zone;

VI. In the comparison with basic and aeration sets, enhanced aeration could increase or decrease the radius of influence of a candle, dependent on the incoming contaminant concentration. Double checking the sufficient mass left for lateral spreading was a key to determine the remediation efficacy or control the aeration rate in a suitable range.

VII. In the slow-release system design, if extra supply of oxidant in a candle was considered and suitable aeration rates was designed, the demand of boring and labor work could be greatly reduced by using larger interval distances. The effective duration time could also be increased.

Finally, the performance of remediation model demonstrated the capacity to handle wide ranges of soil properties in the field. Based on the easy setting of the reaction module, this model is able to be adapted to design the slow-release system for various oxidants and targeting contaminants. In the future, rigorous numerical modeling of aeration should be incorporated to more accurately evaluate the influence of aeration for a complex design. More advanced release kinetic model based on the formula and positions of components should be incorporated to simulate the persulfate release kinetics. Finally, the model should be validated using well-controlled field site experiments.

References

Lee, E. S., Liu, G., Schwartz, F. W., Kim, Y., & Ibaraki, M. (2008). Model-based evaluation of controlled-release systems in the remediation of dissolved plumes in groundwater. *Chemosphere*, *72*(2), 165–173. https://doi.org/10.1016/j.chemosphere.2008.01.078